

Maraa western transect: Sites M0005–M0007¹

Expedition 310 Scientists²

Chapter contents

Operations	1
Sedimentology and biological assemblages	3
Petrophysics	7
Downhole logging	9
Geochemistry	10
References	11
Figures	12

Operations

Holes M0005A and M0005B

The *DP Hunter* arrived at Site M0005 at 2330 h on 6 October 2005 and immediately conducted dynamic positioning (DP) calibration tests ~250 m south of the first hole, Hole M0005A. By 0250 h on 7 October, the vessel was in position to start drilling.

After overcoming problems with a hydraulic ram that caused the moonpool doors to fail to open, Seacore's drilling and reentry template (DART) was deployed on an American Petroleum Institute (API) drill string (used as conductor pipe for this expedition) to just above the seabed. From 1335 h, a seabed survey around the position of the first site was conducted using the downpipe underwater camera. A suitable site was located ~2 m from the planned position, and the DART was placed on the seabed with 8 T of weight. After removing the camera, the HQ (piggyback) drill string was run through the API conductor to the seabed and coring operations in Hole M0005A commenced. The first core arrived on deck at 2000 h. Thereafter, coring continued with difficult barrel latching, and short core runs were used to avoid drilling rather than coring until the best coring parameters were established. The first cores displayed large cavities, and recovery was poor. Core barrel jams and problems with blocked bit-related mismatching led to slow progress in this hole. When reentering the hole after one particular drill string trip to remove a core blockage from the bit, coring appeared to recommence at 10.4 meters below seafloor (mbsf). Good core was obtained, and it appeared that the borehole had been restarted in a deviation or had avoided a previous deviation. This was taken as the start of a new hole, Hole M0005B, at 1840 h on 8 October.

At 0140 h on 9 October, the core barrel failed to latch in at 20 mbsf. A replacement barrel also failed to latch. The hole was verified as clear by the chisel tool. It was suspected that the HQ pipe was bent, and the string was tripped. On deck, the third and second pipe stands (four joints) of the HQ drill string were bent. The decision was made by all to terminate Hole M0005B, not to log, and to make modifications to the DART before continuing with a new hole. The downpipe camera was prepared, and an environmental impact inspection of the coring area was carried out by raising the DART from the seabed and lowering the camera through the DART. There was difficulty in identifying the drilling area because of the minimal impact of the DART on the seabed.

¹Expedition 310 Scientists, 2007. Maraa western transect: Sites M0005–M0007. In Camoin, G.F., Iryu, Y., McInroy, D.B., and the Expedition 310 Scientists. *Proc. IODP*, 310: Washington, DC (Integrated Ocean Drilling Program Management International, Inc.). doi:10.2204/iodp.proc.310.105.2007

²Expedition 310 Scientists' addresses.



The camera was recovered, and the inspection was completed by 0615 h on 9 October.

Starting at 0615 h on 9 October, the API string was tripped and the DART was brought on deck and secured above the moonpool. The vessel departed Site M0005 and headed for a nearby sheltered bay to carry out work on the DART. The DART feet were removed, and a stinger was installed. The vessel departed the sheltered bay and was back at Site M0005 by 1330 h.

Hole M0005C

The *DP Hunter* took position above Hole M0005C, ~10 m east-southeast along slope from Holes M0005A and M0005B, and was ready for operations by 1510 h on 9 October 2005. When lowering the DART on the API string, a burst hydraulic union on the rig hydraulics caused an oil spill on the deck. There was an operational shutdown until the spill was contained and repairs were made. At 1835 h, the downpipe underwater camera was deployed for a predrilling site check, and the stinger was engaged with the seabed under camera observation. The DART was drilled 1.3 m into the seabed and stabilized, ready for the coring string. The HQ coring string was run at 2000 h, and coring operations commenced in Hole M0005C. At 0545 h on 10 October, sand in the drill string caused the core barrel to jam, and the string had to be tripped to free it. At 1110 h, a heading change of the vessel was requested, which was carried out with the HQ string off bottom but still in the hole. After the heading change, the core barrel was unable to be run into the HQ string and it was observed that the API pipe was not central in the moonpool. The HQ string was tripped, and nine stands were removed with bends. A problem with the DP was analyzed and resolved before resetting the DP to average the previous drilling position. At that position, the downpipe camera was run at 1515 h to see if the HQ hole was still in the stinger. No HQ hole was apparent, but the decision was made to trip the HQ string with an insert bit and drill down to the previous depth. Reentry into the earlier borehole was not confirmed even though the template had not moved, so a new hole (Hole M0005D) was started.

Hole M0005D

Coring commenced in Hole M0005D at 2330 h on 10 October 2005. Coring was steady and recovery moderate to good throughout the day on 11 October. At 0510 h on 12 October, the decision was made to stop coring in Hole M0005D after reaching 102 mbsf and without reaching the basaltic basement.

The HQ string was pulled and the logging tools were prepared.

At 0820 h on 12 October, the gamma logging tool was lowered, but it got stuck just below the seabed. It was suspected that the top of the hole was unstable, within a zone of low recovery noted while drilling. The top 5 m of the hole was cased with the HQ pipe. The gamma logging tool was lowered but was still unable to enter the hole from the pipe. The HQ pipe was run all the way to the base of the hole, a gamma log was run inside the HQ pipe, and then, after ensuring that the pipe was free from obstruction, the HQ pipe was pulled back in 25 m increments and the logging was conducted in the open hole below.

The logging operation in Hole M0005D continued with excellent logs being obtained until the hole finally collapsed after pulling back the HQ pipe to 17 mbsf. The logging tools were in danger of becoming stuck in the top-hole section and were retrieved. After a heading change, the remaining HQ pipe was pulled, the DART was lifted, and operations in Hole M0005D ceased at 1310 h on 13 October. A postdrilling seabed survey using the downpipe camera was conducted before leaving the hole.

Hole M0005E

Before departing Site M0005, four hammer samples were taken in Hole M0005E (~5 m along slope from Hole M0005D; 61.34 m water depth). Four samples were taken to a depth of 2 mbsf with typically 80% recovery. After curation, these samples were handed to the microbiologists to sample at will before the remainder was passed to the sedimentologists and coral specialists for description. Operations in Hole M0005E were concluded by 1635 h on 13 October. Before progressing to the next site, the *DP Hunter* conducted a 360° maneuver to verify that positioning offsets at the drill string were zero.

Hole M0006A

A move to deeper water (~80 m) was undertaken, and the *DP Hunter* was repositioned above Hole M0006A in 81.58 m water depth. Another four hammer samples were collected primarily for microbiology before the drill string was lowered onto what appeared to be a very steep slope. Both the ship's transponder and tautwire indicated that they were sliding downslope and suggested that bathymetric data were insufficient to allow a reasonable picture of the seabed. Any slope instability may have led to the DART sliding away downslope, and the decision was made to avoid the outer reef edge until either more seabed information was obtained or modifications were made to the DART to allow greater stabil-

ity on steep slopes. Site M0006 was departed at 2300 h on 13 October 2005.

Hole M0007A

Hole M0007A was located further back from the reef edge than Sites M0005 and M0006, in 44.45 m water depth. The seabed was surveyed using the downpipe camera, and at 0330 h on 14 October 2005, four hammer samples were taken. After hammer sampling, the HQ string was run and rotary coring commenced in the same hole. Coring continued with good recovery for the rest of the day. Total depth (TD; 44.4 mbsf) was reached at 0120 h on 15 October.

Prior to tripping the HQ pipe, the gamma tool was run inside the pipe. Logging results from Hole M0005D indicated that the shape of the gamma trace through the pipe, when scaled accordingly, did not differ significantly when compared to the open-hole trace, although statistically the results are less useful. After gamma logging, the HQ pipe was tripped, the core barrel was removed, and the string was rerun with a casing shoe to 7.5 mbsf. Open-hole logging commenced from TD to the casing shoe. After running the resistivity and hydrochemical tools in the open-hole section, the acoustic imaging tool would not progress much beyond the casing shoe, despite being run with a sinker bar. Logging was terminated in Hole M0007A at 0700 h on 15 October.

Hole M0007B

After a postdrilling seabed survey using the downpipe camera, the *DP Hunter* moved 50 m along slope to Hole M0007B. Two hammer samples were collected before rotary coring commenced in the same hole. Core recovery was poor in the top part of the hole, and the coring parameters were checked for any changes that may have been responsible. Zero bit weight and high rates of penetration confirmed that an open structure was being drilled. The formation became more compact with depth, and recovery improved accordingly. Coring continued until 0630 h on 16 October 2005.

The HQ pipe was tripped and a casing shoe fitted before the pipe was rerun to the base of the hole for in-pipe gamma logging. After gamma logging, the HQ pipe was pulled to 24.6 mbsf and the resistivity, hydrochemical, acoustic imaging, and optical imaging tools were run. It was not possible to log the entire bottom-hole section because of hole blockage (below 30 mbsf). Logging in Hole M0007B was completed by 1410 h on 16 October.

Hole M0007C

Before returning to Site M0007, Sites M0008–M0014 at Tiarei were cored (see the “[Tiarei outer ridge](#)” and “[Tiarei marginal sites](#)” chapters).

Site M0007 was reached at 0200 h on 26 October 2005. Prior to coring in Hole M0007C, a seabed camera survey was conducted, which revealed a surprisingly barren sloping seabed in 43.35 m water depth. Coring operations began at 0315 h and continued until 2215 h. The hole progressed quickly, with core recovery generally poor and little formation resistance being evident on the bit. At ~30 mbsf, the hole started to become sticky and then collapsed at a wireline trip, filling the outer core barrel with cuttings. The string was tripped, the barrel was cleaned out (2 m of coral cuttings), and the HQ string was rerun with an insert bit as the inner core barrel. The base of the hole was reached with difficulty, where rotation also became difficult. The string stuck a few times, and the hole was abandoned at a TD of 32.25 mbsf.

After Hole M0007C was complete, the vessel moved to Site M0015 on the Maraa eastern transect (see the “[Maraa eastern transect](#)” chapter).

Sedimentology and biological assemblages

The western transect drilled offshore Maraa (southwest Tahiti) includes, from land oceanward, Sites M0007, M0005, and M0006, which range in water depth from 41.65 to 81.58 meters below sea level (mbsl).

Modern sediments

Intervals: Cores 310-M0005A-1R through 4R, 310-M0005E-1M through 4M, 310-M0006A-1M through 4M, 310-M0007A-1M through 4M, 310-M0007B-1M, 2M, and 3R, and 310-M0007C-1R through 5R-1

Modern sediments were recovered at all sites along this transect. They consist of a few decimeter-thick beds composed of rhodoliths, skeletal sand, and gravels rich in *Halimeda* segments, mollusk shell fragments, foraminiferal tests, and nongeniculate coralline algal crusts (Fig. F1) (e.g., intervals 310-M0005E-2M-1, 1–6 cm, and 310-M0006A-1M-1, 0–8 cm). They include clasts of *Halimeda* packstone and coral clasts (especially branching and encrusting corals) that are commonly encrusted with nongeniculate coralline algae and worms (Fig. F2) (e.g., interval 310-M0007A-1M-1, 8–16 cm). The surfaces of some clasts are extensively bored and display brown stain-

ing. The cores of the rhodoliths generally correspond to coral fragments that may exhibit traces of bioerosion.

Last deglacial sequence (Unit I)

Coral/algal rubble intervals: Cores 310-M0005A-5R, 310-M0007A-7R, 15R, 21R, 23R, and 25R, 310-M0007B-1M, 2M, 5R, 7R through 9R, and 31R, and 310-M0007C-6R, 9R, and 19R

Skeletal sand intervals: Cores 310-M0007A-15R, 310-M0007B-5R, 18R, 30R, and 31R, and 310-M0007C-7R

Skeletal limestone intervals: Cores 310-M0005A-7R and 310-M0005C-11R

The thickness of the last deglacial sequence (lithologic Unit I) ranges from 33 to 42 m at Sites M0005 and M0007, respectively.

The top of the last deglacial sequence is characterized by the abundance of thin crusts of nongeniculate coralline algae and extensive bioerosion features (e.g., Core 310-M0005A-1R); reddish and brownish staining is conspicuous on the upper surface of the last deglacial rocks and in large borings.

This sequence is primarily composed of coralgamicrobialite frameworks commonly interlayered with skeletal limestone and loose skeletal sediments, including coral and algal rubble and skeletal sand. Coral and algal rubble are mostly composed of accumulations of fragments of corals (branching and robust branching *Pocillopora*, *Acropora*, *Porites*, and *Pavona*), nongeniculate coralline algal crusts, rhodoliths, and lithoclasts that are usually extensively bored. Skeletal sand corresponds to *Halimeda* sand and is rich in echinoid and mollusk grains (Fig. F3) (e.g., intervals 310-M0007B-18R-1, 0–15 cm, and 31R-1, 6–12 cm). Skeletal limestone comprises grainstone and is rich in *Halimeda* segments and coralline algal fragments (including fruticose forms) (Fig. F4) (e.g., interval 310-M0005C-11R-1, 0–10 cm).

The coralgamicrobialite frameworks that form the bulk of the last deglacial sequence are characterized by the widespread development of microbialites, which locally represent the major structural and volumetric component of the reef rock. They develop within the primary cavities of the reef framework, where they generally overlie nongeniculate coralline algal crusts. Microbialites generally comprise a suite of fabrics, including two end-members represented by laminated fabrics and dendritic accretions; the laminated fabrics are generally the most abundant (Figs. F5, F6, F7, F8, F9) (e.g., intervals 310-M0005A-2R-1, 12–24 cm, 310-M0005B-3R-1, 22–36 cm, and 310-M0005C-6R-2, 2–16 cm, 8R-1, 65–79 cm, and 9R-1, 115–134 cm).

The reef sequence is characterized by a general succession of distinctive coral assemblages, although many of them are intergradational, both laterally and vertically. Two successive subunits displaying distinctive coral assemblages and internal structure can be identified, from top to base.

Subunit IA

Intervals: Cores 310-M0005A-1R through 11R, 310-M0005B-1R through 3R, 310-M0005C-2R through 5R, 310-M0007A-3R through 19R, 310-M0007B-3R, 4R, 6R, and 8R through 19R, and 310-M0007C-5R through 15R

Subunit IA, as thick as 20 m, is primarily composed of coralgamicrobialite frameworks dominated by encrusting coral colonies. In the upper part of this subunit, the coral assemblage includes abundant encrusting colonies of *Montipora* and *Porites* and, to a lesser extent, *Pavona*, *Psammocora*, *Astreopora*, agariciids, and faviids (including *Leptastrea* and *Montastrea*) (Figs. F10, F11, F12, F13) (e.g., intervals 310-M0005A-1R-1, 48–59 cm, 310-M0005B-1R-1, 36–46 cm, and 310-M0005C-2R-CC, 10–31 cm, and 3R-1, 11–23 cm). Massive colonies of *Porites*, *Montipora*, *Astreopora*, and faviids occur locally (Fig. F14) (e.g., interval 310-M0007A-6R-1, 20–34 cm). Branching colonies of *Montipora*, *Pocillopora* (including robust branching colonies), and *Acropora* occur as fragments. These coral colonies are coated with thin crusts of nongeniculate coralline algae overlain by massive microbialite coatings (laminated and thrombolitic fabrics) to form loose frameworks (bindstone) (Fig. F15) (e.g., interval 310-M0007A-9R-CC, 1–11 cm). Multiple generations of coral colonies and thin encrustations of nongeniculate coralline algae may alternate locally. Large primary cavities are partly filled with skeletal sand and gravels, including fragments of corals, coralline algae and mollusks, *Halimeda* segments, echinoid spines, and foraminifers; rhodoliths occur locally (e.g., Core 310-M0005B-1R).

In the lower part of this subunit, the coral assemblage is mostly composed of encrusting coral colonies of *Montipora*, faviids, and agariciids (Figs. F16, F17, F18) (e.g., intervals 310-M0007A-8R-1, 51–70 cm, 8R-1, 72–84 cm, and 9R-1, 23–45 cm) associated with branching colonies of *Porites* that are locally dominant (e.g., Cores 310-M0007B-16R through 18R), robust branching colonies of *Pocillopora* (e.g., Cores 310-M0007A-15R and 310-M0007C-15R and interval 310-M0007A-15R-1, 30–45 cm) (Fig. F19), tabular colonies of *Acropora* (e.g., Cores 310-M0007B-12R, 15R, and 16R, and 310-M0007C-7R through 9R), and massive colonies of *Porites*, *Montipora*, *Astreopora*, and faviids; some sections of massive *Porites*

colonies are up to 60 cm thick (Fig. F20) (e.g., Cores 310-M0005B-1R and 3R, 310-M0007A-6R through 9R, 11R, 13R through 15R, and 18R, and 310-M0007B-5R-2, 6R, 8R, 9R, and 11R and interval 310-M0007A-7R-1, 18–30 cm). In this part of the subunit, frameworks usually exhibit a denser internal structure and are characterized by thicker crusts of nongeniculate coralline algae. Microbialite crusts display widespread development in those frameworks.

Subunit IB

Intervals: Cores 310-M0005A-12R, 310-M0005B-3R through 8R, 310-M0005C-6R through 16R, 310-M0005D-1R through 6R, 310-M0007A-20R through 35R, 310-M0007B-17R through 34R, and 310-M0007C-16R through 22R

Subunit IB, as thick as 25 m, comprises coralgamicrobialite frameworks made of tabular and robust branching coral colonies that are usually heavily encrusted with nongeniculate coralline algae, locally associated with vermetid gastropods and serpulids, and overlain by very thick and massive microbialite crusts (Fig. F21) (e.g., interval 310-M0005B-6R-1, 9–39 cm). Large primary cavities are partially filled with skeletal sand and are rich in *Halimeda* segments and coral fragments (Fig. F22) (e.g., interval 310-M0007C-22R-1, 10–26 cm).

The coral assemblage is dominated by tabular colonies of *Acropora* associated with robust branching colonies of *Pocillopora*, *Acropora*, and *Pavona* (especially in the lower part of this interval) (Figs. F23, F24, F25, F26, F27, F28, F29) (e.g., intervals 310-M0005B-4R-1, 19–41 cm, 310-M0005C-8R-1, 38–62 cm, 11R-1, 48–62 cm, and 13R-1A, 66–85 cm, 310-M0007A-30R-1, 7–20 cm, and 31R-1, 45–65 cm, and 310-M0007B-30R-1, 35–56 cm). Other corals include massive colonies of *Porites* (Figs. F30, F31) (e.g., Cores 310-M0005A-12R, 310-M0005B-5R and 6R, 310-M0007A-19R-2 and 20R-1, and 310-M0007B-20R and 21R and intervals 310-M0005B-4R-1, 87–101 cm, and 310-M0007B-20R-1, 86–106 cm), *Montipora*, and *Montastrea*, branching colonies of *Porites* (locally dominant), and encrusting colonies of *Montipora*, *Porites*, *Leptastrea*, *Pavona*, *Montastrea*, *Millepora*, *Favia*, and agariciids (Figs. F32, F33, F34) (e.g., intervals 310-M0005C-10R-1, 33–46 cm, and 15R-1, 1–15 cm, and 310-M0007B-34R-CC, 0–20 cm).

At Site M0007, the base of the coralgamicrobialite frameworks of the last deglacial sequence is characterized by lithified skeletal grainstone that contains fine sand-sized volcanic grains; a 30 cm thick interval composed of branching coralline algae occurs in Section 310-M0007B-34R-CC.

Older Pleistocene sequence (Unit II)

The top of the older Pleistocene sequence (lithologic Unit II) is located at 86 and 92 mbsl at Sites M0005 and M0007, respectively. This sequence was drilled down to 161.56 mbsl in Hole M0005D.

The older Pleistocene sequence is composed of eight distinctive lithologic units, which are discussed in order from top to base.

Subunit IIA

Intervals: Cores 310-M0007A-35R and 36R, 310-M0007B-34R and 35R, and 310-M0005D-8R and 9R

Subunit IIA is made up of beige to gray well-lithified limestone comprising coralgamicrobialite frameworks associated with rudstone-floatstone beds. The coral assemblage is dominated by encrusting colonies of *Montipora*, tabular colonies of *Acropora*, and branching colonies of *Pocillopora*. Fragments of *Acropora* and *Porites* branches are commonly associated. Coral colonies are bounded by very thick crusts of nongeniculate coralline algae in which vermetid gastropods and serpulids occur (Fig. F35) (e.g., interval 310-M0007A-35R-1, 90–110 cm). Associated rudstone-floatstone beds consist of large fragments of corals and nongeniculate coralline algae in a matrix that includes a mixture of skeletal (*Halimeda* segments and fragments of mollusks and echinoids) and volcanic grains (Fig. F36) (e.g., interval 310-M0007B-35R-1, 82–102 cm).

Postdepositional diagenetic processes are indicated by the recrystallization and transformation of coral skeletons and the occurrence of abundant centimeter-sized solution cavities. Cement crusts in those cavities are usually stained reddish. The contact between this limestone and the underlying subunit corresponds to an unconformity; distinctive diagenetic features characterize these subunits.

Subunit IIB

Interval: Core 310-M0005D-9R through Section 16R-1

Subunit IIB contains well-lithified skeletal floatstone-rudstone rich in rhodoliths, fragments of corals (branching *Pocillopora* and *Porites*, encrusting *Montipora* and *Porites*, and massive *Porites*) and mollusks, and *Halimeda* segments; volcanic grains are common (Figs. F37, F38, F39, F40, F41) (e.g., intervals 310-M0005D-9R-1, 42–53 cm, 10R-1, 8–18 cm, 10R-1, 68–76 cm, 15R-2, 7–16 cm, and 16R-1, 2–10 cm). Abundant centimeter-sized cavities as well as dissolution of skeletal grains (*Halimeda* segments, fragments of mollusks, and corals that form the core

of rhodoliths) and recrystallization and transformation of coral skeletons indicate that these limestones were subject to postdepositional diagenetic processes.

Subunit IIC

Interval: Core 310-M0005D-16R through Section 20R-1

Subunit IIC comprises poorly sorted and ungraded unlithified volcanoclastic silt to sand, including scattered skeletal grains (*Halimeda* segments, fragments of mollusks and echinoids, and foraminifers), reworked pebbles of *Halimeda* floatstone, and angular clasts of siltstone of the same composition (Fig. F42) (e.g., interval 310-M0005D-16R-1, 97–105 cm). Sand-sized volcanic grains are angular to subangular. Bioturbation is locally abundant, and burrows are filled with *Halimeda* floatstone. These volcanoclastic sediments are locally interlayered with skeletal floatstone rich in *Halimeda* and grade downward (from Core 310-M0005D-18R) through skeletal siltstone to sandstone rich in fragments of corals (massive *Porites* and encrusting agariciids).

Subunit IID

Interval: Sections 310-M0005D-20R-1 through 25R-1

Subunit IID contains beige to brownish coralgal frameworks in which corals are thinly coated with nongeniculate coralline algae and then heavily encrusted with microbialites composed of laminar and thrombolitic fabrics (Fig. F43) (e.g., interval 310-M0005D-21R-2, 0–12 cm). Large colonies of massive *Porites* were recovered in this subunit; other corals include robust branching colonies of *Pocillopora* and *Pavona*, tabular colonies of *Acropora*, and encrusting colonies of *Montipora*, *Leptastrea*, *Porites*, and agariciids (Fig. F44) (e.g., interval 310-M0005D-21R-1, 0–15 cm). Corals contain evidence of severe bioerosion and diagenetic alteration (Fig. F45) (e.g., interval 310-M0005D-21R-1, 38–48 cm). Volcanic grains commonly occur in the matrix of the frameworks (Fig. F46) (e.g., interval 310-M0005D-21R-1, 65–75 cm). Solution cavities are usually filled with a mixture of skeletal and volcanic grains. Associated beds include skeletal packstone to grainstone, including foraminifers and fragments of mollusks, coralline algae and echinoids, and rhodolith floatstone that includes volcanic grains (Fig. F47) (e.g., interval 310-M0005D-23R-1, 10–15 cm).

Subunit IIE

Interval: Core 310-M0005D-25R through Section 29R-1

Subunit IIE is a sandy skeletal grainstone to packstone rich in volcanic grains, large coral fragments of massive *Porites*, and skeletal fragments of nongeniculate coralline algae and corals (Fig. F48) (e.g., interval 310-M0005D-29R-1, 5–14 cm). Some in situ massive colonies of *Porites* (e.g., Cores 310-M0005D-27R-1 and 29R-1) and encrusting colonies of agariciids (Fig. F49) (e.g., interval 310-M0005D-29-1, 50–70 cm) occur in this subunit.

Subunit IIF

Interval: Sections 310-M0005D-29R-1 through 30R-1

Subunit IIF contains coral and algal rudstone to floatstone composed of rhodoliths (Fig. F50) (e.g., interval 310-M0005D-29R-1, 116–131 cm), lithoclasts, and fragments of corals (massive, encrusting, and branching corals), coralline algae, echinoids, and mollusks in a coarse sandstone matrix rich in volcanic and skeletal grains (Figs. F51, F52) (e.g., intervals 310-M0005D-29R-1, 80–110 cm, and 30R-1, 17–26 cm).

Subunit IIG

Interval: Core 310-M0005D-30R through Section 35R-1

Subunit IIG consists of coralgal frameworks interbedded with skeletal grainstone to packstone rich in volcanic grains and sandstone (Figs. F53, F54, F55) (e.g., intervals 310-M0005D-31R-2, 0–12 cm, 32R-1, 109–133 cm, and 32R-3, 15–27 cm). The abundance and grain size of the volcanoclastic intervals increase downhole (Fig. F56) (e.g., interval 310-M0005D-34R-1, 28–40 cm). Coral assemblages included are dominated by massive colonies of *Porites* and *Montastrea* associated with tabular colonies of *Acropora*, robust branching colonies of *Pocillopora* and *Pavona*, and encrusting colonies of *Porites* and faviids (Figs. F57, F58, F59, F60, F61) (e.g., intervals 310-M0005D-30R-1, 117–128 cm, 30R-2, 30–46 cm, 30R-2, 79–97 cm, 30R-2, 95–110 cm, and 33R-3, 0–25 cm). Corals are diagenetically altered.

Subunit IIH

Interval: Section 310-M0005D-35R-2 and Core 36R

Subunit IIH comprises skeletal grainstone to floatstone rich in fragments of corals (robust branching *Pavona* and encrusting *Montipora*), echinoids and coralline algae, and volcanic grains (Fig. F62) (e.g., interval 310-M0005D-35R-2, 70–97 cm). Strong diagenetic imprints are manifest because coral skeletons have been altered and large solution cavities occur. The base of this subunit includes poorly lithified carbonates rich in volcanic grains.

Petrophysics

Recovery at Maraa western transect sites, on the southern side of the island of Tahiti, was low (Hole M0005A = 32%, Fig. F63; Hole M0007C = 36%, Fig. F64), partial (Hole M0005C = 53%, Fig. F65; Hole M0007B = 56%, Fig. F66), and good (Hole M0005B = 74%, Fig. F67; Hole M0005D = 64%, Fig. F68; Hole M0007A = 69%, Fig. F69). Hole M0006A was cored only with hammer coring for microbiology investigation. Multisensor core logger (MSCL) measurements were not possible on the rubble recovered from this hole (Hole M0006A). Cores 310-M0007B-31R and 36R and 310-M0007C-7R were left unsaturated and thus have different data coverage and quality (see the “Methods” chapter for more details). Water depths are as follows: Hole M0005A = 59.13 mbsl, Hole M0005B = 59.13 mbsl, Hole M0005C = 59.63 mbsl, Hole M0005D = 59.63 mbsl, Hole M0005E = 61.34 mbsl, Hole M0007A = 44.45 mbsl, Hole M0007B = 41.65 mbsl, and Hole M0007C = 43.35 mbsl.

Density and porosity

Bulk density at Maraa western transect sites was measured on discrete 1 inch core plugs (MAD) and using the MSCL (GRA). The last deglacial sequence (lithologic Unit I) was recovered in Holes M0005A–M0005C (Figs. F63, F65, F67) where density and porosity values are highly scattered downhole. Density values range from 1.8 to 2.4 g/cm³. The porosity profile also lacks any clear downhole trend with highly variable readings from 20% to 55%. Holes M0007A–M0007C (Figs. F64, F66, F69) have much more continuous data coverage, with densities varying between 1.9 and 2.3 g/cm³ and a mean constant value of ~2.1 g/cm³. Porosity directly follows the density profile, with average porosities of ~35%, a minimum of 20%, and a maximum of up to 55%.

The transition from Unit I to the older Pleistocene sequence (Unit II) is sharp and abrupt (e.g., Hole M0007A, 41 mbsf; Fig. F69) or lacks data coverage because of bad recovery due to poor lithification (e.g., Hole M0007B, 44 mbsf; Fig. F66).

Six distinct intervals are recognized in the older Pleistocene sequence based on density, porosity, and velocity trends. Intervals 2 to 6 were only recovered in Hole M0005D (Fig. F68).

- Interval 1: Holes M0005D (Fig. F68): 23–33 mbsf (Cores 310-M0005D-1R through 6R); M0007A (Fig. F69): 41 mbsf to the bottom of the hole (Cores 310-M0007A-35R through 36R); and M0007B (Fig. F66): 44 mbsf to the bottom of the hole (Cores 310-M0007B-34R through 36R). After a sharp and abrupt increase in density from the

overlying last deglacial sequence, density and porosity are constant at 2.4 g/cm³ and ~15%, respectively.

- Interval 2: Hole M0005D (Fig. F68): 33–49 mbsf (Cores 310-M0005D-7R through 16R). Density sharply increases at 33 mbsf, and from 33 to 36 mbsf density continues to increase to 2.4 g/cm³. Variable densities gradually decrease to 1.8 g/cm³, reflecting strong lithification at the top of this interval changing to weak to moderate lithification downcore (~49 mbsf).
- Interval 3: Hole M0005D (Fig. F68): 49–59 mbsf (Cores 310-M0005D-17R through 20R). The underlying unit is composed of massive moderately lithified volcanoclastic sandstone with densities ranging between 1.8 and 2.2 g/cm³. Porosities are equally high, between 35% and 55%.
- Interval 4: Hole M0005D (Fig. F68): 59–71 mbsf (Cores 310-M0005D-21R through 24R). Coralgall frameworks alternate with microbialites and skeletal sand. Density is between 2.0 and 2.4 g/cm³ with a slight decrease toward the bottom of this interval, to ~2.0 g/cm³. Porosity shows a reverse trend, with porosities ranging from 15% to 35% in the top part and averaging 40% at the bottom part of the interval.
- Interval 5: Hole M0005D (Fig. F68): 71–78 mbsf (Cores 310-M0005D-25R through 28R). This interval is poorly recovered, most likely because of poorer lithification, and consists of sandy bioclastic limestone with scattered density observations of ~2.0 g/cm³.
- Interval 6: Hole M0005D (Fig. F68): 78 mbsf to the bottom of the hole (Cores 310-M0005D-29R through 36R). The lowermost interval shows strong diagenetic overprint on sandy coralgall framework and coarse floatstone and rudstone. Large solution cavities are present. Density profile shows continuous high values between 2.1 and 2.5 g/cm³ and porosity varying between 15% and 35%.

MAD measurements are in correspondence with GRA density and porosity values and range from 17% to 42% (average = 24%). Grain density averages 2.72 g/cm³ for lithologic Unit I and increases to 2.74 g/cm³ for lithologic Unit II.

P-wave velocity

P-wave velocities were measured with the MSCL P-wave logger (PWL) on whole cores and the PWS3 contact probe system on discrete 1 inch core plugs.

P-wave velocity profiles in the last deglacial sequence (Unit I) are highly variable with small-scale variations and velocities ranging between 1800 and 4300

m/s (Hole M0007A, Fig. F69; Hole M0007B, Fig. F66). Discrete measurements show similar variation with high velocity values corresponding to dense microbialite matrix sediments (e.g., Hole M0007B, 12 mbsf) and lower velocities in highly porous sand-dominated samples. Samples measured correlate to peaks of velocities in the PWL and sometimes exceed PWL velocities by as much as 300 m/s. The velocity profile in the last deglacial sequence shows that this extreme variation results from the open character of the coralgal-microbialite framework where porosity changes from 50% to 10% occur over a centimeter scale.

Velocity changes abruptly at the lithologic Unit I/II boundary. The velocity profile is constant in the high-velocity domain with values of ~4300 m/s on average and seldom below 4000 m/s (e.g., Hole M0007A, 42 mbsf; Fig. F69). The velocity profile mimics the density and porosity zone subdivision with decreasing velocities from 4200 to 2200 m/s in Interval 2 reflecting the decrease in density and increase in porosity. The massive sandstone in Interval 3 has constant low velocities of ~1800 m/s, as would be expected for moderately lithified sand-size sediments. Interval 4 follows the density profile with values of ~4000 m/s at the top of the interval and a decrease in velocity toward 3000 m/s in the lower part of the profile. Interval 5 shows scattered velocity observations, mostly ~2000 m/s. The last interval, Interval 6, reflects the diagenetic overprint modification toward higher densities also with equally high velocities varying between 3800 and 4300 m/s.

A cross plot of velocity versus porosity for the Maraa western transect shows a general inverse relationship (Fig. F70). For the time-average empirical equation of Wyllie et al. (1956) and Raymer et al. (1980), the traveltime of an acoustic signal through rock is a specific sum of the traveltime through the solid matrix and the fluid phase. Moderately lithified sandstone forms a distinct group in porosity-velocity space, occupying a region of relatively low velocities compared to densities. For carbonates, the general trend appears to be rather linear, with the largest deviations from the general trends between porosities of 0% and 15% and only scattered observations between 35% and 50%. A comparison of the V_p MSCL data with wireline downhole sonic logging data shows clear correlation of high-velocity excursions (Fig. F71). Sonic velocities are ~500 m/s slower, most likely because of scaling effects. Where MSCL measures velocity directly only on matrix sediments, the sonic log provides an average over an interval of 1 ft (~31 cm) in which velocity is averaged over large primary pores containing seawater (~1535 m/s) and rock. Direct shear waves show a range of 800–2800

m/s, closely following trends in compressional wave sonic data.

Magnetic susceptibility

Magnetic susceptibility in the last deglacial sequence is generally $<100 \times 10^{-5}$ SI units with a few outliers as high as 220×10^{-5} SI units. No clear downhole trends are observed. Below the boundary with the older Pleistocene sequence, the upper magnetic susceptibility profile changes immediately. Values in Interval 2 are constantly low, $<200 \times 10^{-5}$ SI units, but in Interval 3 a sharp increase occurs, corresponding to the occurrence of volcanoclastic sandstone. Magnetic susceptibility values range between 0 and 720×10^{-5} SI units and show small-scale variation. In Intervals 4 and 5, overall magnetic susceptibility values are generally high, ranging between 0 and 500×10^{-5} SI units, because of the influx of sand and small pebbles of volcanic origin. The lowermost interval, Interval 6, shows continuous high magnetic susceptibility with values above 100×10^{-5} SI units. The uppermost part of Interval 6 (83–88 mbsf) displays values up to 735×10^{-5} SI units. Volcanic grains are abundant in this entire interval (see “[Sedimentology and biological assemblages](#)”).

Resistivity

The electrical resistivity of rocks depends on several factors, including the presence of conductive minerals such as base metal sulfides or oxides and graphite in the rock. Rocks without these minerals are usually poor conductors, and their resistivities are governed primarily by their porosity, their degree of fracturing, the salinity of the pore water, the degree of saturation of the pore spaces, and, to a lesser extent, the intrinsic minerals that constitute the rock. Diagenetic processes such as silicification and cementation tend to reduce porosity and thus increase the resistivity of the rock. In igneous and metamorphic rocks, the resistivity log is mainly useful for mapping conductive minerals and fracture zones. In sedimentary rocks, the resistivity log is frequently used in lithologic mapping because changes in lithology are often associated with changes in porosity.

During Expedition 310, good resistivity measurements were difficult to obtain. This may have been caused by the following reasons:

- Defective sensor because of entrance of water into the electronics, affecting all sections logged subsequent to Core 310-M0015B-20R (see the “[Methods](#)” chapter), and
- Low volume of monomineral rock versus high porosity saturated with seawater, affecting all sections logged.

Rocks are poor electrolytic conductors whose effective resistivity varies with the volume and arrangement of the pores and with the conductivity of the pore fluid. During Expedition 310, all cores were saturated with seawater. When comparing coreline with downhole measurements of electrical conductivity, no clear correlations are visible and absolute values are incomparable. It is thought that drilling disturbances in combination with the low rock:water volume ratios of the measured liners (including the core) resulted in MSCL resistivity values near those of seawater (Fig. F72).

Diffuse color reflectance spectrophotometry

Color reflectance in the last deglacial sequence varies between 40% and 85% L^* units. Downhole trends are not present in any borehole. Slightly higher values are present just below the seafloor where modern reef sediment (corals) was recovered. In the interval from Core 310-M0005D-16R to Core 19R within the older Pleistocene sequence, color reflectance has lower L^* values of 13%–67% L^* units (Fig. F73). This interval corresponds to volcanoclastic sandstone lithofacies. Increases and decreases of L^* values in this interval may therefore be indicative of influx of the volcanoclastic grains.

Hole-to-hole correlation

Borehole correlation at the Maraa western transect is straightforward along the Unit I/II boundary. Deeper intervals are only cored in Hole M0005D (Fig. F68), however, and results do not permit any crosshole trends. The top few meters in Hole M0005D (Fig. F68) do not show the same clear petrophysical expression (i.e., high density, low porosity, and high velocity) as in Holes M0007A (Fig. F69) and M0007B (Fig. F66).

Downhole logging

Hole M0005D

Geophysical wireline operations were completed in Hole M0005D (59.63 mbsl) from 98.01 mbsf upward, with data coverage by all slimhole tools over the lowermost older Pleistocene sequence. A spectral gamma ray log was made through the steel drill pipes to obtain a continuous log over the entire interval comprising lithologic Units I and II (i.e., last deglacial and older Pleistocene sequences). From the seafloor to 32.36 mbsf, total gamma radiation (TGR) was very low (~15 cps), despite logging speeds up to a maximum of 1.1 m/min. A marked increase in TGR was observed within the older Pleistocene sequence

in the interval between 32.36 and 52.0 mbsf, where U contributes most to TGR in the upper part (32.36–46.71 mbsf) and Th and minor K contribute most to TGR in the lower part. In the remainder of the older Pleistocene sequence, U contributes most to TGR values (Fig. F74).

Open borehole logging was performed in three different stages because of borehole instability:

1. By positioning an open shoe casing at 75.49 mbsf, the bottom part of Hole M0005D could be logged. Borehole conditions were exceptionally good for the lower part of the older Pleistocene sequence. From 77.66 mbsf to the base of the casing (75.49 mbsf; Core 310-M0005D-27R), the caliper showed a large increase in borehole diameter (from ~9.7 to 14.6 cm). Optical images were slightly affected by murky borehole waters at the top, but quality increased toward the base. Acoustic images were not affected by this and are high-quality virtual representations of the lithologies cored. Repetitive spectral gamma ray logs over this interval show that logging through the steel casing reduces the number of counts per second (in TGR) for each sample but that trends in natural radiation values with depth are the same (Fig. F74). Resistivity values range from 2.8 to 11 m (Fig. F74). Resistivity values drop significantly above 77.66 mbsf, corresponding to an increase in borehole diameter and soft formation reflectivity values in the acoustic image. Sonic P -wave velocities (V_p) range from 2300 to 4400 m/s. The top 2 m show a marked decrease in V_p to values as low as 1738 m/s. Sonic Stoneley-wave velocities range from 1085 to 1477 m/s, dropping to values of 333 m/s in the uppermost 2 m (Fig. F74). The temperature of the borehole fluid is ~22.8°C, pH values are ~8.07, and electrical conductivity is ~51.7 mS/cm (0.193 m).
2. By positioning the open shoe casing at 57.45 mbsf, the middle part (57.45–75.49 mbsf; Cores 310-M0005D-20R through 27R) of Hole M0005D in Unit II could be logged. Borehole conditions were very poor in this interval, as observed from the caliper logs. Borehole diameter was highly variable (from 10 to 15.7 cm). Optical images could not be recorded at this level because of unstable borehole conditions, which caused difficulties entering the borehole and pulling the tool up. Acoustic images were recorded from a maximum depth of 71.07 mbsf and show highly variable lithologic stacking based on acoustic reflectivity values. Overall, this interval is characterized by very low acoustic amplitudes; high impedance features appear only sporadically within the interval (Fig. F75). Between 60.40 and 62.75 mbsf, the acoustic borehole televiewer ABI40 image shows

- high impedance dense coral framework. Resistivity values are very low in the bottom part of this interval (~1.1 m) and increase from 67.36 mbsf to a maximum of 5.26 m at 61.11 mbsf (Fig. F74). The temperature of the borehole fluid increases from 22.56° to 23.84°C, pH values are ~7.78, and electrical conductivity is ~51.45 mS/cm (0.194 m).
- By positioning an open shoe casing at 17.45 mbsf, the upper part of the older Pleistocene sequence and the lower 10 m of the last deglacial sequence (17.45–57.45 mbsf; Cores 310-M0005D-10R through 20R) of Hole M0005D could be logged. Borehole conditions were very poor in this interval, and only resistivity and spectral gamma tools could be run safely. Both tools, however, could not reach below 32.36 mbsf. Resistivity values range from 1.1 m at the base to 4.54 m in the middle of this interval (Fig. F74). No decoupling between deep and medium resistivity values was observed until reaching maximum overall resistivity values in the middle part.

Hole M0007A

At Site M0007, borehole conditions were extremely hostile and great difficulties were encountered while deploying the logging tools.

Geophysical wireline operations were completed in Hole M0007A (44.45 mbsl) from 41.63 mbsf upward, with data coverage by only three tools (Spectral Natural Gamma Probe [ASGR], Induction Resistivity Probe [DIL45], and Hydrogeologique Probe [IDRONAUT]) in the last deglacial carbonate sequence. Despite many efforts, tools with centralizers could not pass an obstruction directly below the shoe casing; however, a spectral gamma ray log through the steel drill pipes provided a continuous log of the drilled interval in Hole M0007A (Fig. F76).

Hole M0007B

In Hole M0007B (41.65 mbsl), geophysical wireline operations were completed from 45.08 mbsf upward, with data coverage by five tools (no Full Waveform Sonic Probe and Caliper Probe) in the short interval between 24.88 and 31.15 mbsf (Cores 310-M0007B-20R through 25R). A spectral gamma ray log through the steel drill pipes provided a continuous log of the drilled interval in Hole M0007B (Fig. F77). An open shoe casing was placed at 24.88 mbsf, and open borehole logging was only possible below this depth. The following geophysical characterization of Unit I at Site M0007 was made by integrating both boreholes. TGR was very low (~9 cps) from the seafloor to the base (0–45.08 mbsf; Cores 310-M0007B-1R through 34R), and a clear indication of what specific element contributed most to these counts cannot be

made. Resistivity values range from a maximum of 3.38 m at 27.19 mbsf to 1.09 m at 16.31 mbsf. The temperature of the borehole fluid ranges from 26.5° to 27.2°C, pH values are ~8.1, and average electrical conductivity is ~56.3 mS/cm, whereas in Hole M0007B a sharp decrease to values below 49 mS/cm was observed from 29.31 mbsf. This decrease can be attributed to a large cavity and very open framework, which was observed in the acoustic image (ABI40 amplitude) of the borehole wall (ABI40 amplitude; Fig. F78).

Geochemistry

All geochemical pore water data are presented in tables allsitesIW.xls and IWsaturation.xls in “[Supplementary Material](#).”

pH, alkalinity, ammonia, chloride, and sulfate

pH and alkalinity values of Maraa western transect pore waters are essentially that of Tahitian seawater with the exception of the slightly lower pH and alkalinity values found in Hole M0005D samples (Fig. F79A, F79B). Sample 310-M0007B-5R-1, 16 cm, yielded an anomalously high alkalinity of 10.3 mmol/L even by repeated measurements of different dilutions. Ammonia was only detectable in two samples from Hole M0007B (Fig. F79C). Chloride concentrations in Maraa western transect pore waters do not significantly deviate from seawater values, precluding any significant influence of freshwater on interstitial water (IW) geochemistry (Fig. F79D). Sulfate concentrations of all samples are similar to seawater.

Mg, K, Ca, and Sr

Concentrations of both Mg and K in Maraa western transect pore waters do not vary significantly from seawater concentrations (Fig. F79E, F79F). Most of those samples exhibit seawater-like Ca concentrations except those of Hole M0007B, which are slightly depleted (Fig. F79G). Sr concentrations in these pore waters are similar to seawater, apart from significant elevations in Hole M0005D samples (Fig. F79H). This could indicate some aragonite dissolution occurring in Hole M0005D material, resulting from the lower pH values of Hole M0005D pore waters.

Li, P, Mn, Fe, and Ba

Li is enriched relative to seawater in IW samples from the shallowest depths at Maraa western transect sites (Fig. F79I). This indicates a sedimentary

source of Li to the pore waters at these depths. Similarly, P, Mn, and Ba concentrations are elevated in the uppermost IW samples (Fig. F79J–F79L), suggesting all these trace elements share a common source at these depths in that area. This source may result from the dissolution of phosphatic-iron-manganese crusts associated with microbialites (Camoin et al., 2006). Fe was only detected in Section 310-M0006A-3R-1 (1.32 mbsf; 82.90 mbsl). In contrast, at Maraa western transect sites both Mn and Ba display enrichments with no associated changes in the Li or P of these samples (Fig. F79I–F79L). This indicates a separate source for Mn and Ba at depth in the Maraa western transect sections.

References

- Camoin, G., Cabioch, G., Eisenhauer, A., Braga, J.-C., Hamelin, B, and Lericolais, G., 2006. Environmental significance of microbialites in reef environments during the last deglaciation. *Sediment. Geol.*, 185(3–4):277–295. doi:10.1016/j.sedgeo.2005.12.018
- Raymer, L.L., Hunt, E.R., and Gardner, J.S., 1980. An improved sonic transit time-to-porosity transform. *Trans. SPWLA 21st Annu. Log. Symp.*, Pap. P.
- Wyllie, M.R.J., Gregory, A.R., and Gardner, L.W., 1956. Elastic wave velocities in heterogeneous and porous media. *Geophysics*, 21(1):41–70. doi:10.1190/1.1438217

Publication: 4 March 2007

MS 310-105

Figure F1. Modern sediment rich in coralline algal crusts (interval 310-M0005E-2M-1, 1–6 cm).



Figure F2. Modern sediment dominated by rhodoliths and *Halimeda* segments (interval 310-M0007A-1R-1, 8–16 cm).

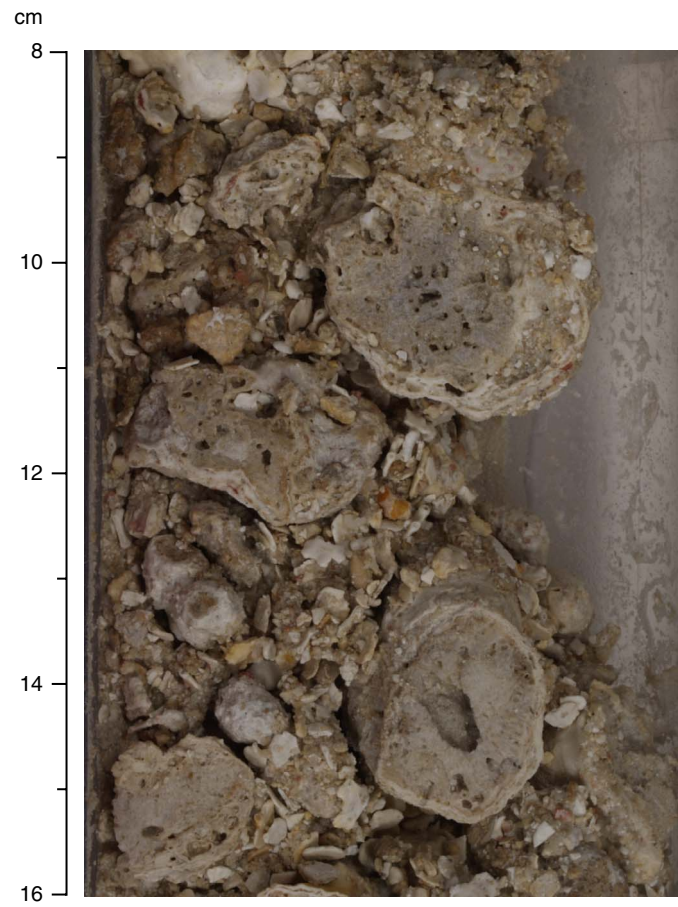


Figure F3. Skeletal sand (Unit I; interval 310-M0007B-18R-1, 0–15 cm).

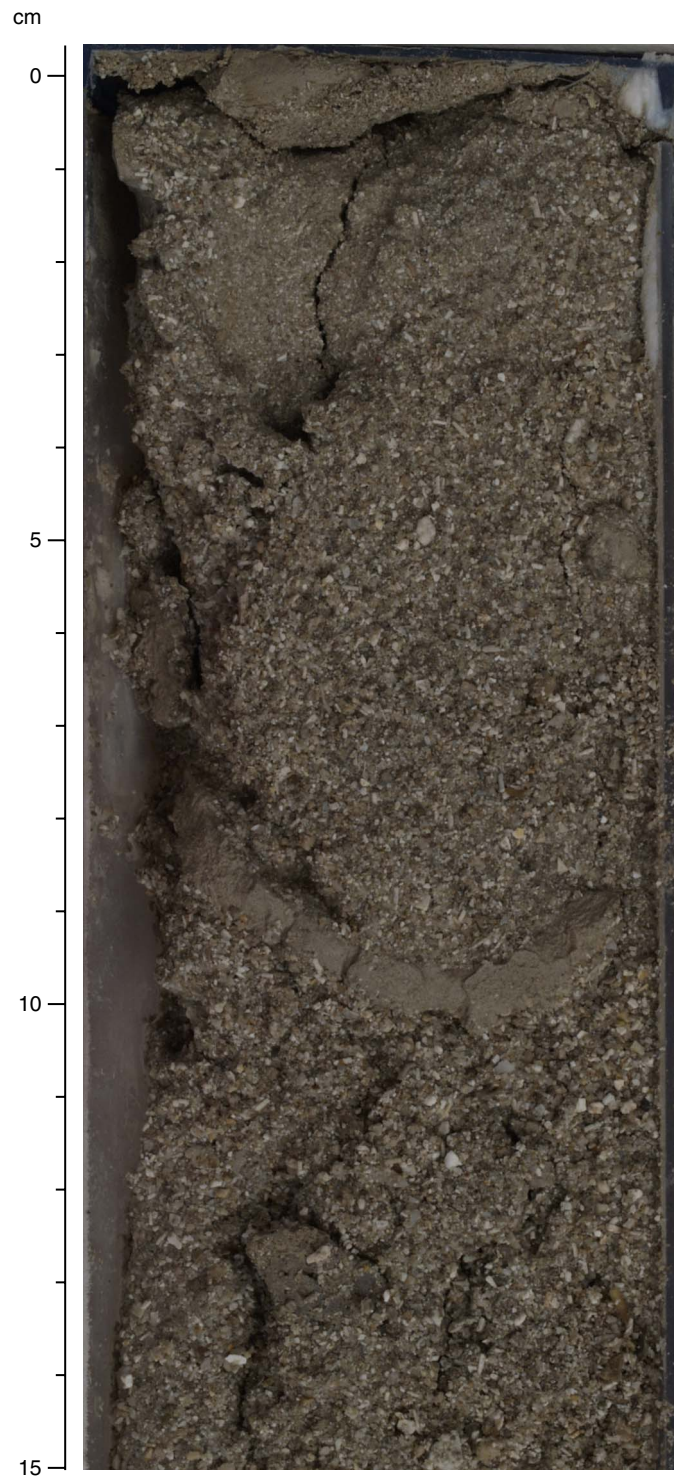


Figure F4. Grainstone rich in *Halimeda* segments (Unit I; interval 310-M0005C-11R-1, 0–10 cm).

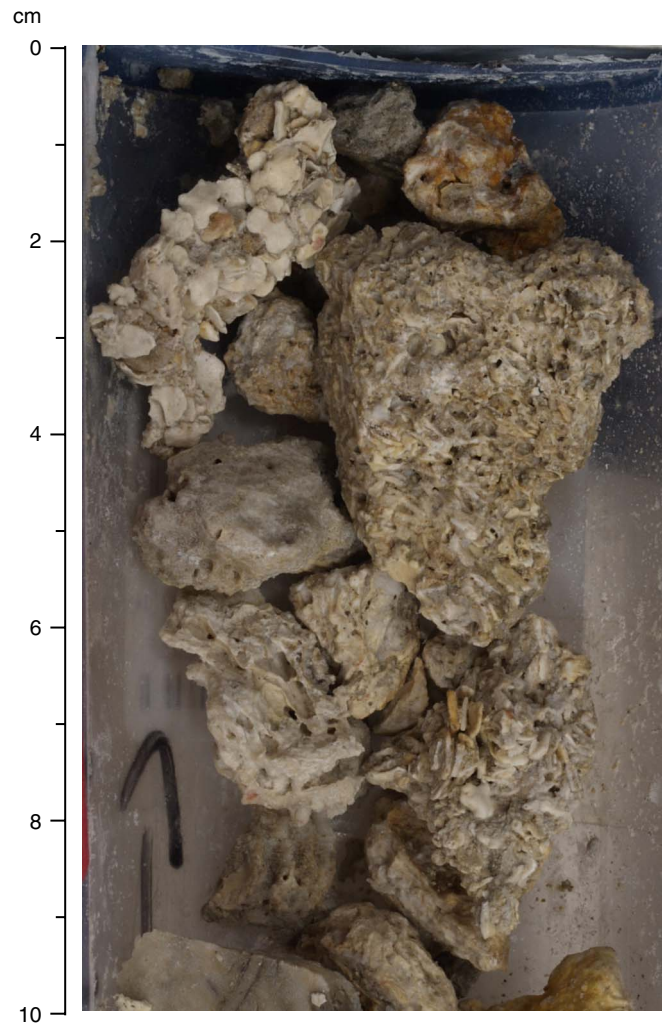


Figure F5. Microbialites represented by laminated fabrics (Unit I; interval 310-M0005A-2R-1, 12–24 cm).

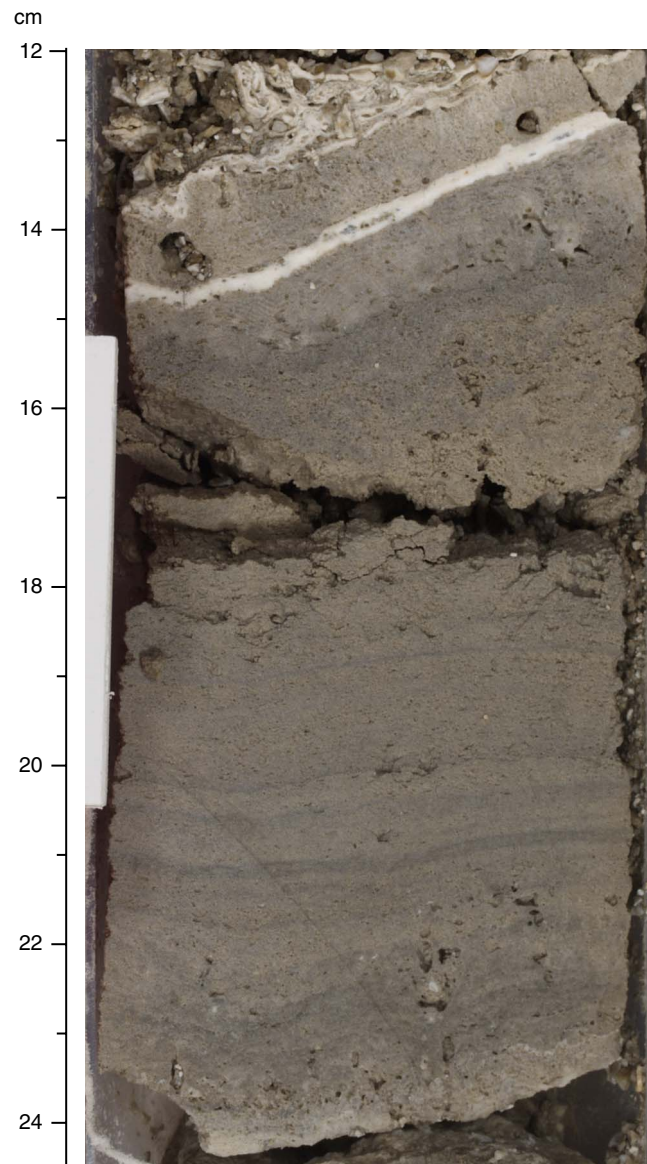


Figure F6. Microbialites represented by dendritic and columnar accretions developed on nongeniculate coralline algal-encrusted coral branches (Unit I; interval 310-M0005B-3R-1, 22–36 cm).

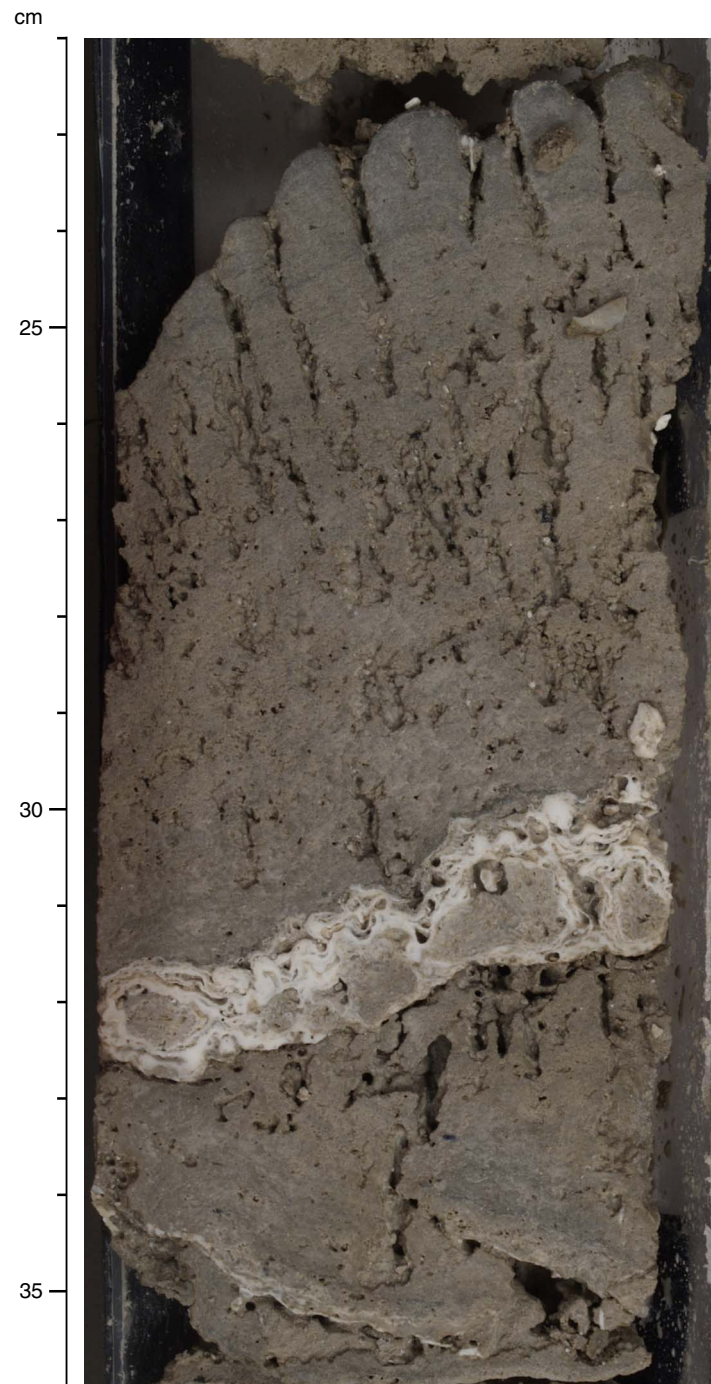


Figure F7. Microbialites represented by laminated fabrics and thrombotic masses (Unit I; interval 310-M0005C-6R-2, 2–16 cm).

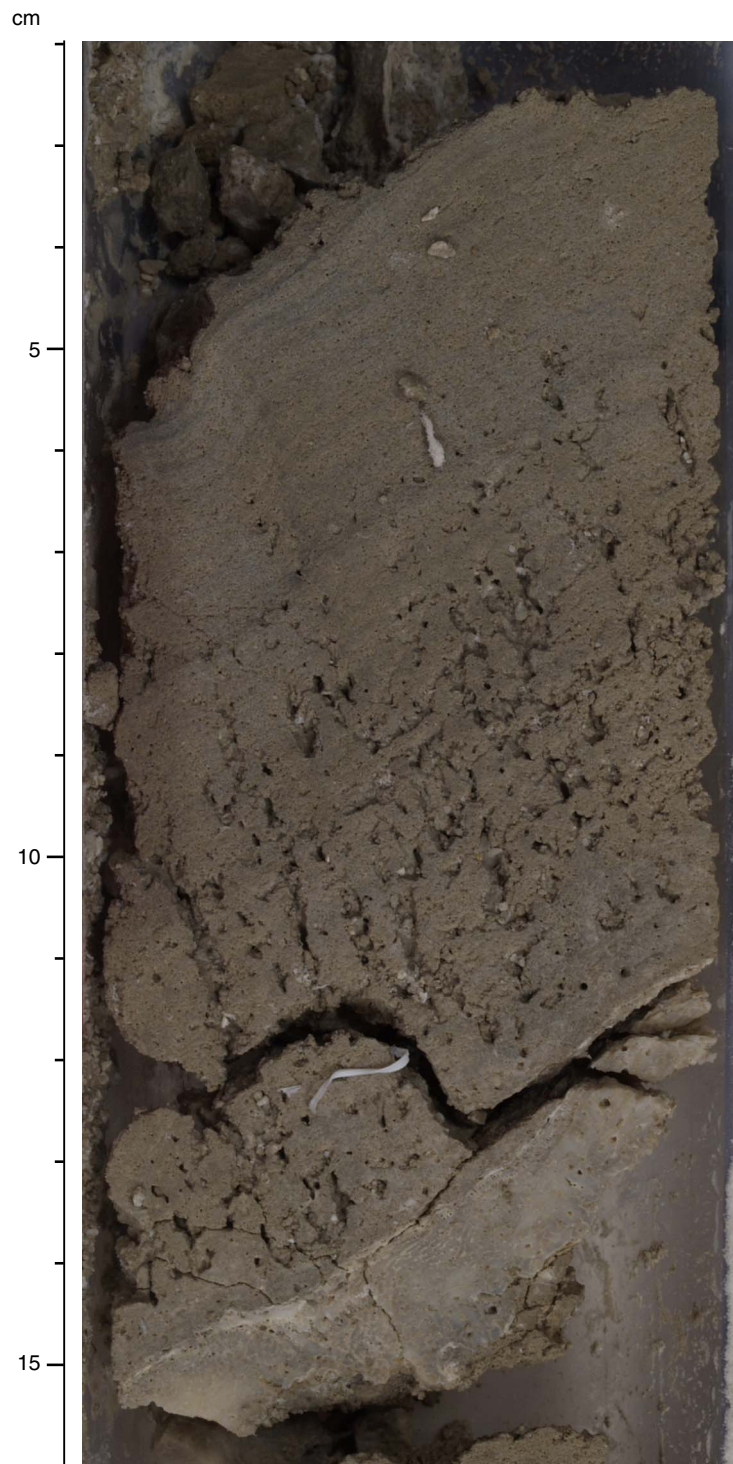


Figure F8. Laminated to columnar microbialite (Unit I; interval 310-M0005C-8R-1, 65–79 cm). Note the accumulation of *Halimeda* segments between columnar microbial accretions.

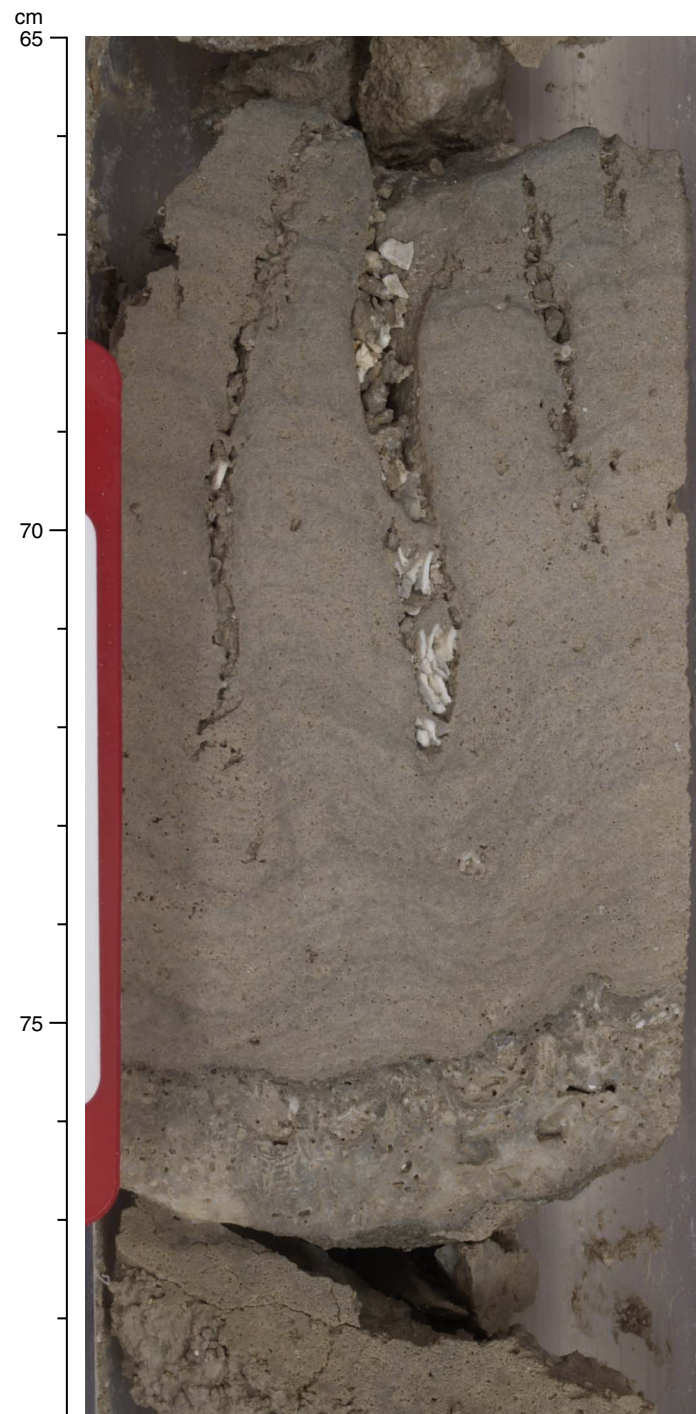


Figure F9. Laminated to dendritic microbialites that represent the last shape of encrustation of coralgall framework (Unit I; interval 310-M0005C-9R-1, 115–134 cm).

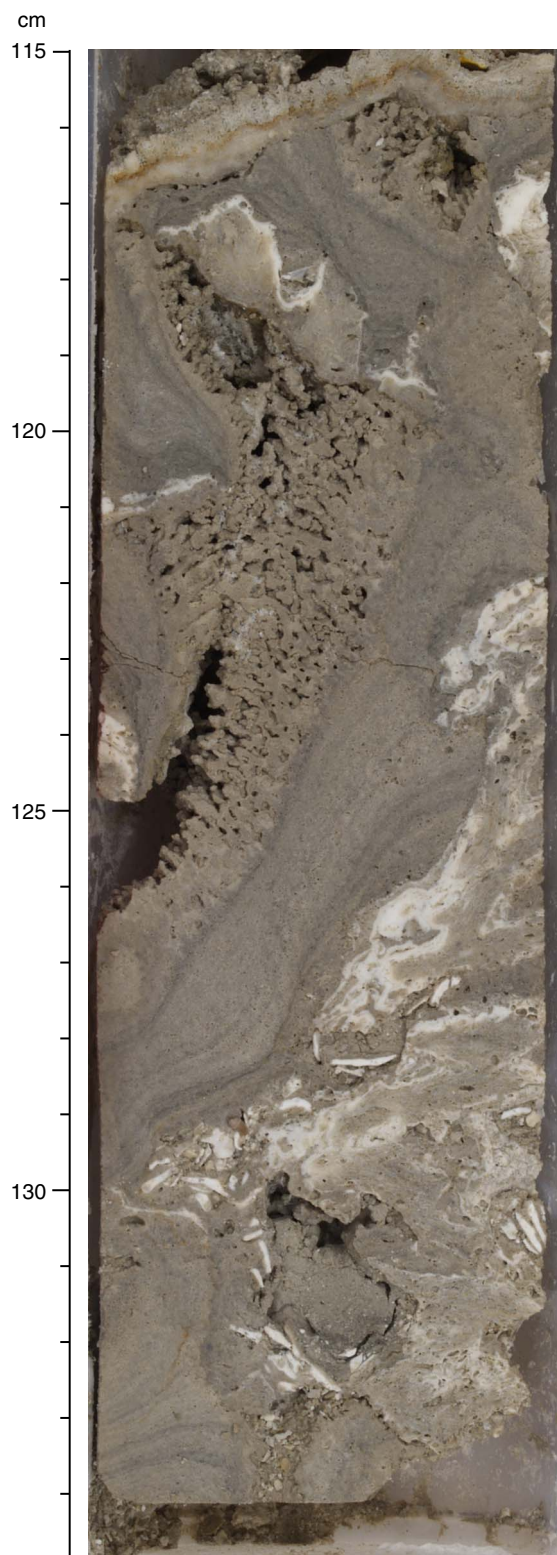


Figure F10. Encrusting colonies of *Montipora*, *Psammocora*, and agariciids and interfingered encrusting coralline algae (Subunit IA; interval 310-M0005A-1R-1, 48–59 cm). Note bioerosion in coral colonies.

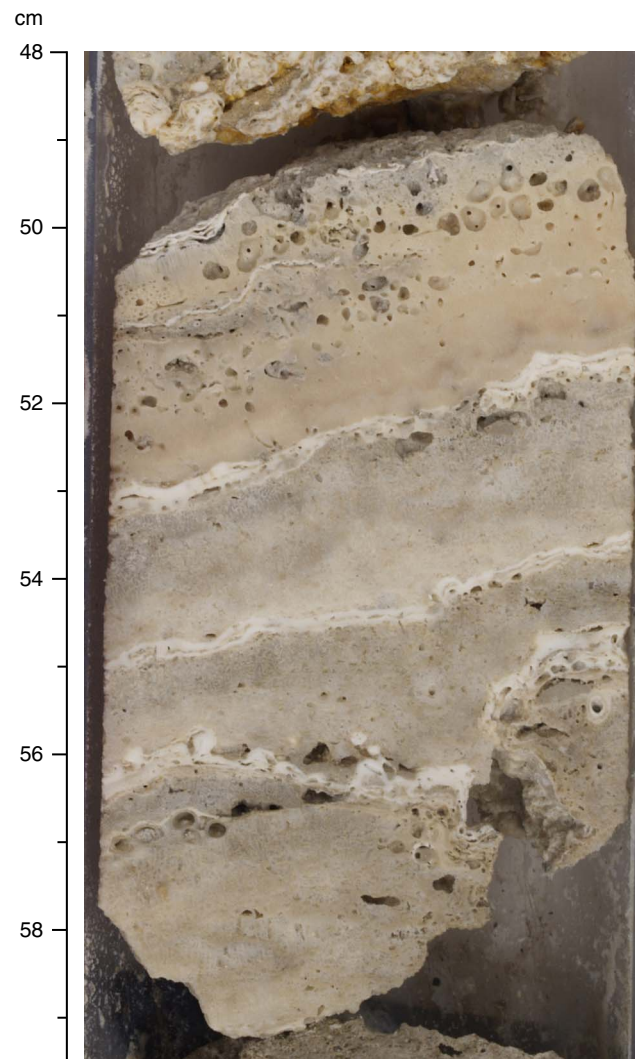


Figure F11. Encrusting colonies of *Porites* interlayered with thin coralline algal crusts (Subunit IA; interval 310-M0005B-1R-1, 36–46 cm). Note the bioerosion in coral colonies.

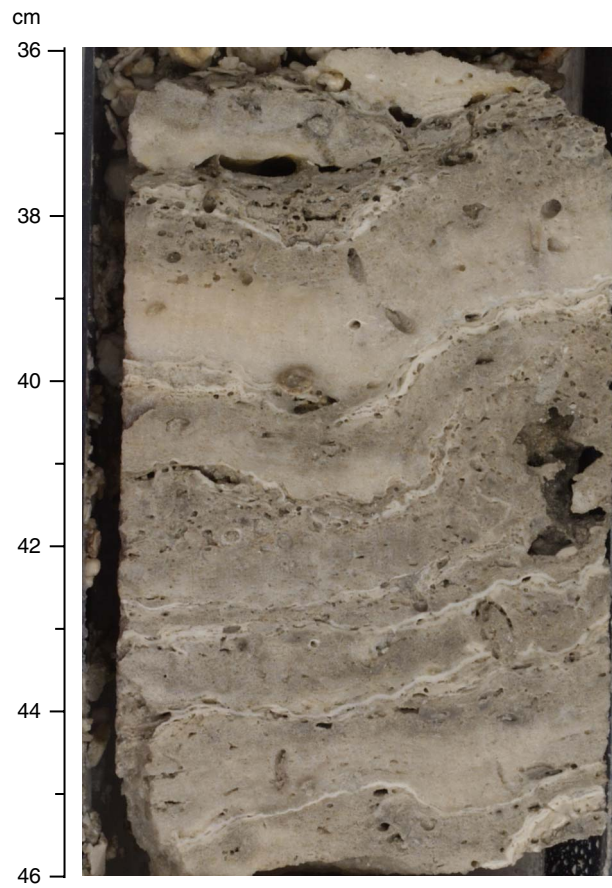


Figure F12. Encrusting colonies of *Porites* and *Montastrea* with interlayered thin crusts of coralline algae (Sub-unit IA; interval 310-M0005C-6R-CC, 9–33 cm).

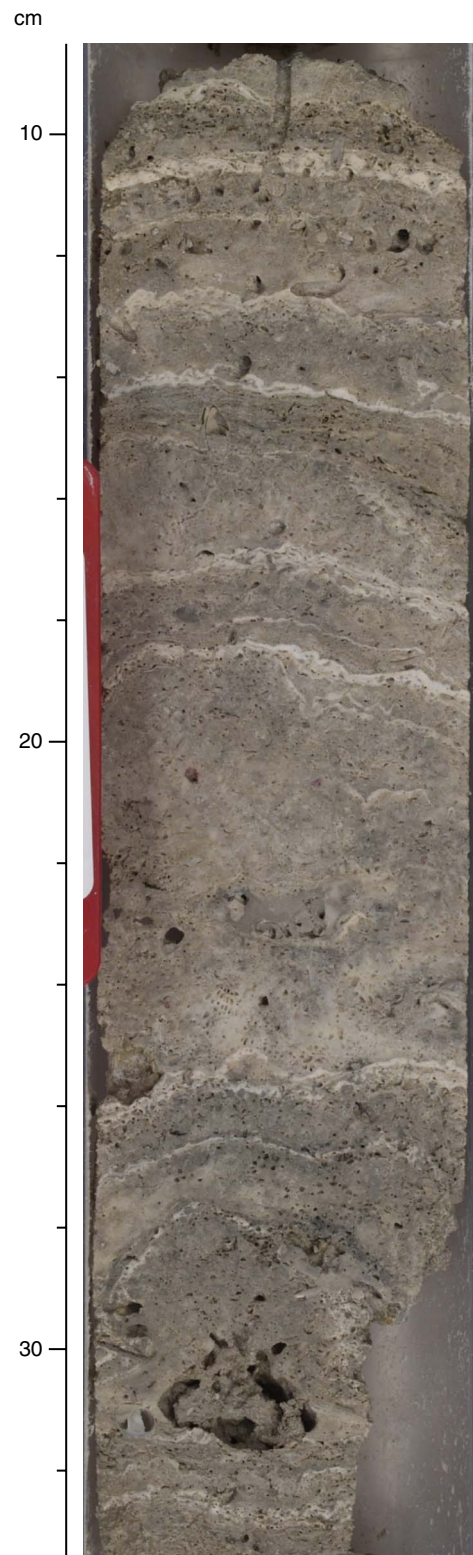


Figure F13. Encrusting colonies of *Porites* and agariciids interlayered with multiple thin coralline algal crusts (Subunit IA; interval 310-M0005C-3R-1, 11–23 cm). Corals are extensively bioeroded.

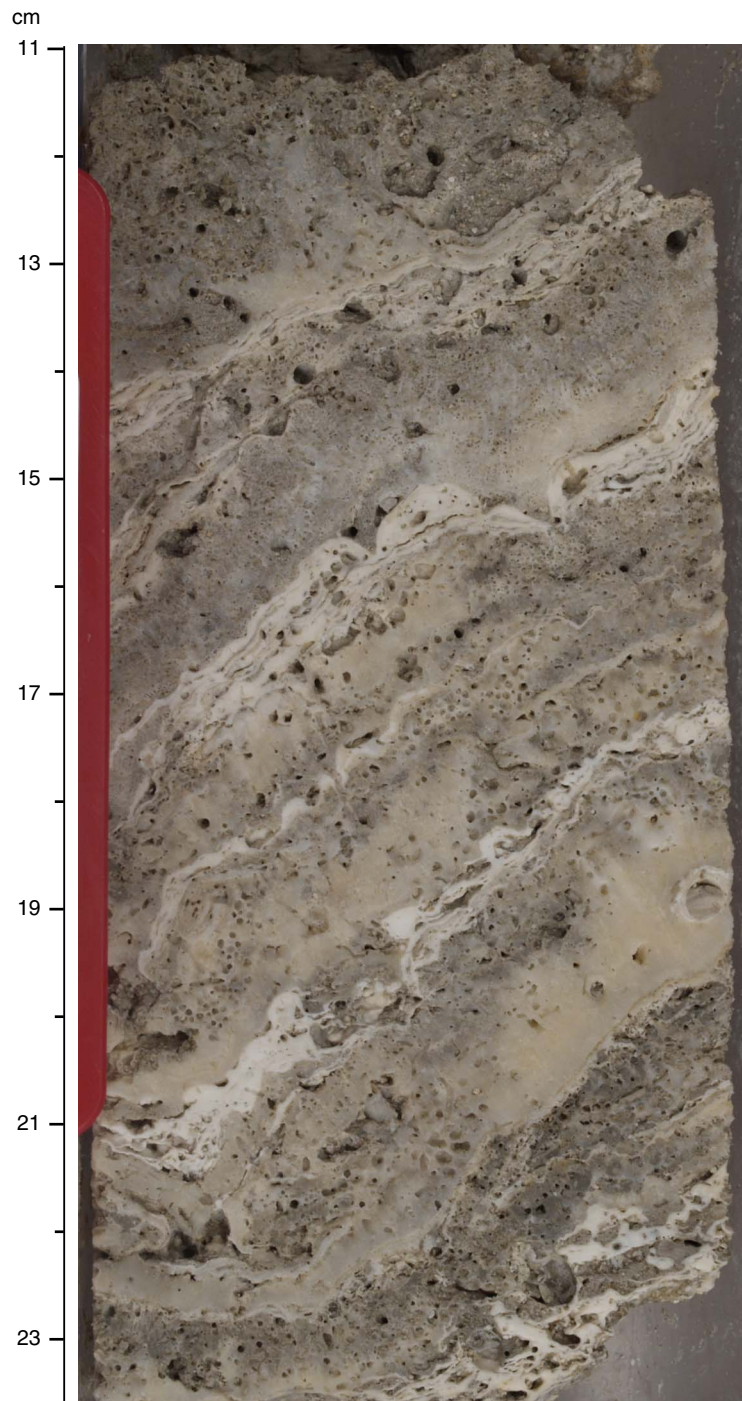


Figure F14. Encrusting colonies of *Montipora* and *Pavona* interlayered with coralline algal crusts (Subunit IA; interval 310-M0007A-6R-1, 20–34 cm).

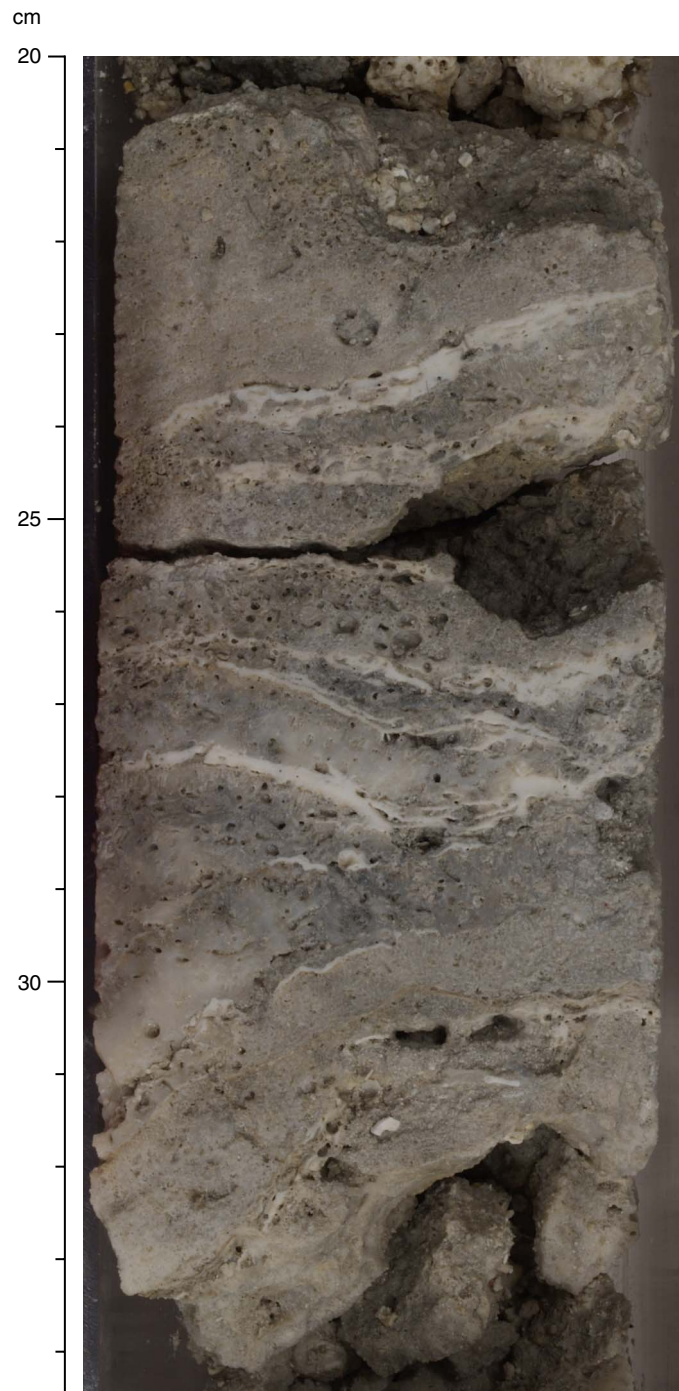


Figure F15. Encrusting colonies of faviids covered with multiple thin crusts of coralline algae and thrombolitic microbialite masses (Subunit IA; interval 310-M0007A-9R-CC, 1–11 cm).



Figure F16. Encrusting colonies of *Montipora*, faviids, and agariciids interlayered with thin coralline algal crusts (Subunit IA; interval 310-M0007A-8R-1, 51–70 cm). Note intense boring in the lower part.

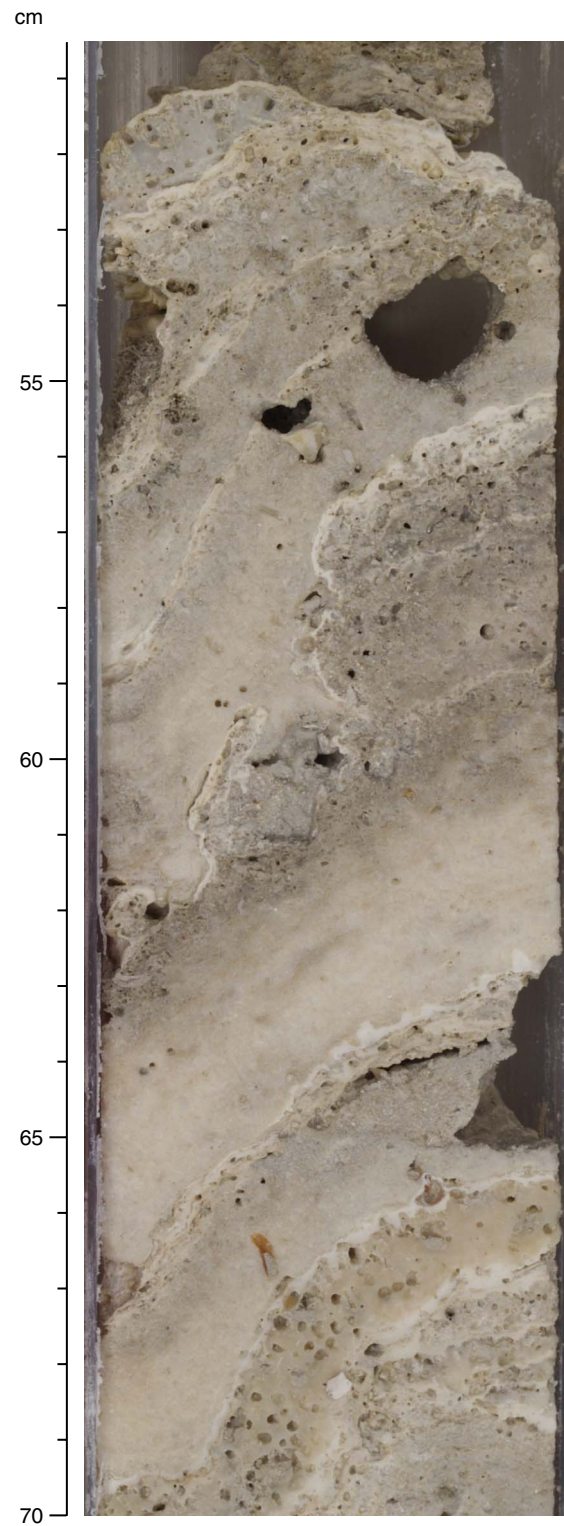


Figure F17. Encrusting colonies of *Montipora* and agariciids and a massive colony of *Astreopora* (Subunit IA; interval 310-M0007A-8R-1, 72–84 cm).

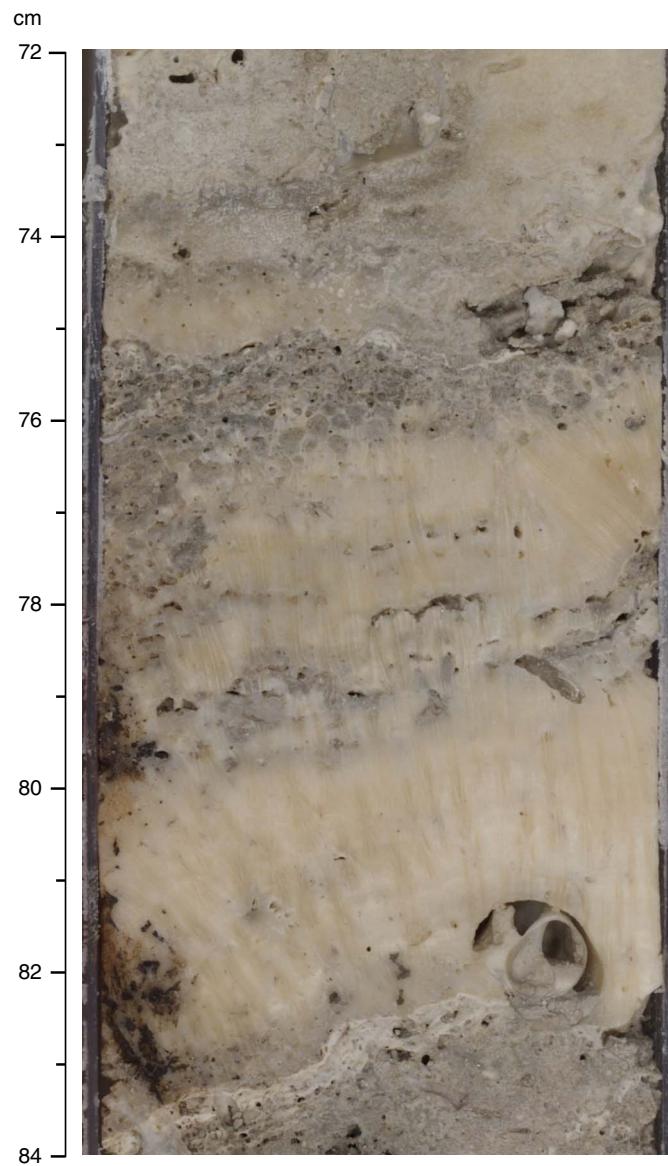


Figure F18. Encrusting colonies of *Porites* and agariciids interlayered with coralline algal crusts (Subunit IA; interval 310-M0007A-9R-1, 23–45 cm).



Figure F19. Robust branching colony of *Pocillopora* encrusted with thrombolitic microbialite masses (Subunit IA; interval 310-M0007A-15R-1, 30–45 cm).

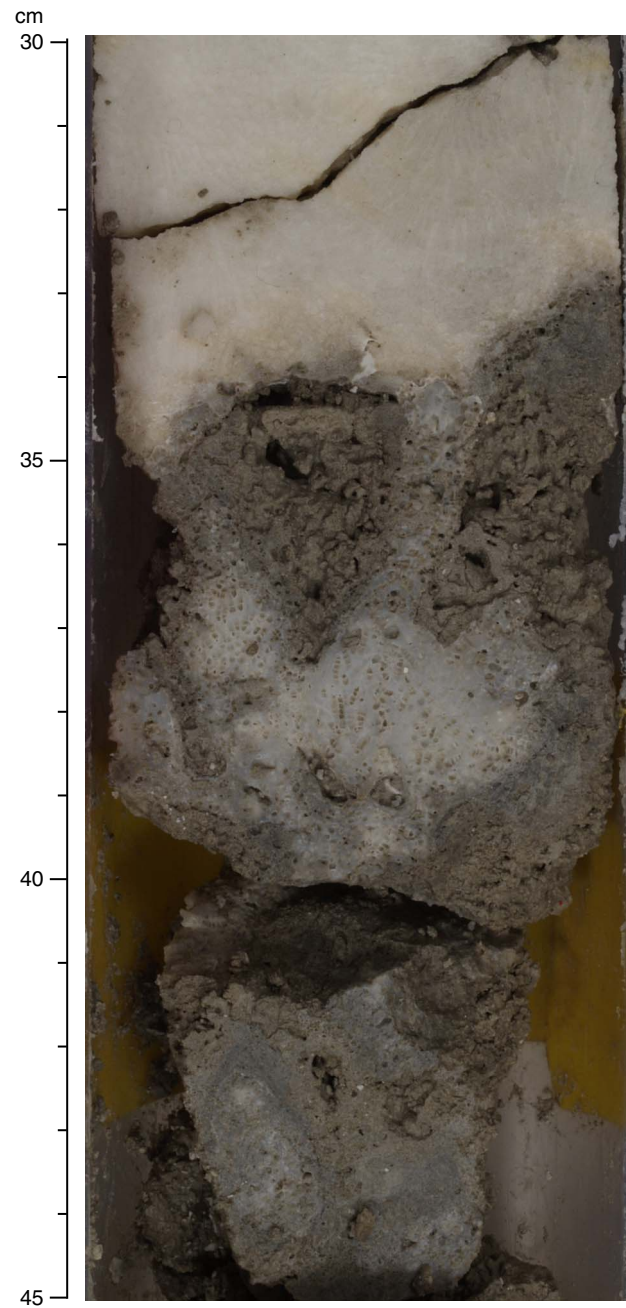


Figure F20. Massive colony of *Porites* with a thin crust of coralline algae between 24 and 25 cm (Subunit IA; interval 310-M0007A-7R-1, 18–30 cm).

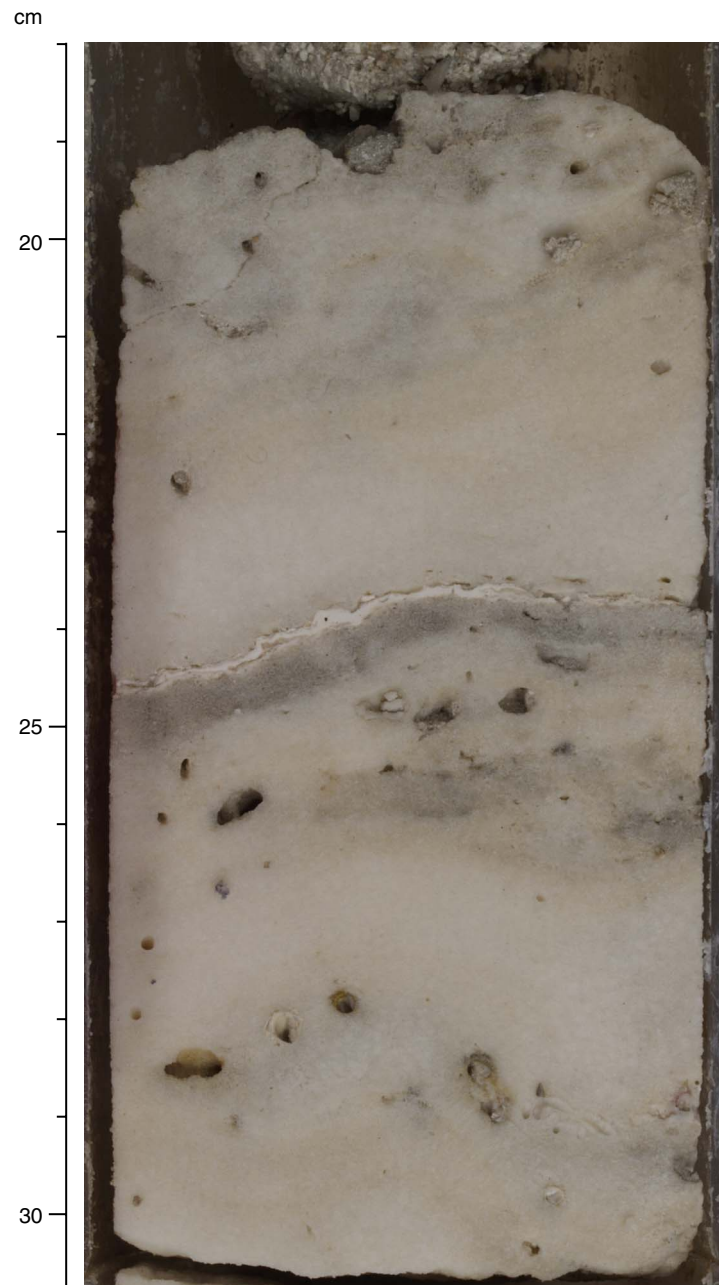


Figure F21. Tabular *Acropora* and encrusting *Porites* colonies (Subunit IB; interval 310-M0005B-6R-1, 9–34 cm). Note thick coralline algal crusts. Last stage of encrustation with laminated microbialites.

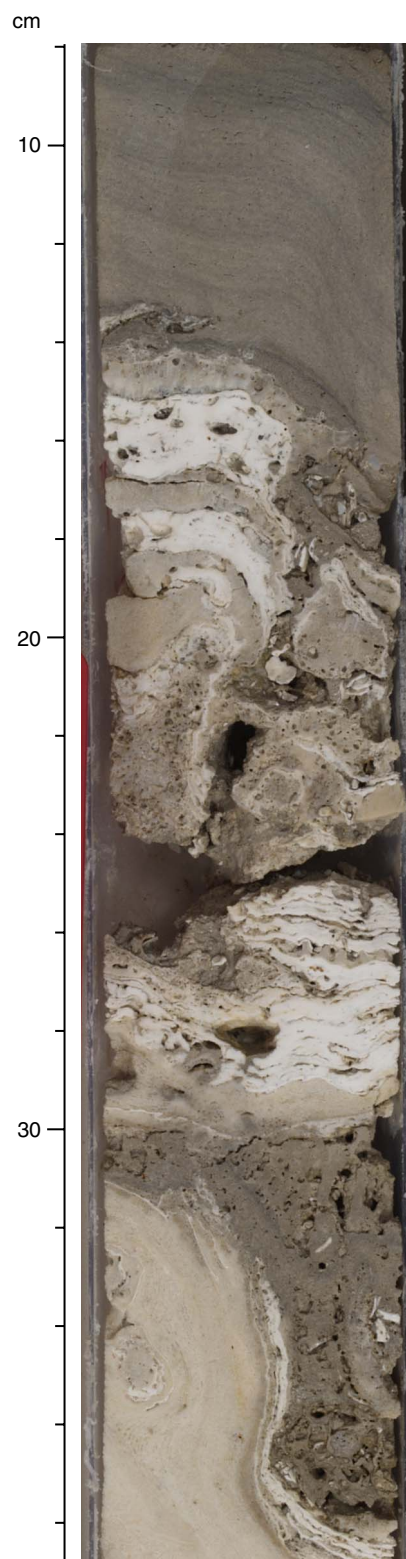


Figure F22. Branching colonies of *Pavona* encrusted with microbialites (Subunit IB; interval 310-M0007C-22R-1, 10–26 cm). Primary cavities are partially filled with skeletal sand rich in *Halimeda* segments.

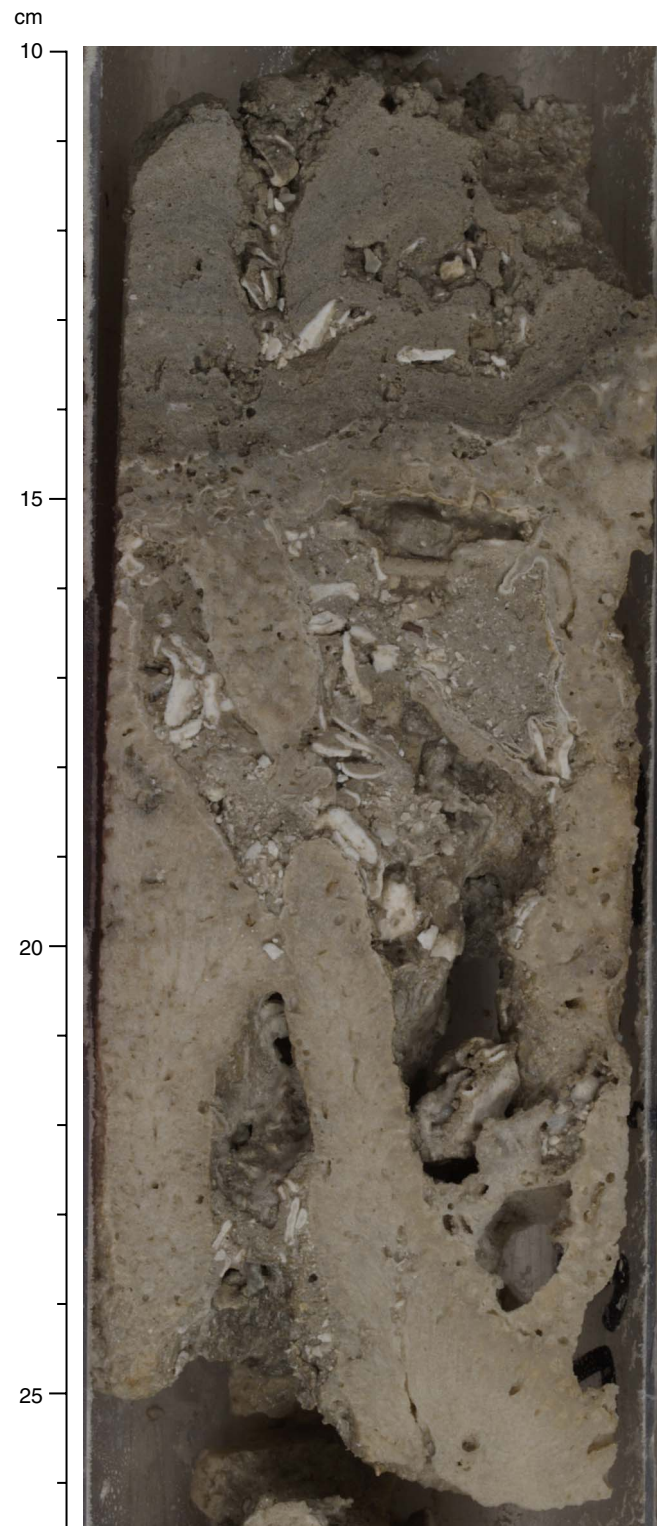


Figure F23. Robust branching colonies of *Pocillopora* with coralline algal crusts on tips and subsequent microbial encrustations (Subunit 1B; interval 310-M0005B-4R-1, 19–41 cm).

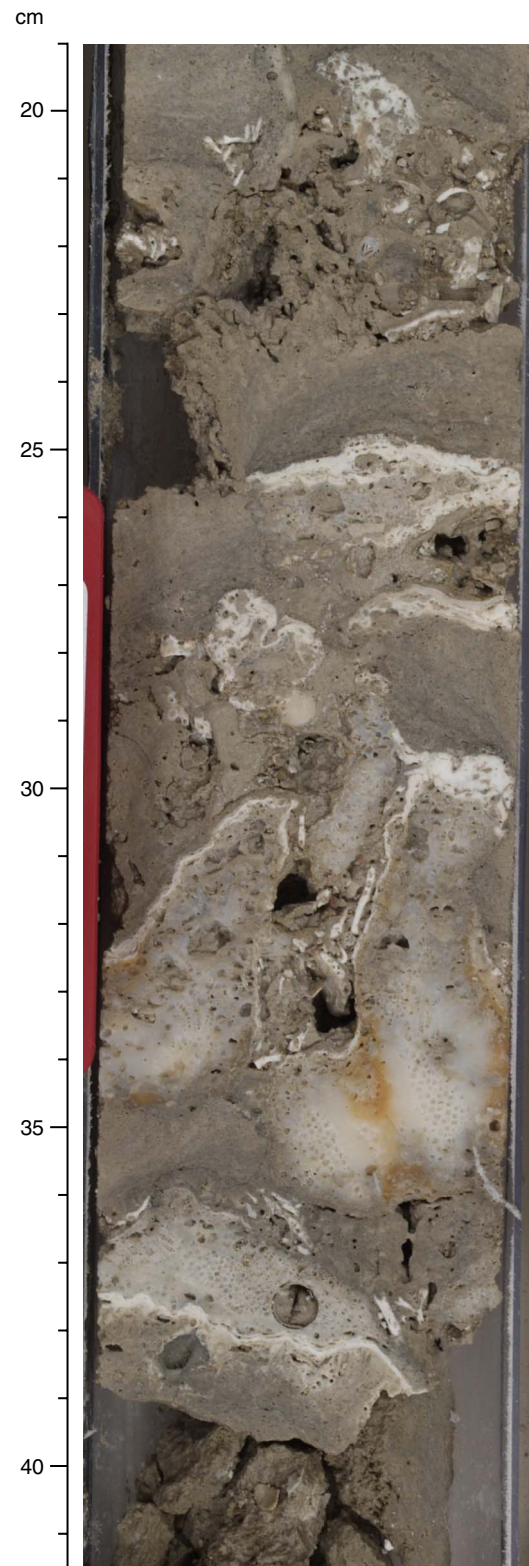


Figure F24. Tips of robust branching colonies of *Pocillopora* encrusted with coralline algal crusts (Subunit IB; interval 310-M0005C-8R-1, 38–62 cm). Coarse skeletal sand fills primary voids.



Figure F25. Tabular colony of *Acropora* encrusted with coralline algae and subsequent laminated microbialites (Subunit IB; interval 310-M0005C-11R-1, 48–62 cm).



Figure F26. Tabular colony of *Acropora* (Subunit IB; interval 310-M0005C-13R-1, 64–85 cm). Primary voids in the reef framework are partly infilled with *Halimeda*-rich sediment and laminated microbialites.

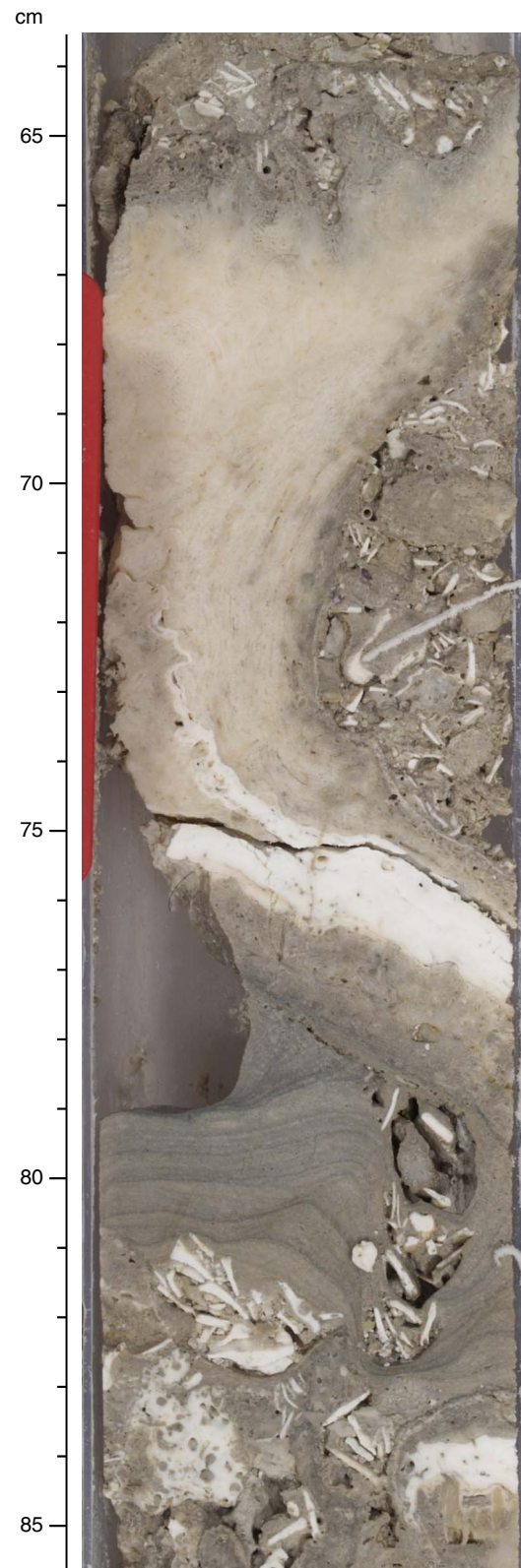


Figure F27. Robust branching colony of *Pocillopora* encrusted with laminated microbialites (Subunit IB; interval 310-M0007A-30R-1, 7–20 cm).

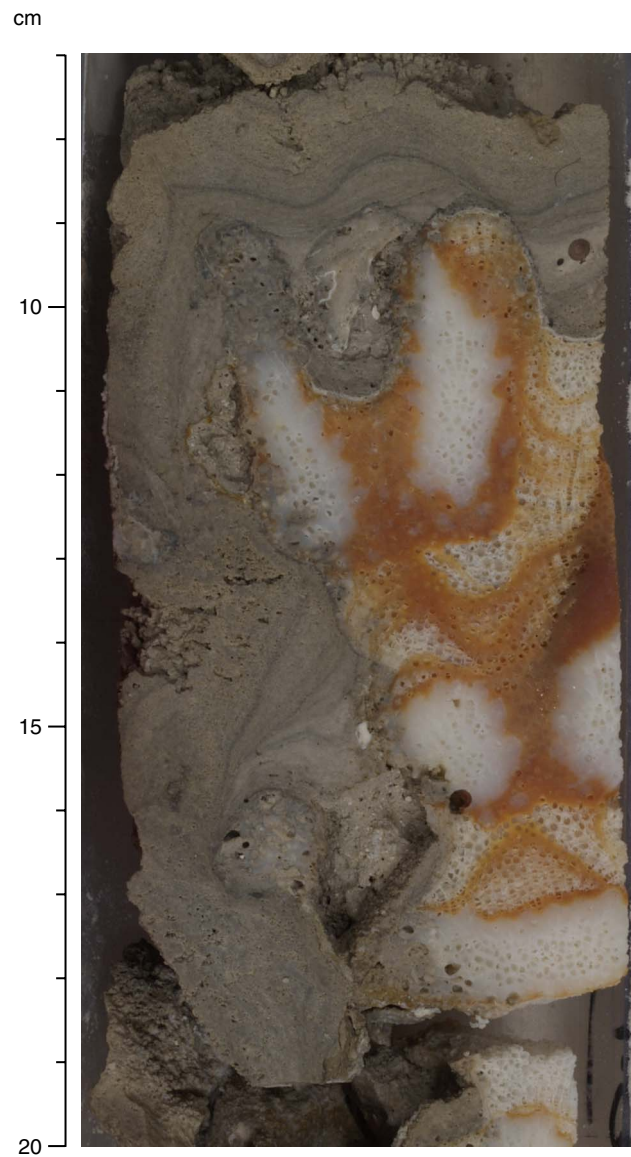


Figure F28. Robust branching colonies of *Pocillopora*. Upper surfaces of colonies are encrusted with thick crusts of coralline algae and subsequent laminated to thrombolitic microbialites (Subunit IB; interval 310-M0007A-31R-1, 45–65 cm). *Halimeda* segments occur in primary pore spaces.

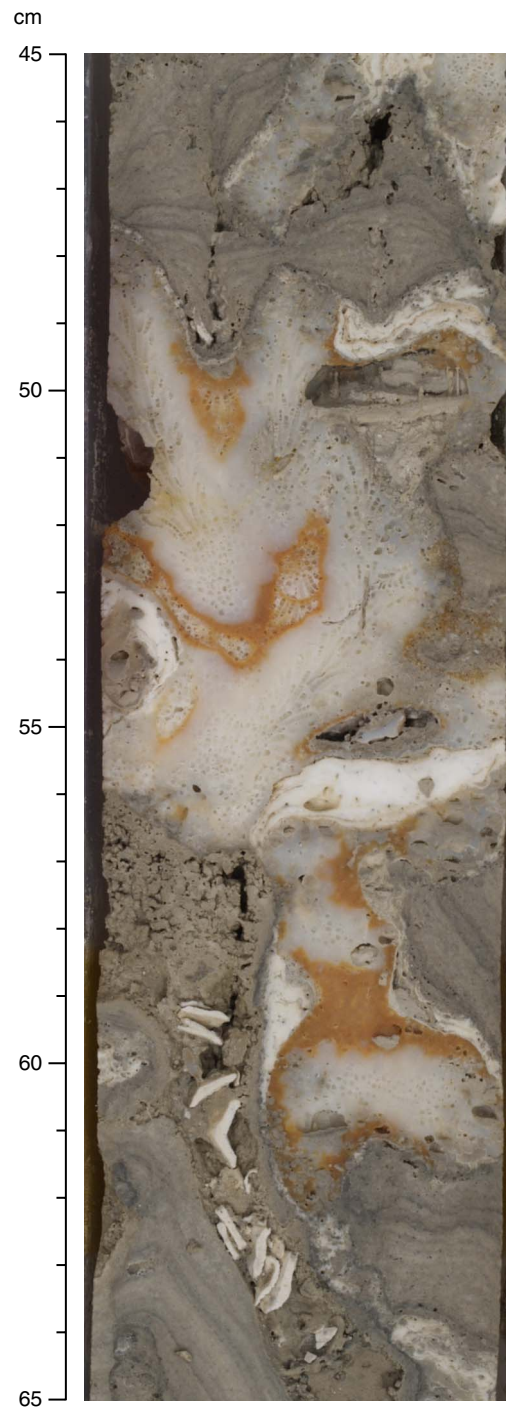


Figure F29. Tabular colony of *Acropora* with thick crusts of coralline algae and subsequent laminated microbialites (Subunit IB; interval 310-M0007B-30R-1, 35–56 cm).

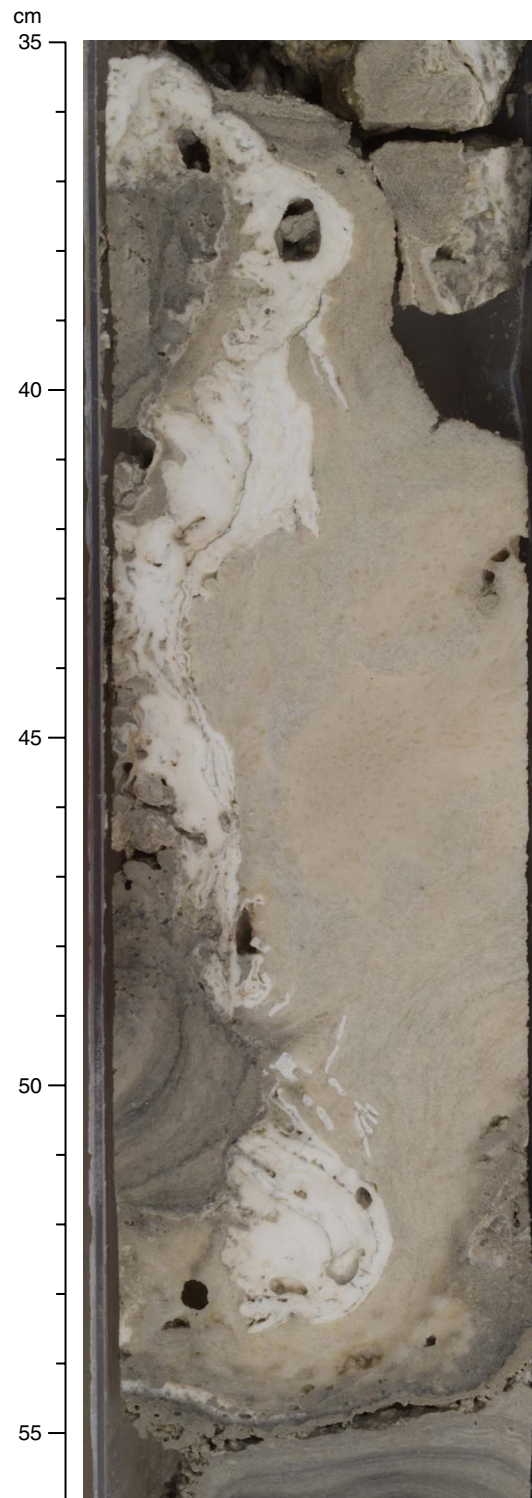


Figure F30. Robust branching colonies of *Pavona* with thick coralline algal crusts on tips and massive *Porites* (Subunit IB; interval 310-M0005B-4R-1, 87–101 cm). Note bioerosion in corals and algae.

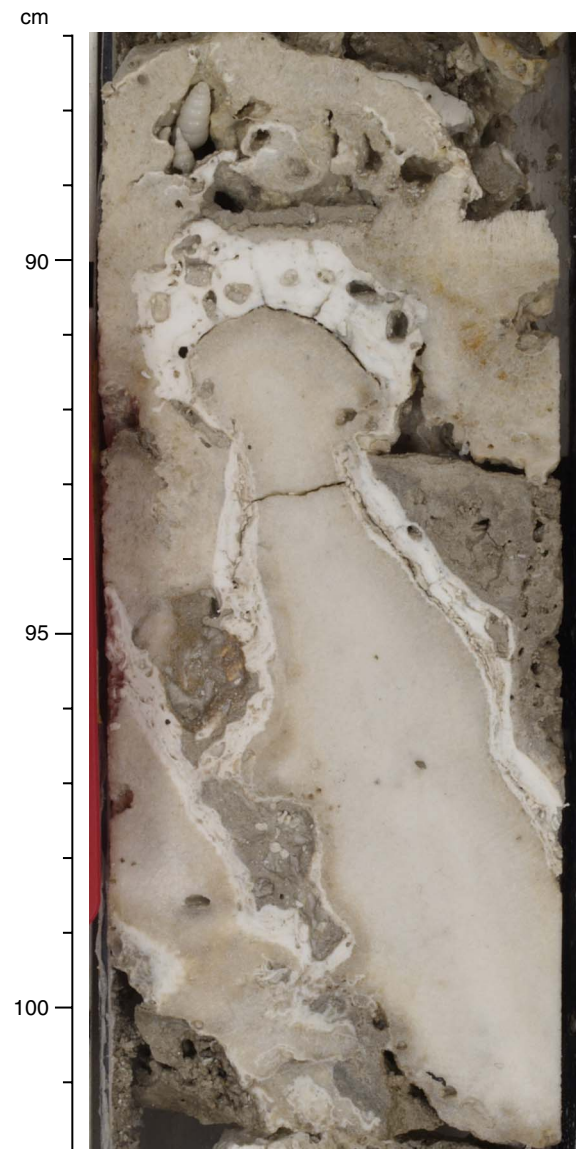


Figure F31. Encrusting and massive colonies of *Porites* with a robust branching colony of *Pocillopora* (Subunit IB; interval 310-M0007B-20R-1, 86–106 cm). Upper coral surfaces are encrusted with coralline algae and columnar microbialites.

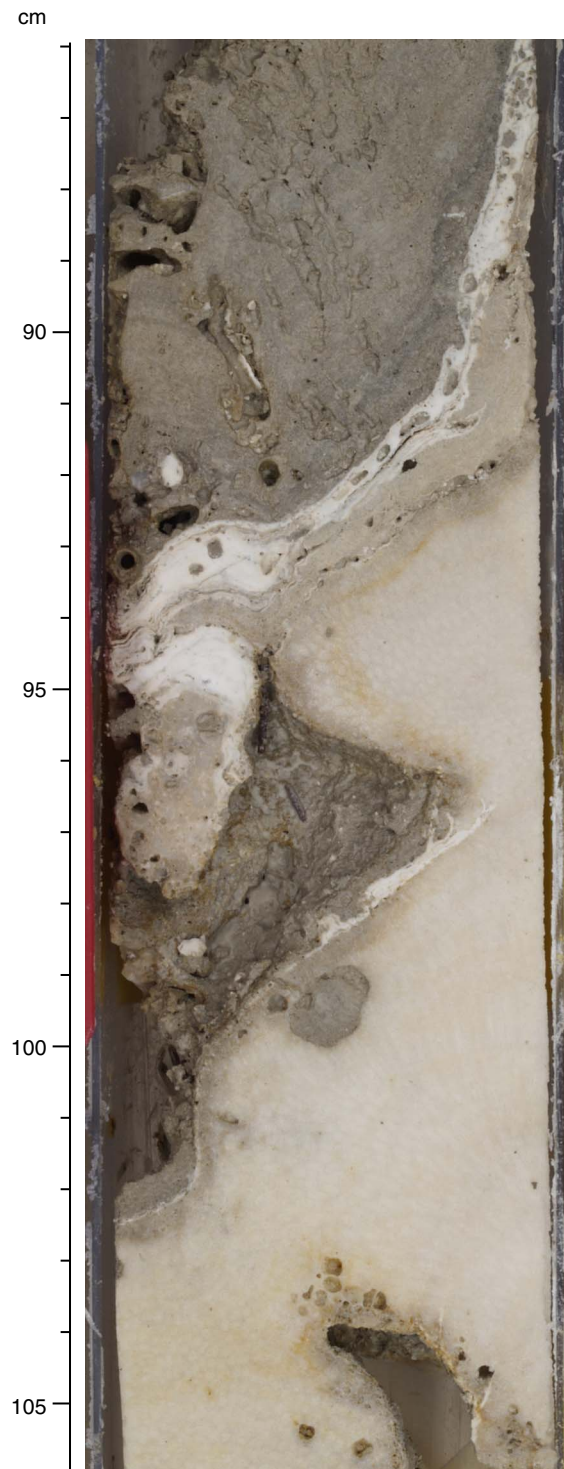


Figure F32. Branching colonies of *Porites* and *Pocillopora* encrusted with coralline algae and subsequent microbialites (Unit I; interval 310-M0005C-10R-1, 33–46 cm).

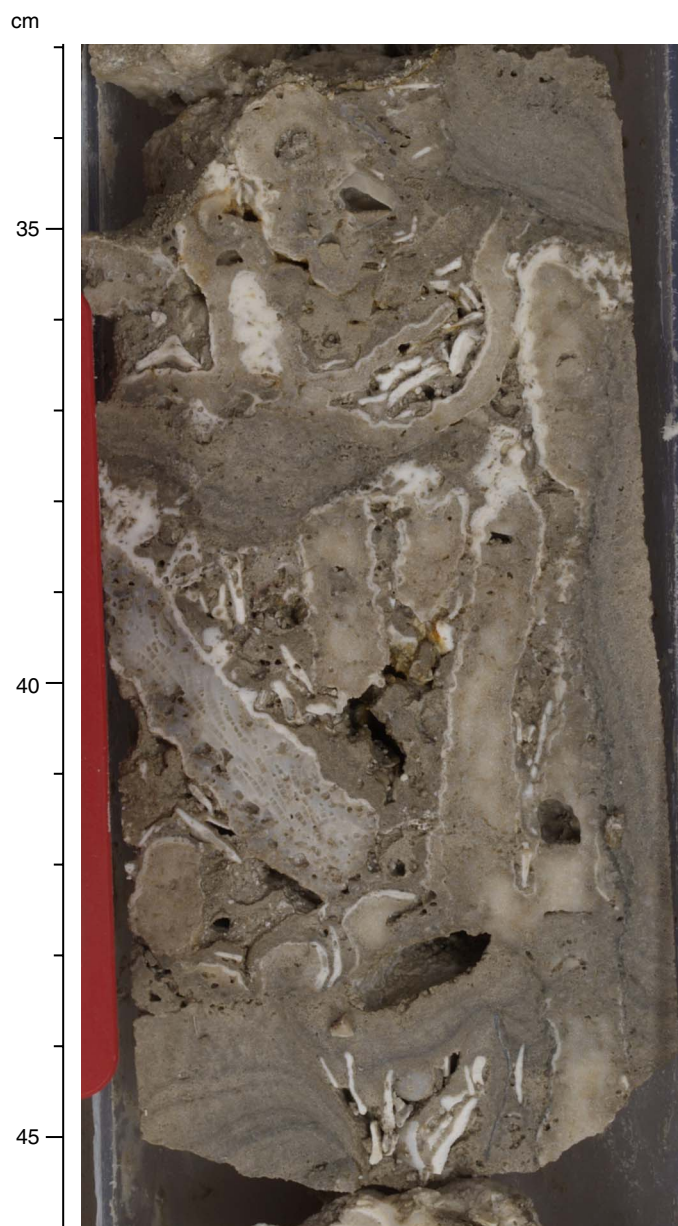


Figure F33. Branching colonies of *Porites* grown on thick layers of coralline algae (Subunit IB; interval 310-M0005C-15R-1, 1–15 cm). Primary vugs in coral framework are infilled with *Halimeda*-rich sediment and laminated microbialites.

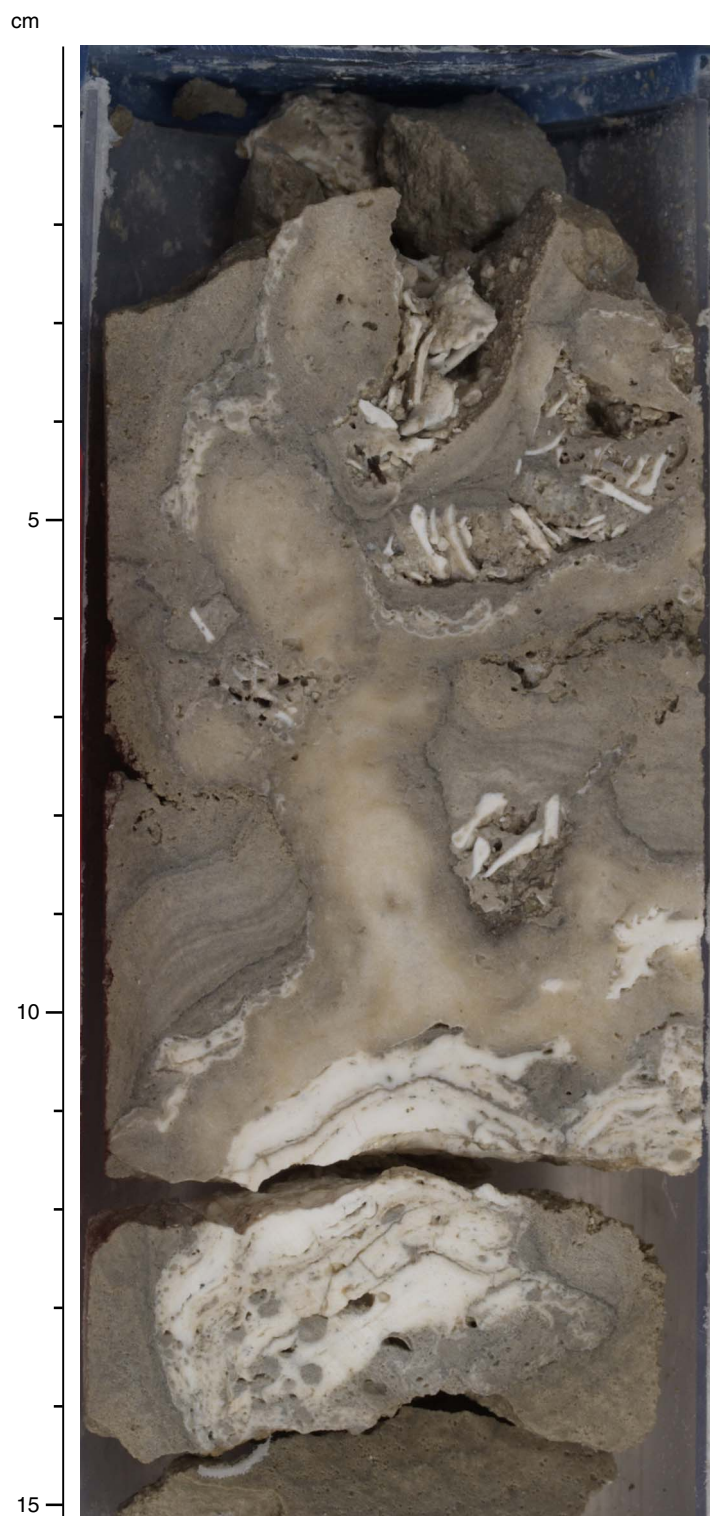


Figure F34. Encrusting colonies of *Porites* with thick crusts of coralline algae (Subunit IB; interval 310-M0007B-34R-CC, 0–20 cm).

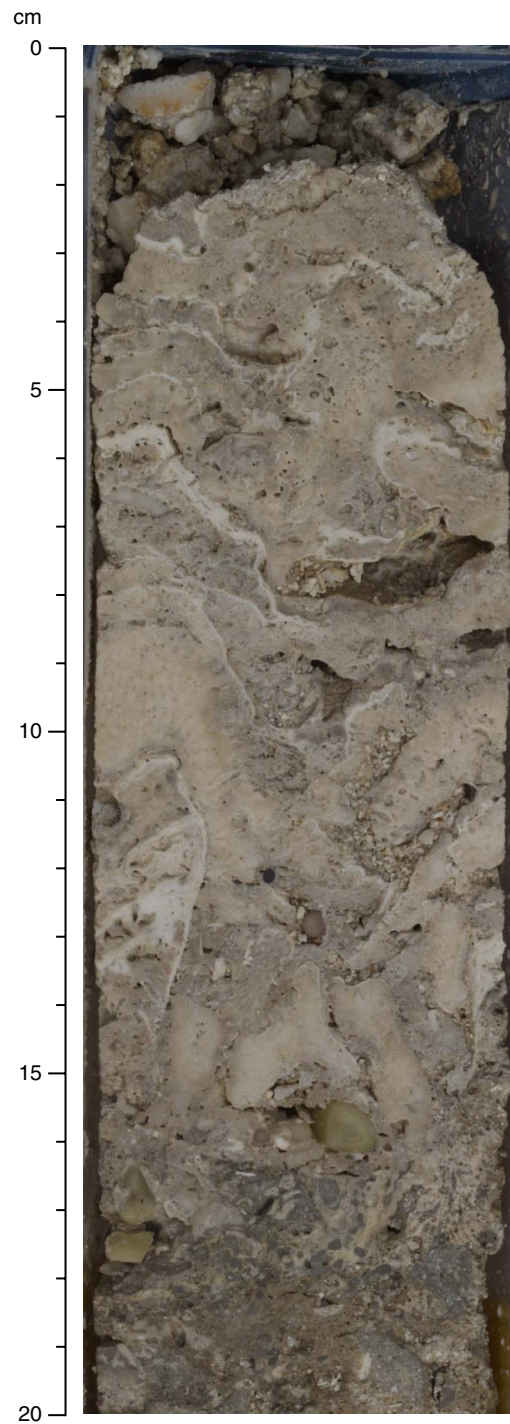


Figure F35. Tabular colonies of *Acropora* and robust branching colonies of *Pocillopora* encrusted with thick multiple crusts of coralline algae (Subunit IA; interval 310-M0007A-35R-1, 90–110 cm). Note bioerosion of algal crusts. The matrix comprises coarse skeletal sediments.

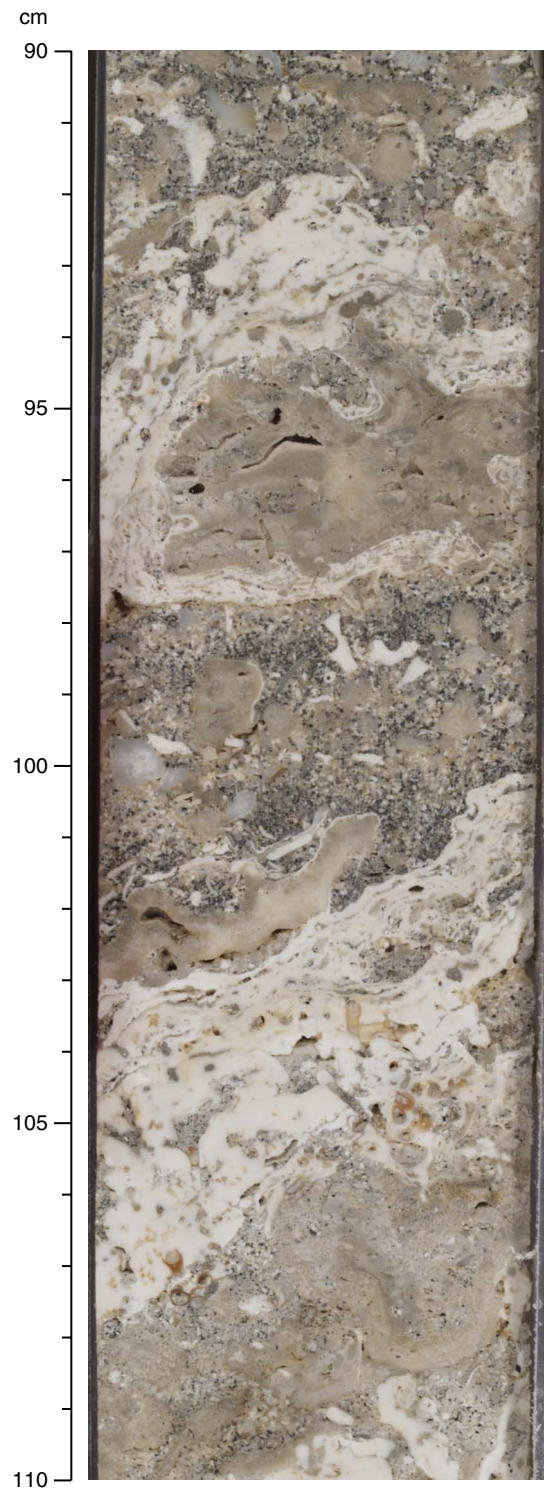


Figure F36. Rudstone/floatstone with large fragments of tabular *Acropora* and volcanic grains (Subunit IA; interval 310-M0007B-35R-1, 82–102 cm).

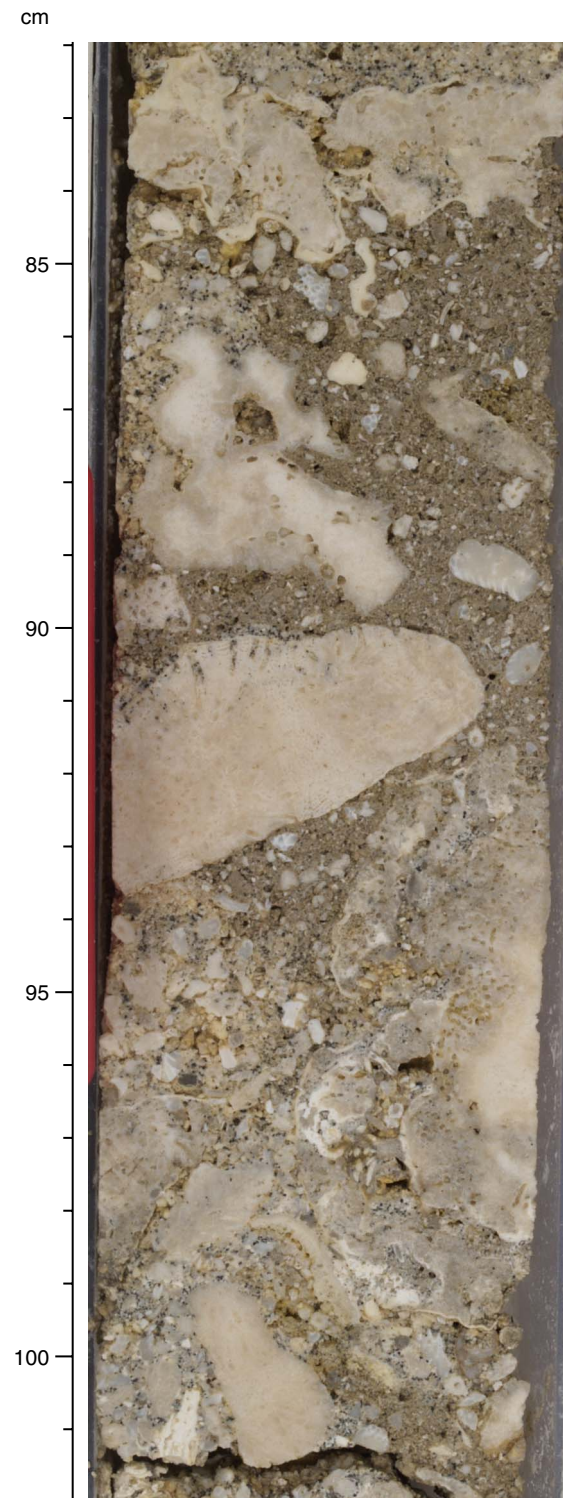


Figure F37. Skeletal rudstone that includes rhodoliths and fragments of branching and encrusting corals (Sub-unit IIB; interval 310-M0005C-11R-1, 42–53 cm).

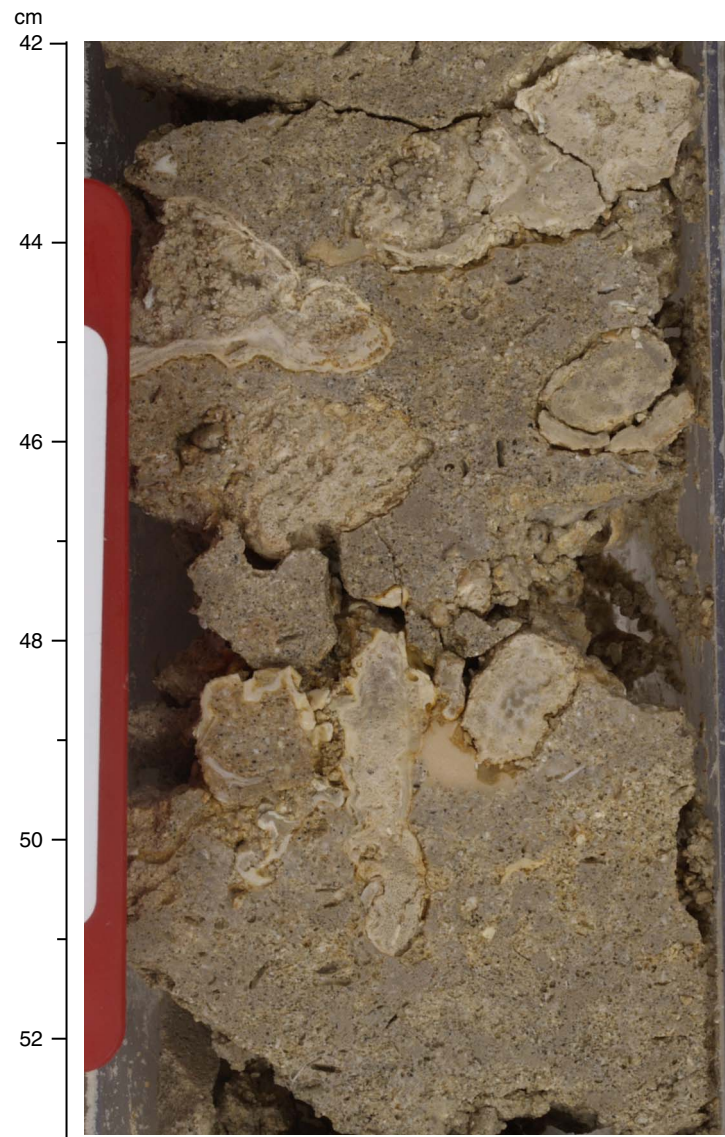


Figure F38. Skeletal rudstone, including rhodoliths and a molluscan shell (Subunit IIB; interval 310-M0005D-10R-1, 8–18 cm). Note dissolution of skeletal components.

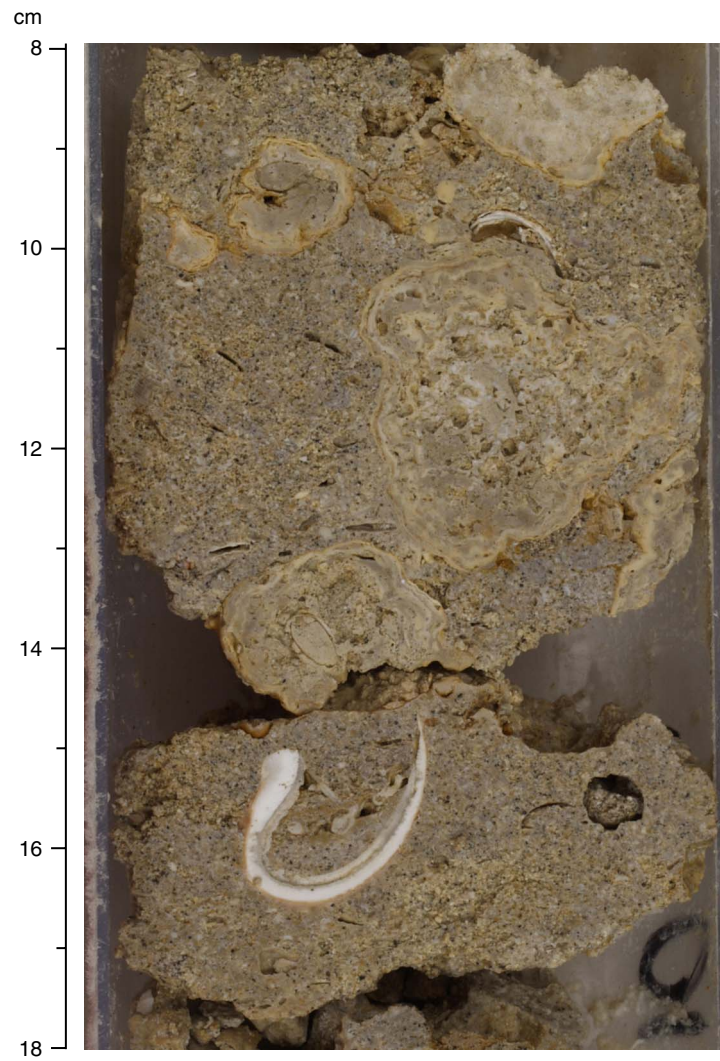


Figure F39. Skeletal rudstone with rhodoliths (Subunit IIB; interval 310-M0005D-10R-1, 68–76 cm).



Figure F40. Skeletal rudstone with rhodoliths (Subunit IIB; interval 310-M0005D-15R-2, 7–16 cm).

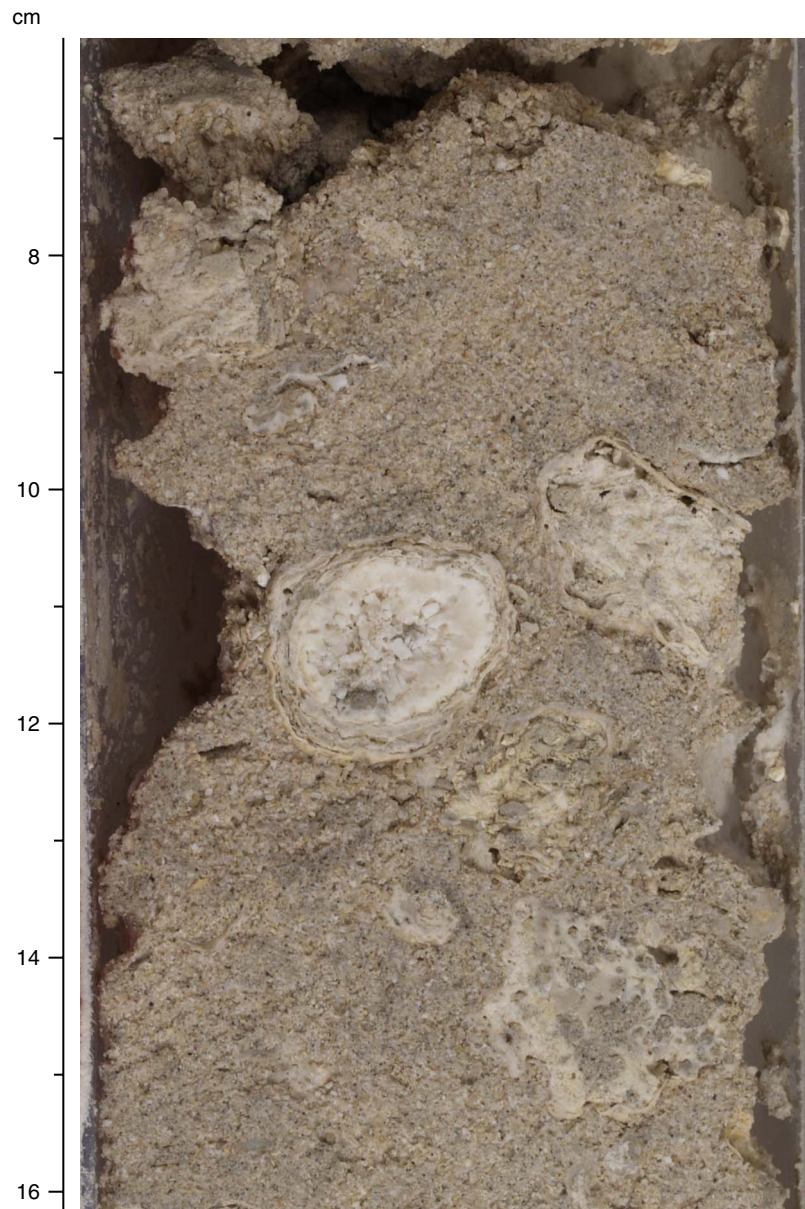


Figure F41. Skeletal floatstone composed of molluscan shells and *Halimeda* segments (Subunit IIB; interval 310-M0005D-16R-1, 2–10 cm).

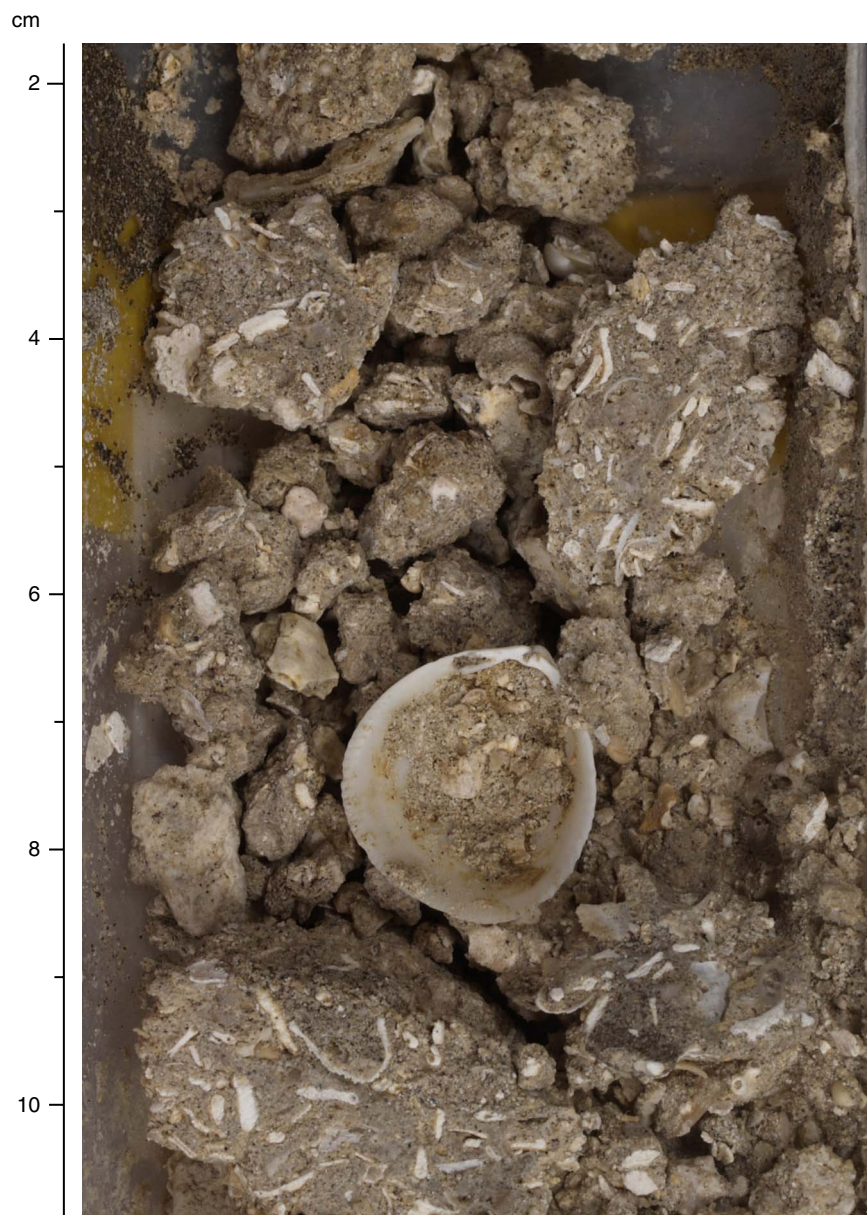


Figure F42. Volcaniclastic silt to sand with bioturbation filled with *Halimeda* floatstone (Subunit IIC; interval 310-M0005D-16R-1, 97–105 cm).

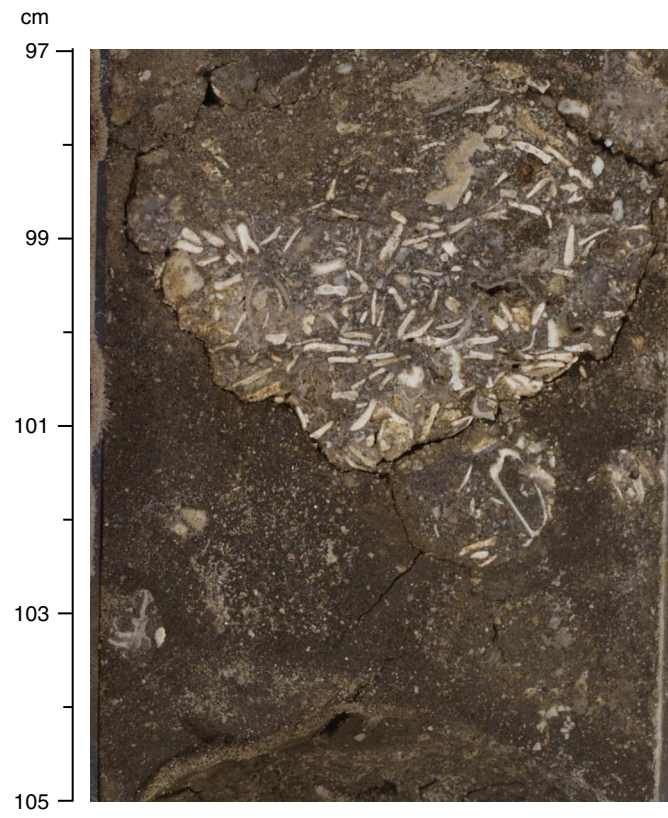


Figure F43. Laminated microbialite forming thick columnar accretions; spaces between microbial accretions are infilled with coarse, volcanic-rich skeletal sediment (Subunit IID; interval 310-M0005D-21R-2, 0–12 cm).

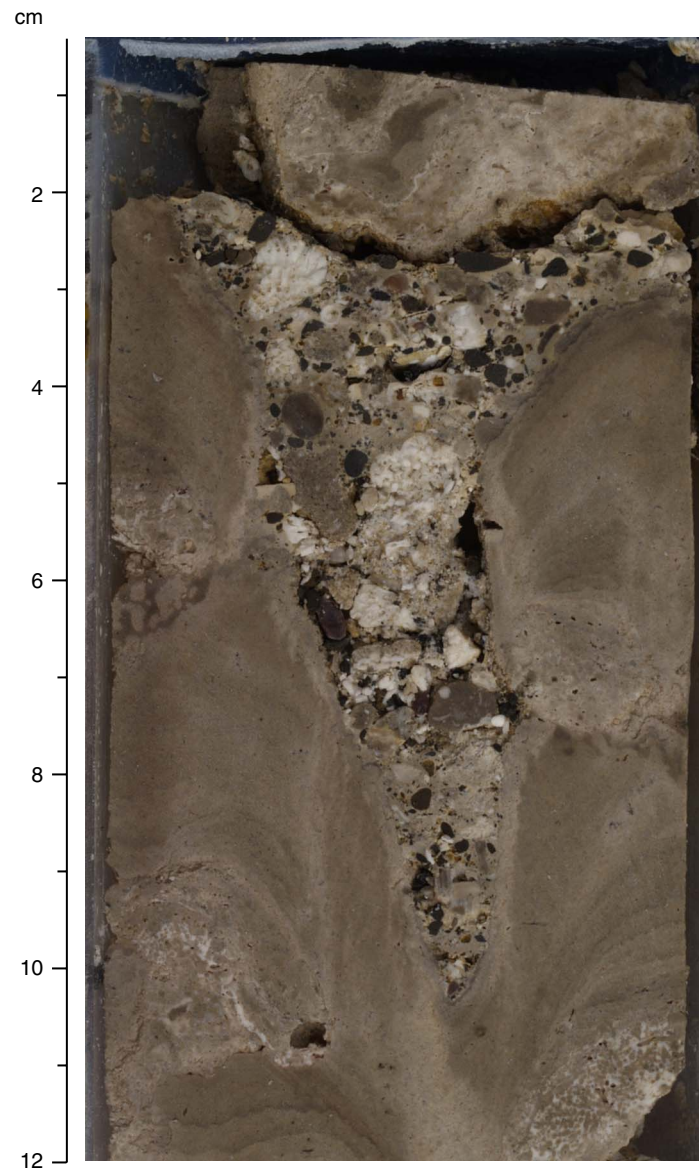


Figure F44. Encrusting colonies of agariciids thinly encrusted with coralline algae (Subunit IID; interval 310-M0005D-21R-1, 0–15 cm).

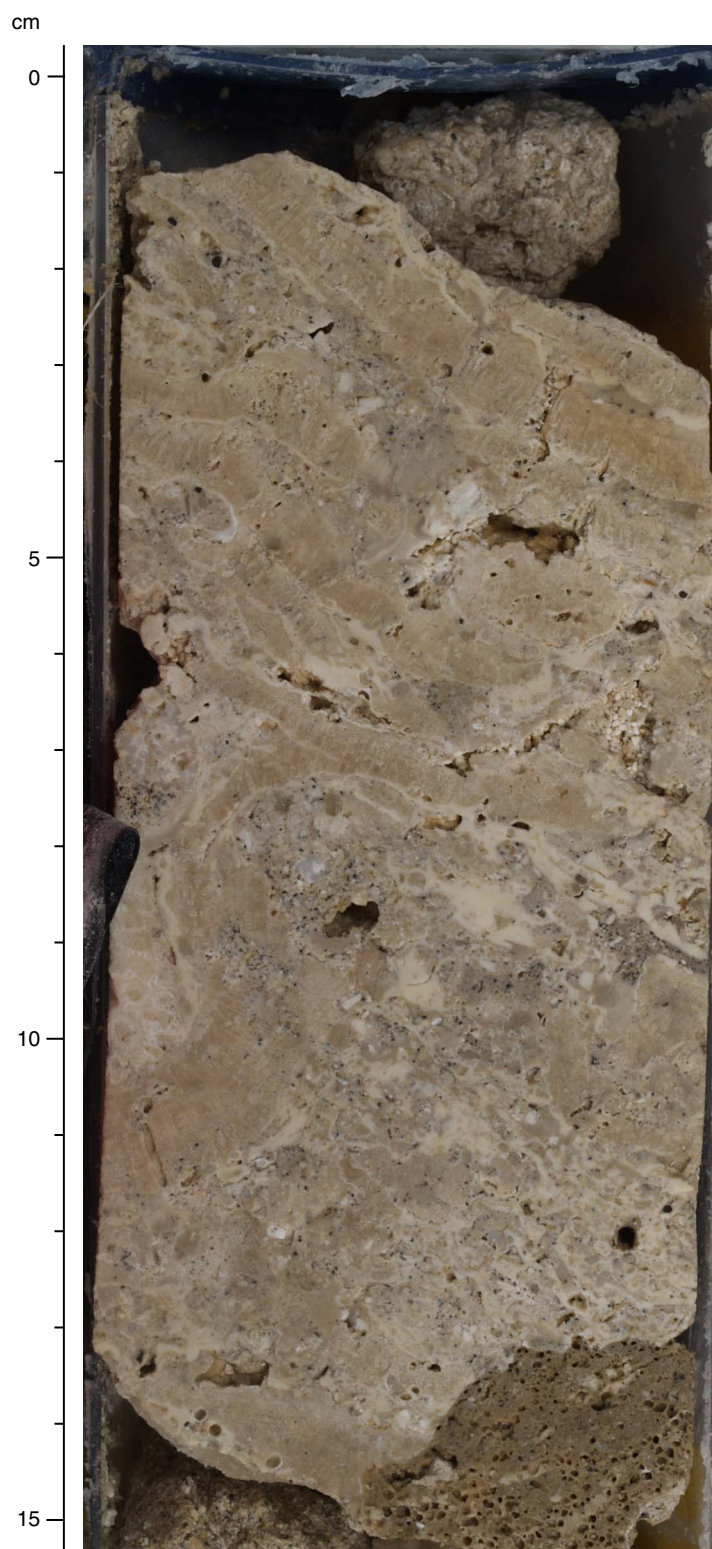


Figure F45. Extensively bioeroded coral; borings are partly filled with internal sediments displaying geopetal structure (Subunit IID; interval 310-M0005D-21R-1, 38–48 cm). Sedimentary matrix is rich in volcanic grains.

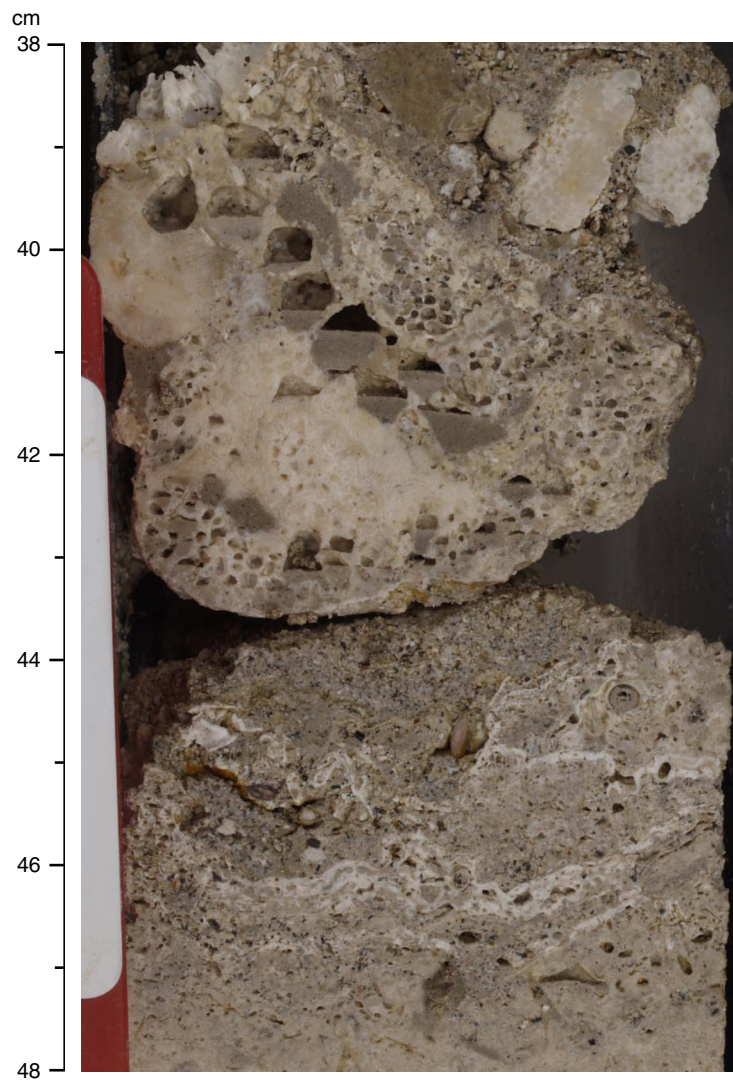


Figure F46. Volcanic grains in the matrix of coralgall frameworks (Subunit IID; interval 310-M0005D-21R-1, 65–75 cm).

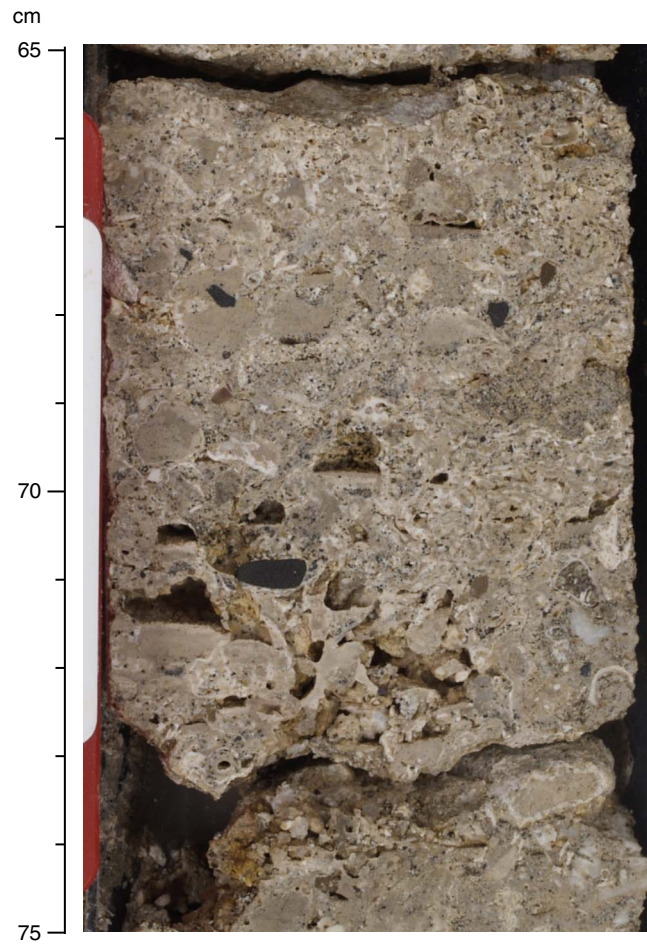


Figure F47. Sandy skeletal grainstone rich in volcanic grains (Subunit IID; interval 310-M0005D-23R-1, 10–15 cm).



Figure F48. Packstone, including volcanic grains and skeletal fragments (coral and nongeniculate coralline algae) (Subunit IIE; interval 310-M0005D-29R-1, 5–14 cm). Note thin coralline algal crusts.

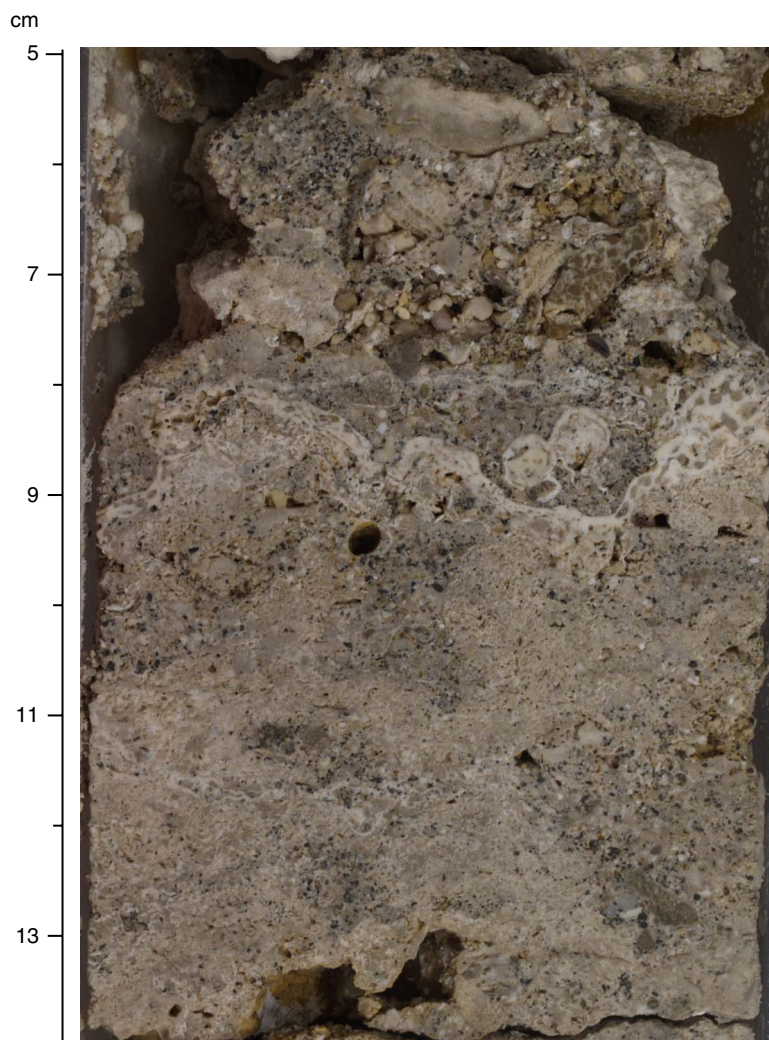


Figure F49. In situ massive colonies of *Porites* thinly encrusted with coralline algae and embedded in volcanic-rich sediment (Subunit IIE; interval 310-M0005D-29R-1, 50–70 cm).

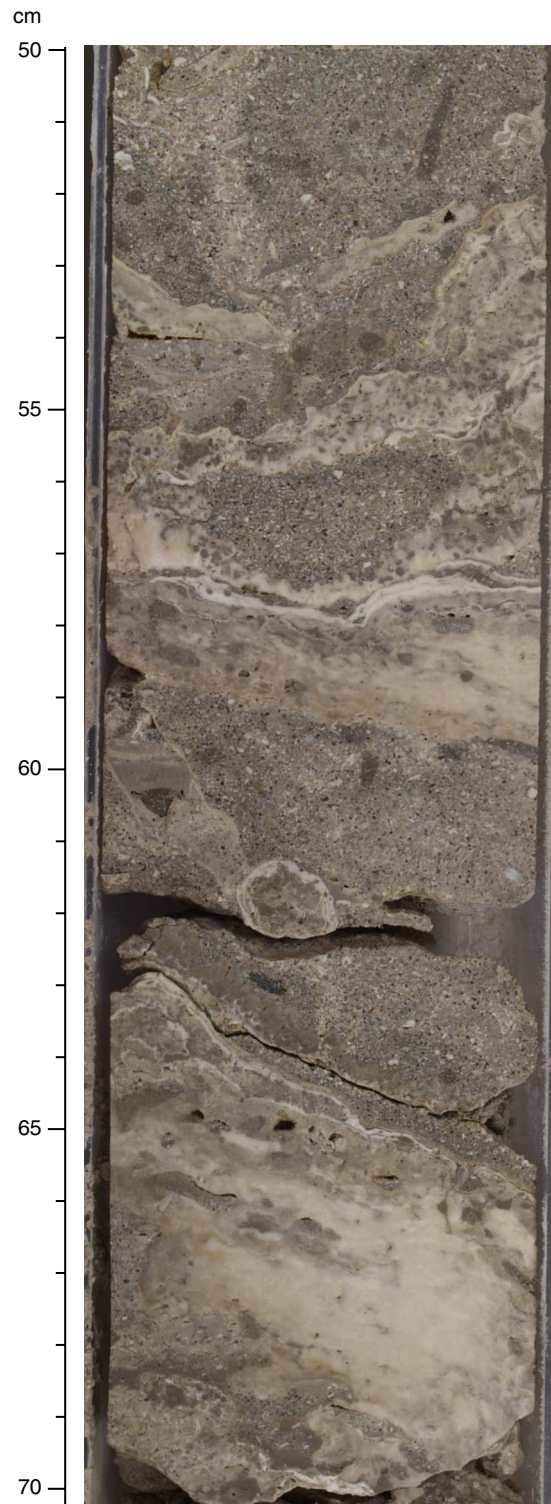


Figure F50. Coralgall floatstone rich in rhodoliths (Subunit IIF; interval 310-M0005D-29R-1, 116–131 cm).

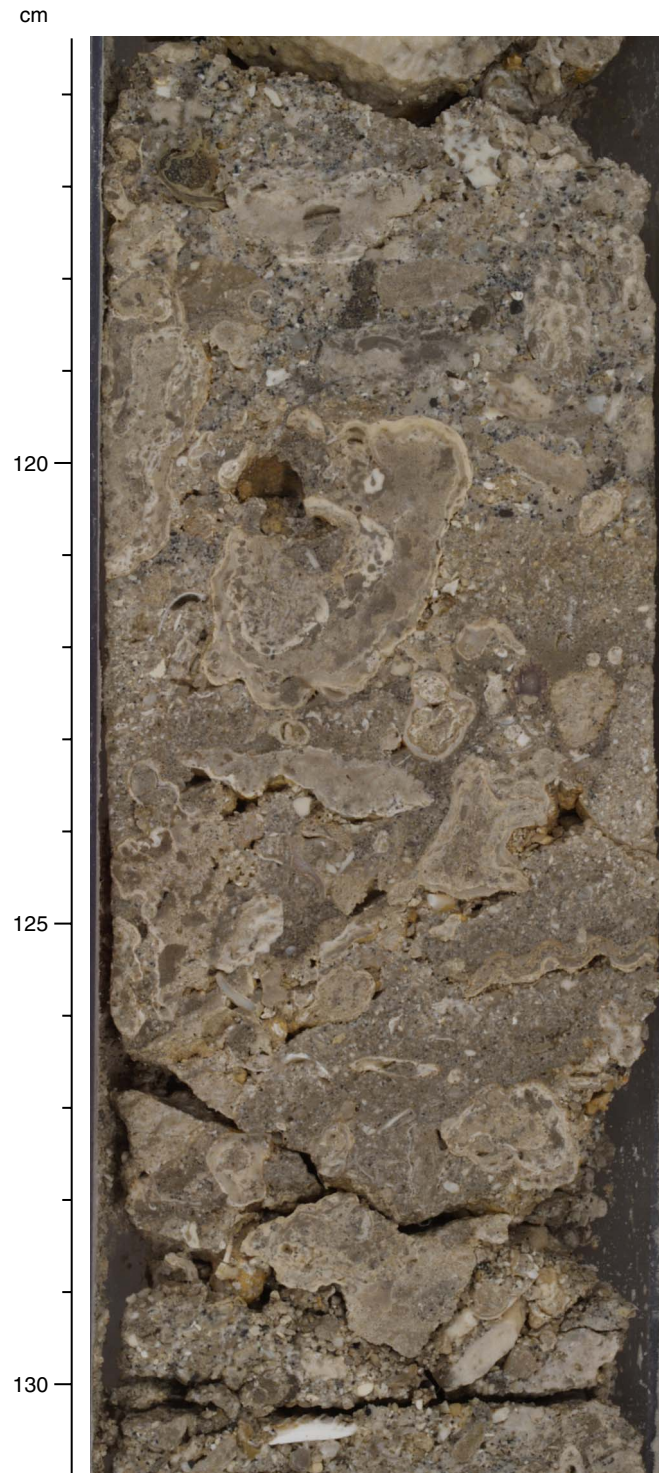


Figure F51. Coralgall rudstone, including lithoclasts and volcanic grains (Subunit IIF; interval 310-M0005D-29R-1, 80–110 cm).

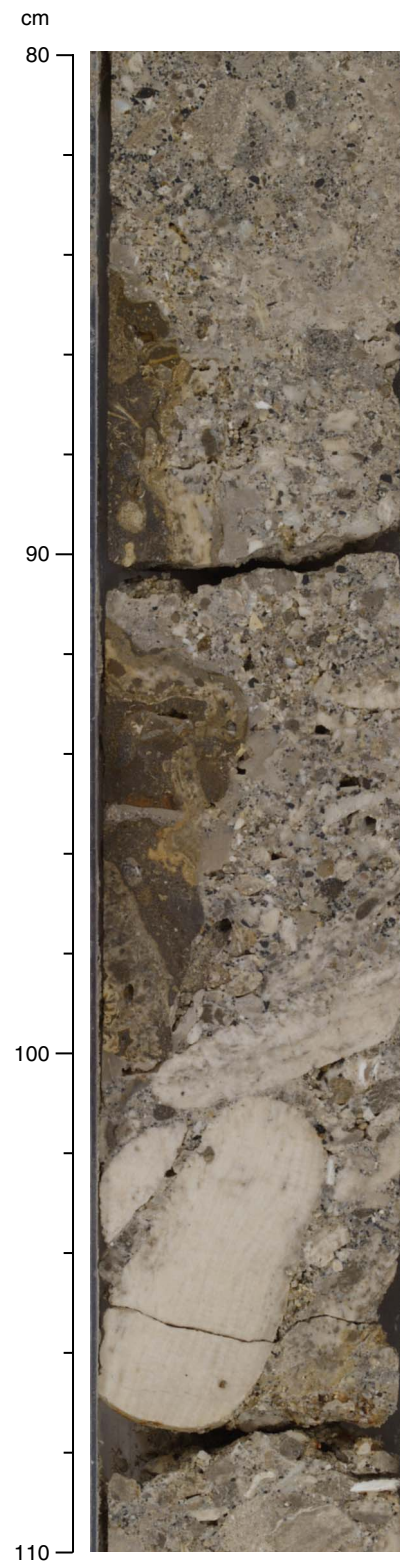


Figure F52. Coralgall rudstone, including fragments of massive *Porites* in a volcanic-rich sedimentary matrix (Subunit IIF; interval 310-M0005D-30R-1, 17–26 cm).

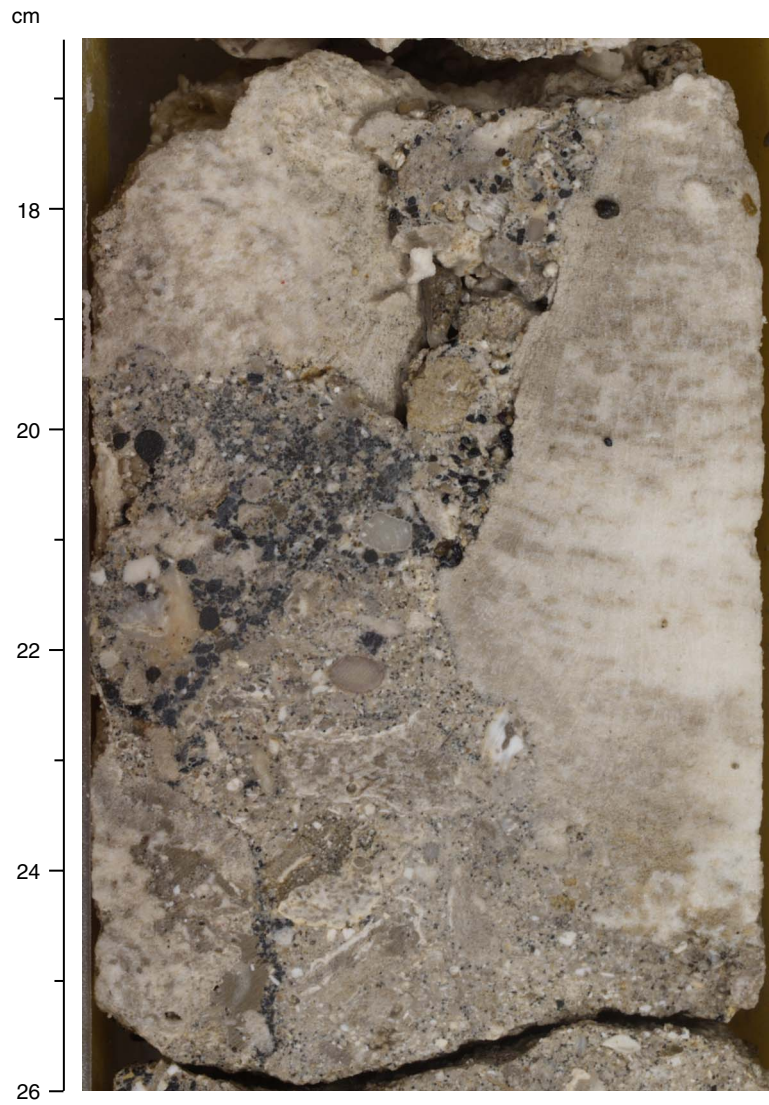


Figure F53. Encrusting colonies of *Porites* in a volcanic sediment-rich matrix, thinly encrusted with coralline algae (Subunit IIG; interval 310-M0005D-31R-2, 0–12 cm). Note bioerosion of corals.

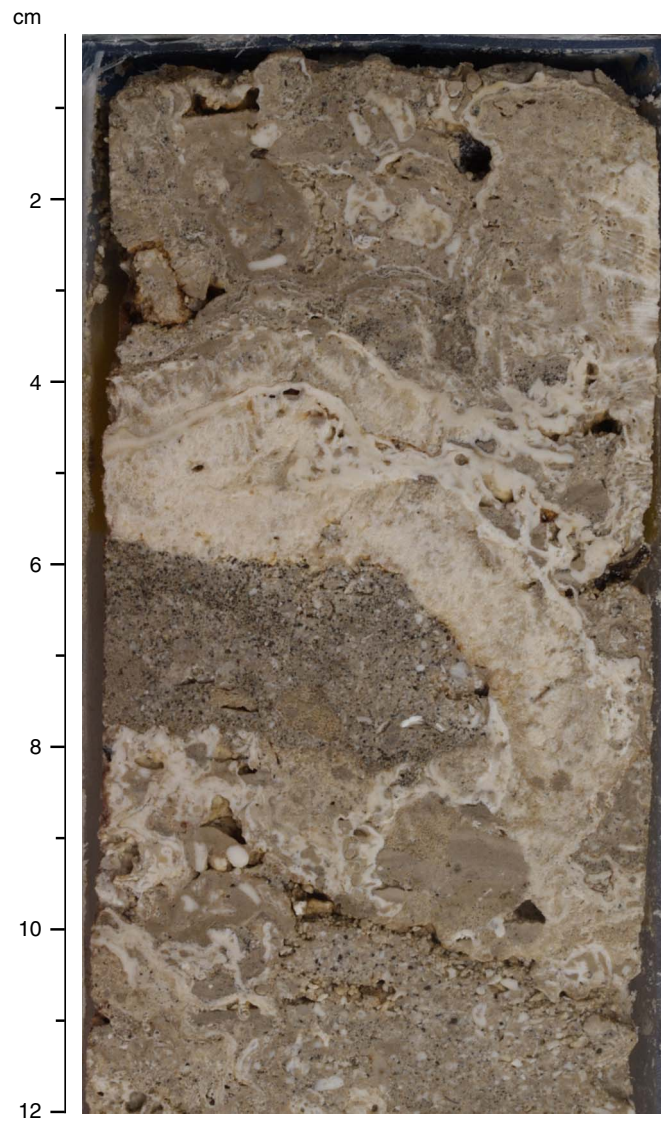


Figure F54. Encrusting colonies of *Porites* in a volcanic sediment-rich matrix (Subunit IIG; interval 310-M0005D-32R-1, 109–133 cm).



Figure F55. Coralgall frameworks composed of encrusting colonies of *Porites* and tabular colonies of *Acropora*(?) interbedded with grainstone rich in volcanic grains and skeletal fragments (Subunit IIG; interval 310-M0005D-32R-3, 15–27 cm).

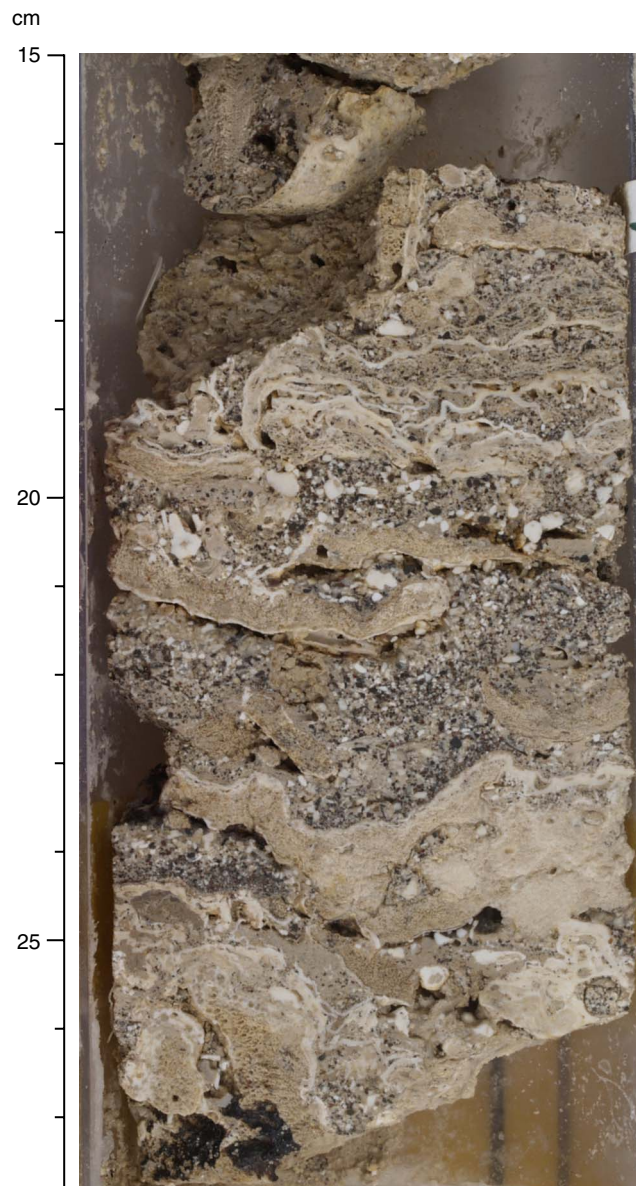


Figure F56. Encrusting colonies of *Porites* in a volcanic sediment-rich matrix (Subunit IIG; interval 310-M0005D-34R-1, 28–40 cm).

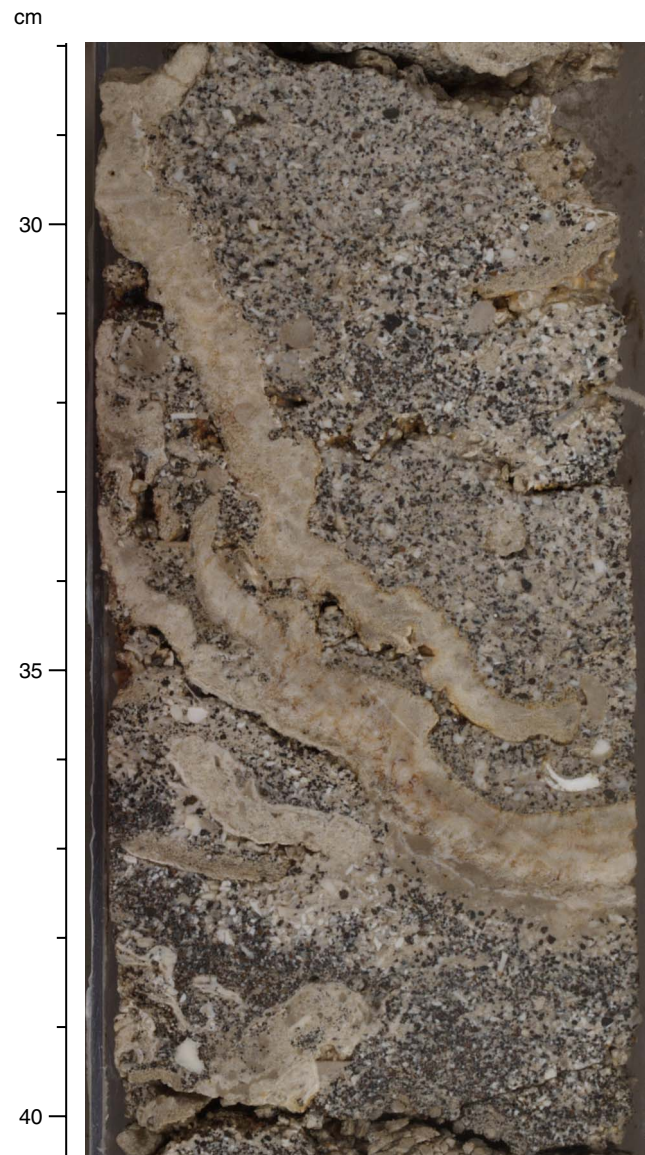


Figure F57. Massive colony of *Porites* with severe bioerosion close to upper surface (Subunit IIG; interval 310-M0005D-30R-1, 117–128 cm).

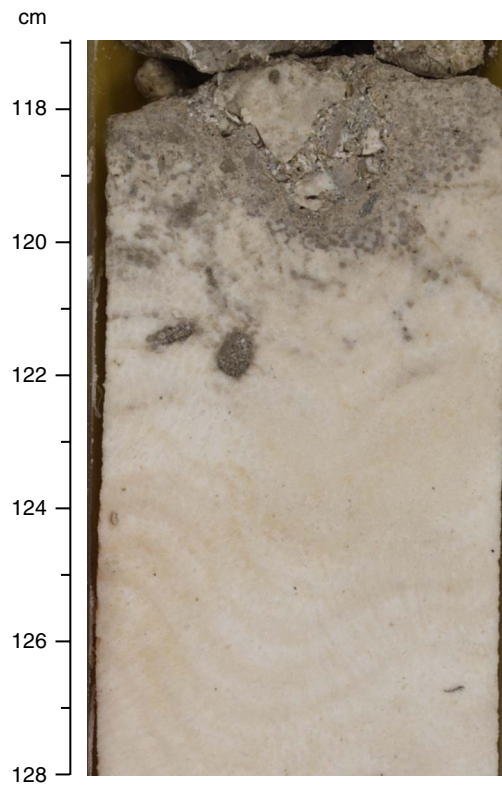


Figure F58. Robust branching colony of *Pocillopora* (Subunit IIG; interval 310-M0005D-30R-2, 30–46 cm). Note strong bioerosion of corals.

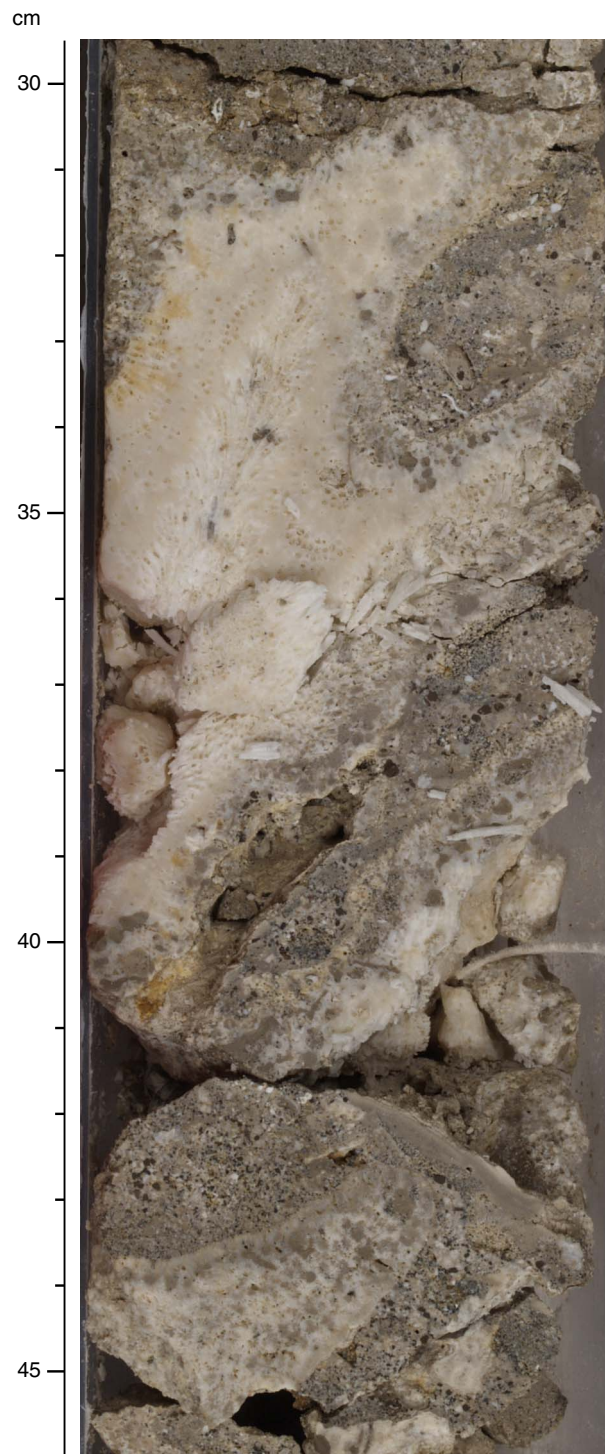


Figure F59. Encrusting colonies of *Porites* encrusted with thin nongeniculate coralline algal crusts (Subunit IIG; interval 310-M0005D-30R-2, 79–97 cm). Note solution cavities.

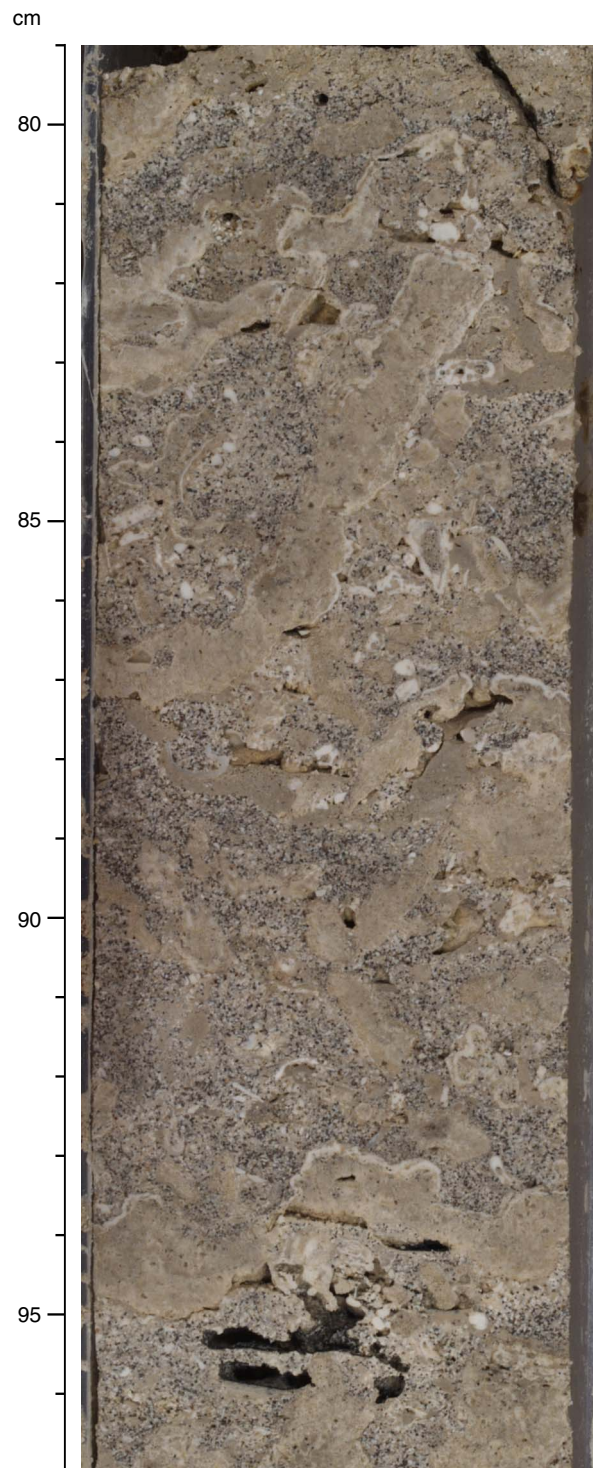


Figure F60. Tabular colony of *Acropora* in a volcanic sediment-rich matrix (Subunit IIG; interval 310-M0005D-30R-2, 95–110 cm). Note geopetal infill of borings.

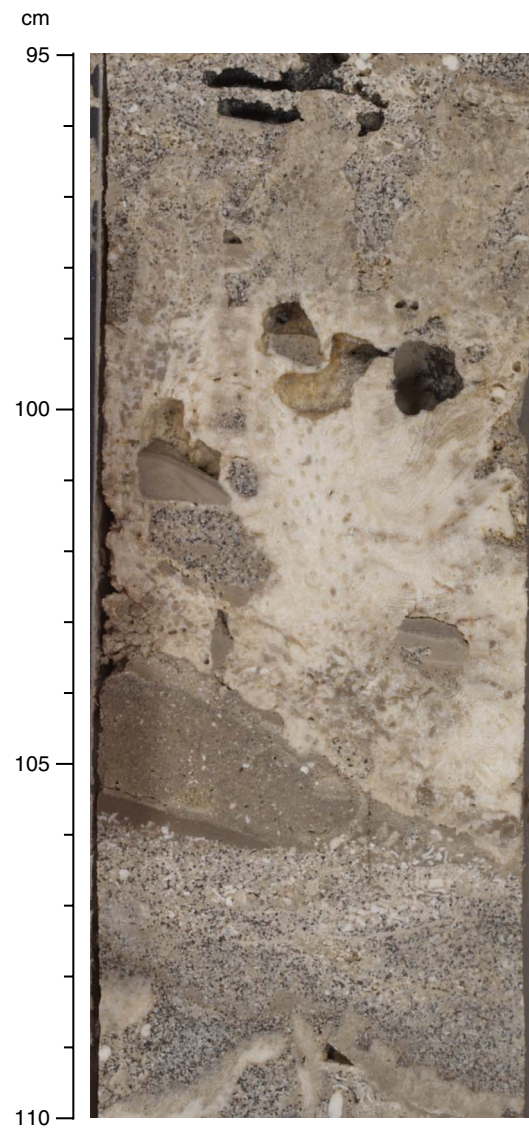


Figure F61. Encrusting colony of *Montastrea* and tabular colony of *Acropora* in a volcanic sediment-rich matrix (Subunit IIG; interval 310-M0005D-33R-3, 0–25 cm).

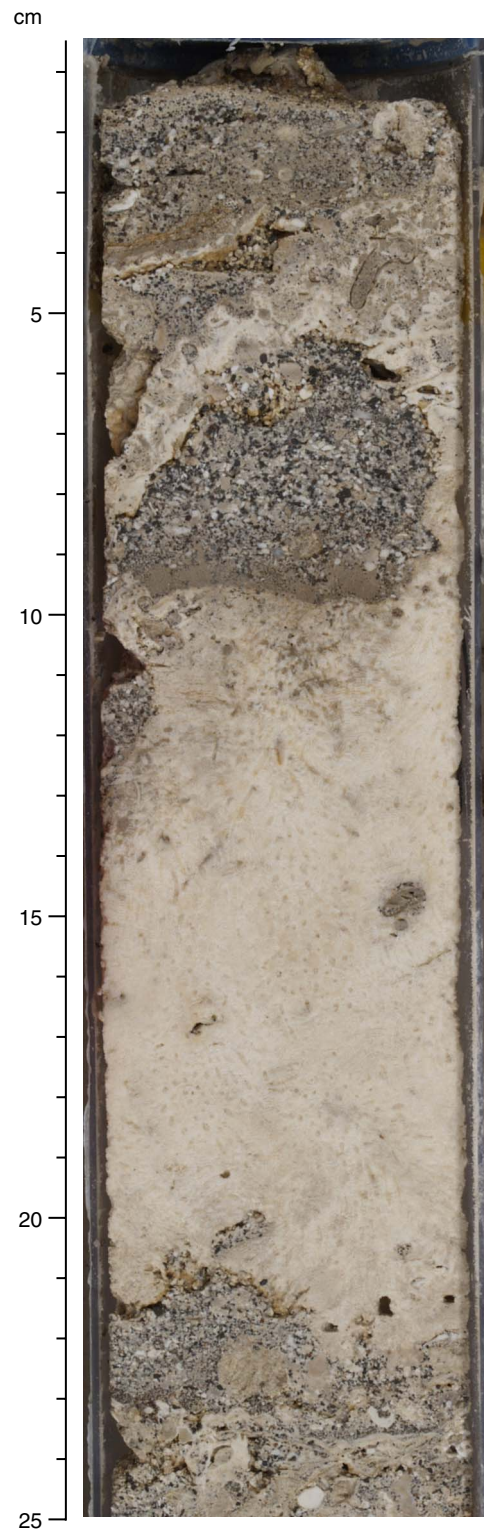


Figure F62. Floatstone rich in fragments of robust branching *Pavona* with a volcanic sediment-rich grainstone matrix (Subunit IIH; interval 310-M0005D-35R-2, 70–97 cm).



Figure F63. Velocity, bulk density, magnetic susceptibility, and porosity as a function of depth in Hole M0005A. Discrete measurements are superimposed (red circles).

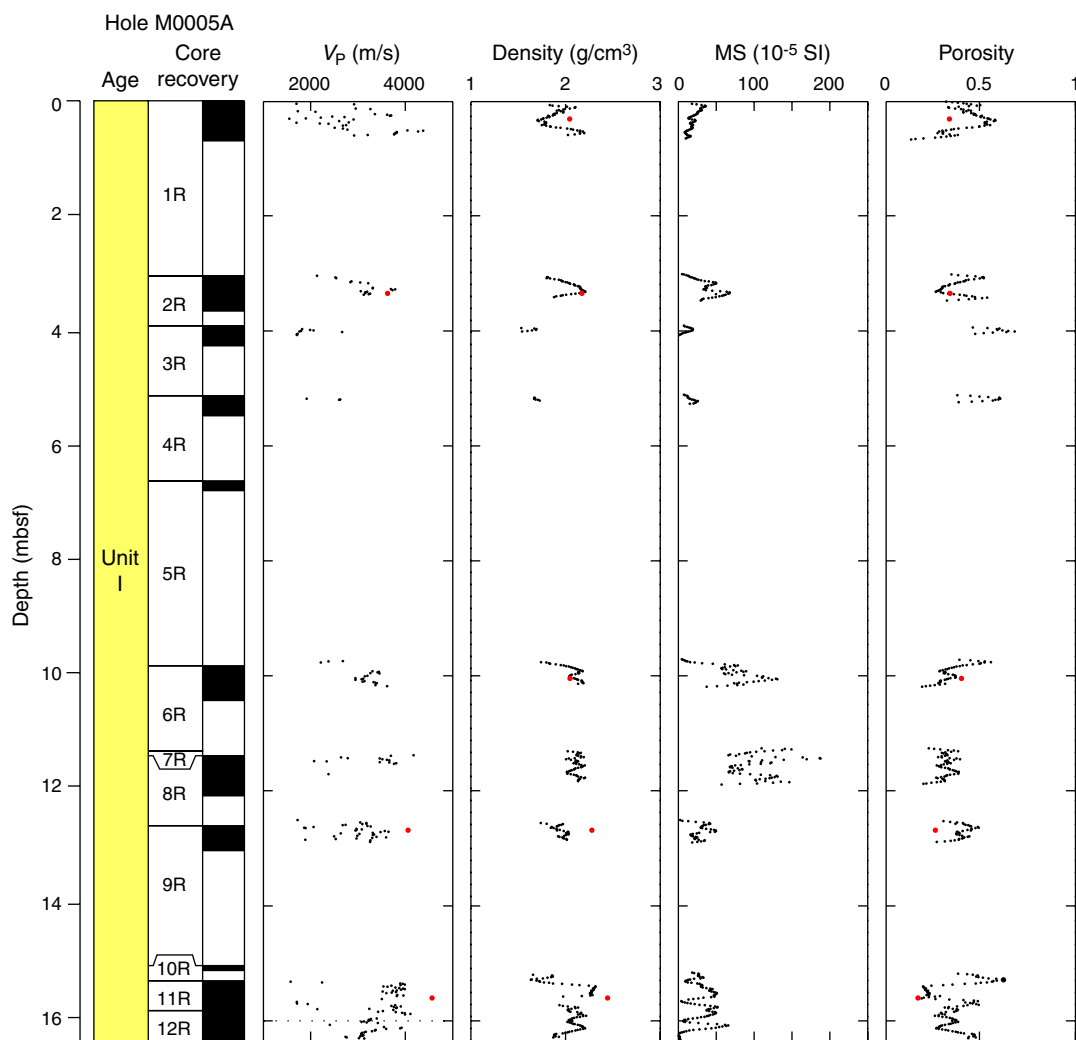


Figure F64. Velocity, bulk density, magnetic susceptibility, and porosity as a function of depth in Hole M0007C. Discrete measurements are superimposed (red circles).

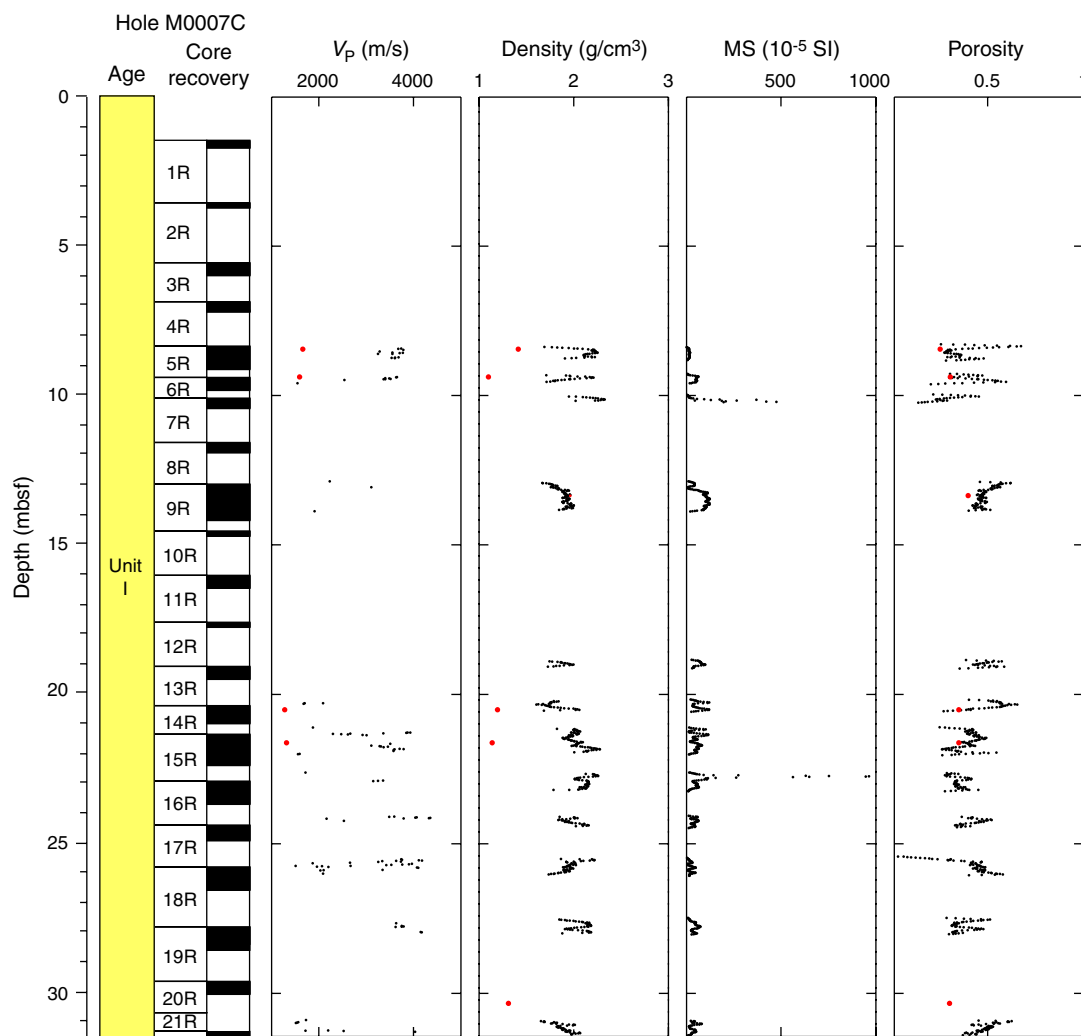


Figure F65. Velocity, bulk density, magnetic susceptibility, and porosity as a function of depth in Hole M0005C. Discrete measurements are superimposed (red circles).

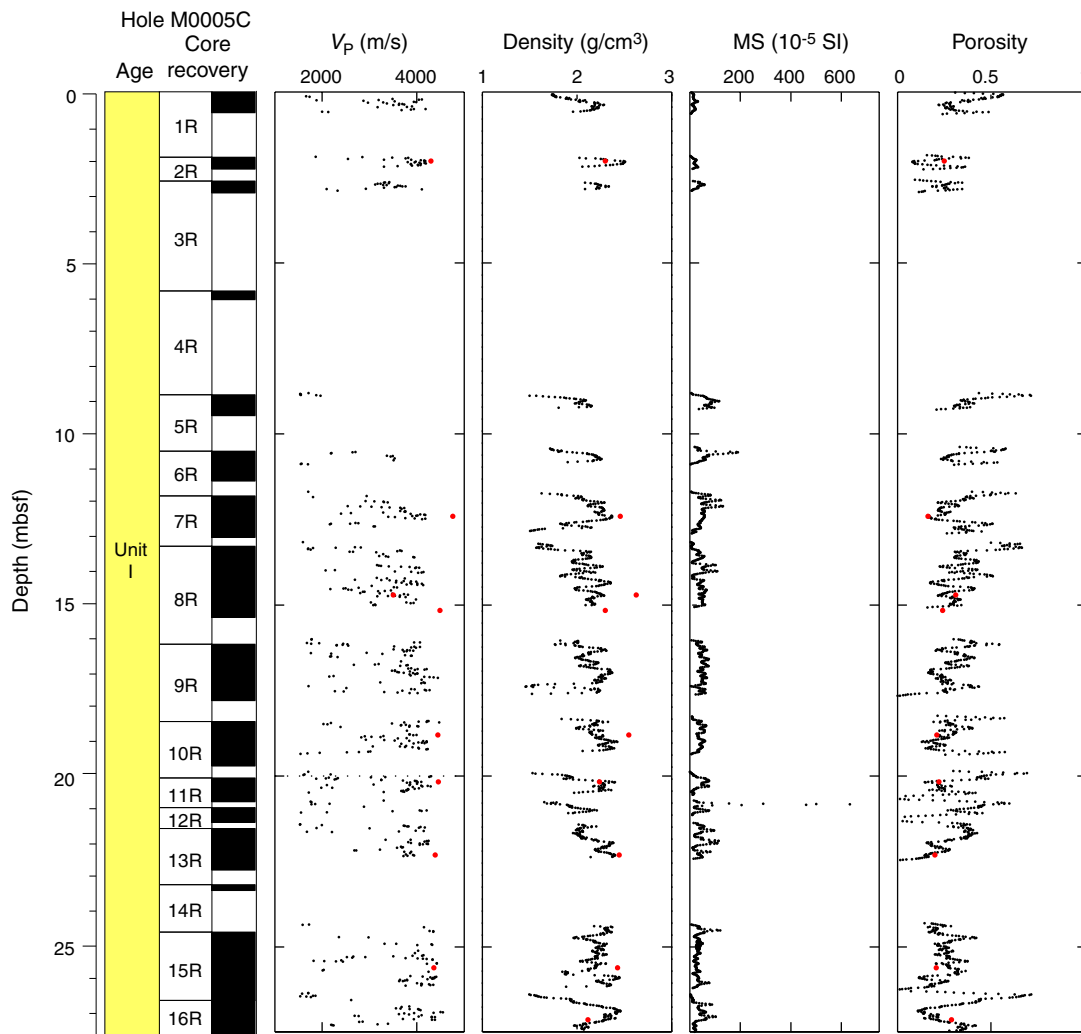


Figure F66. Velocity, bulk density, magnetic susceptibility, and porosity as a function of depth in Hole M0007B. Discrete measurements are superimposed (red circles).

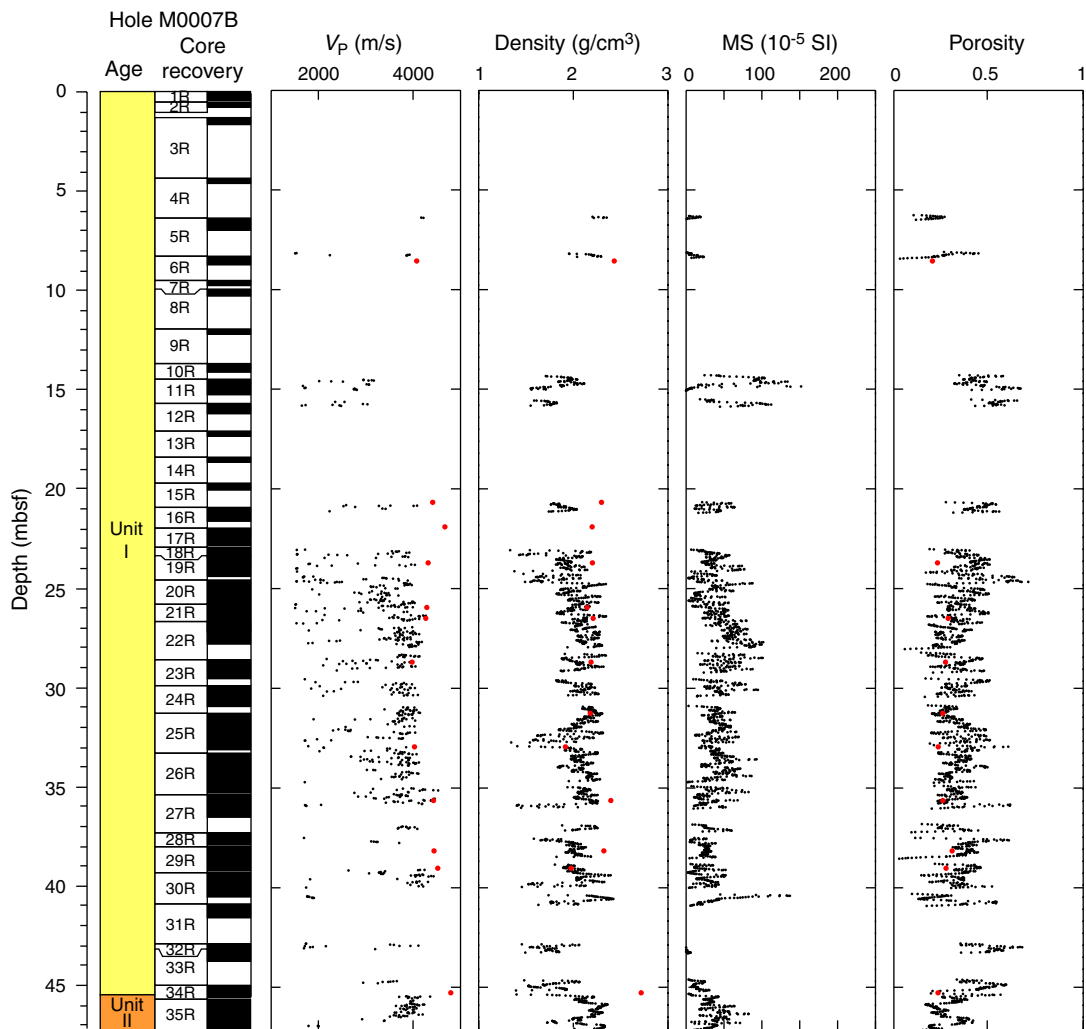


Figure F67. Velocity, bulk density, magnetic susceptibility, and porosity as a function of depth in Hole M0005B. Discrete measurements are superimposed (red circles).

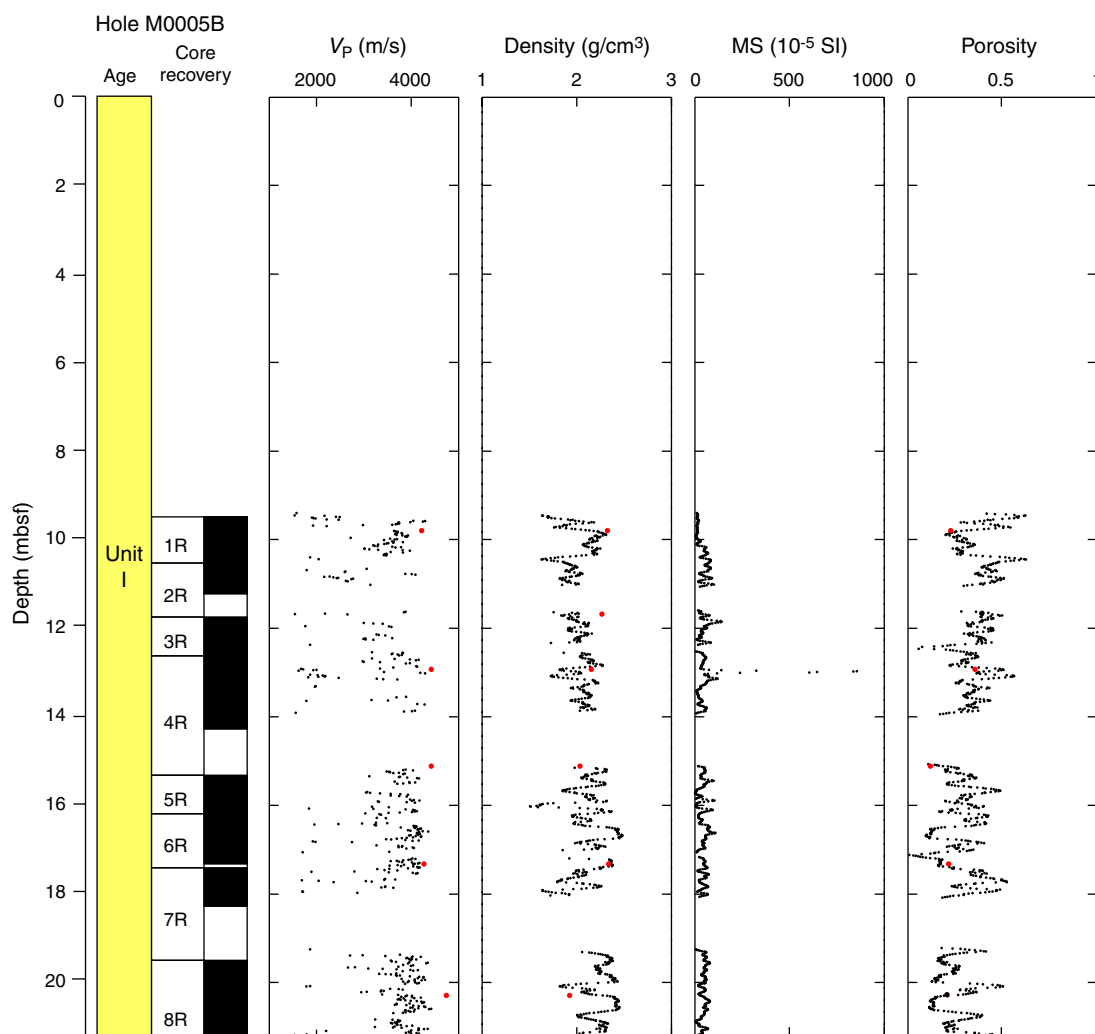


Figure F68. Velocity, bulk density, magnetic susceptibility, and porosity as a function of depth in Hole M0005D. Discrete measurements are superimposed (red circles).

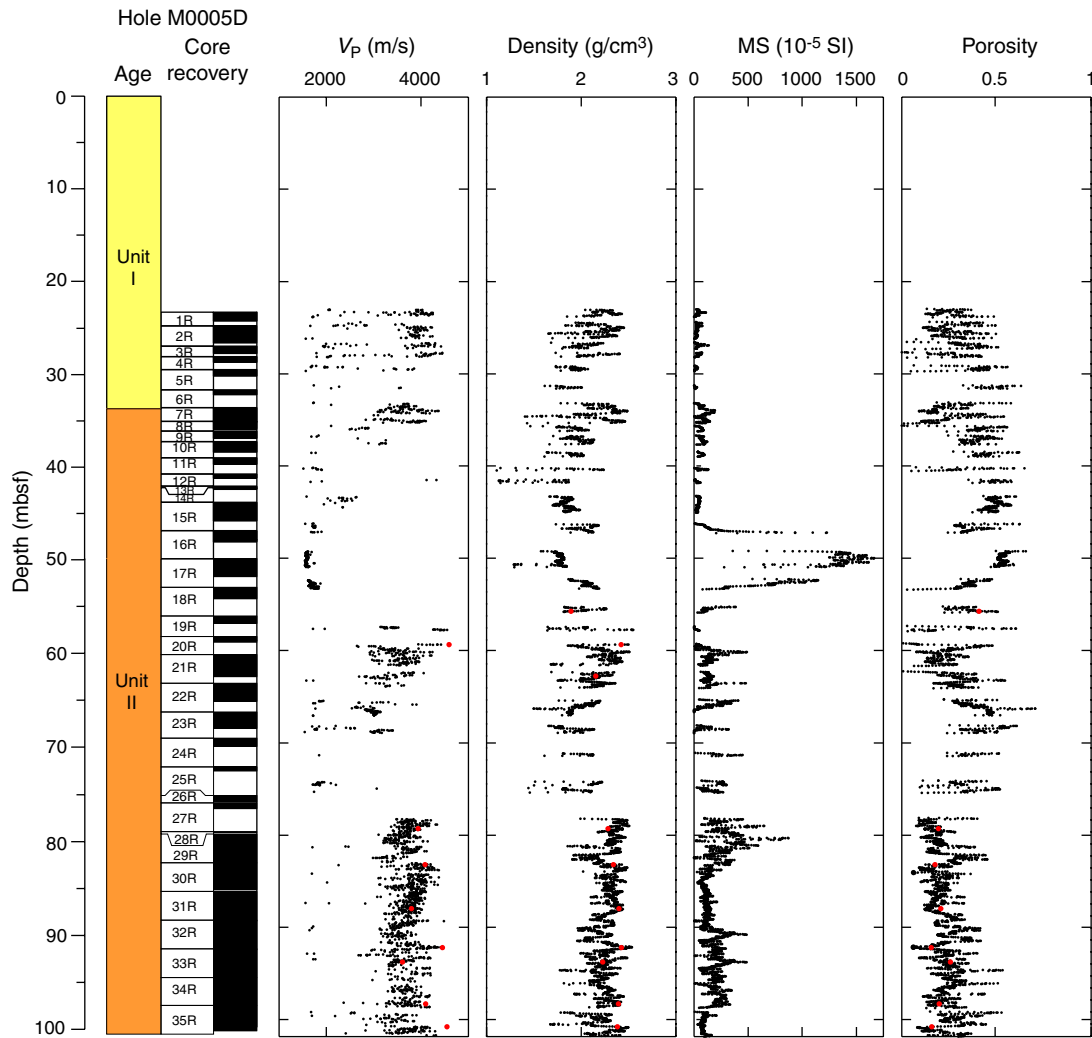


Figure F69. Velocity, bulk density, magnetic susceptibility, and porosity as a function of depth in Hole M0007A. Discrete measurements are superimposed (red circles).

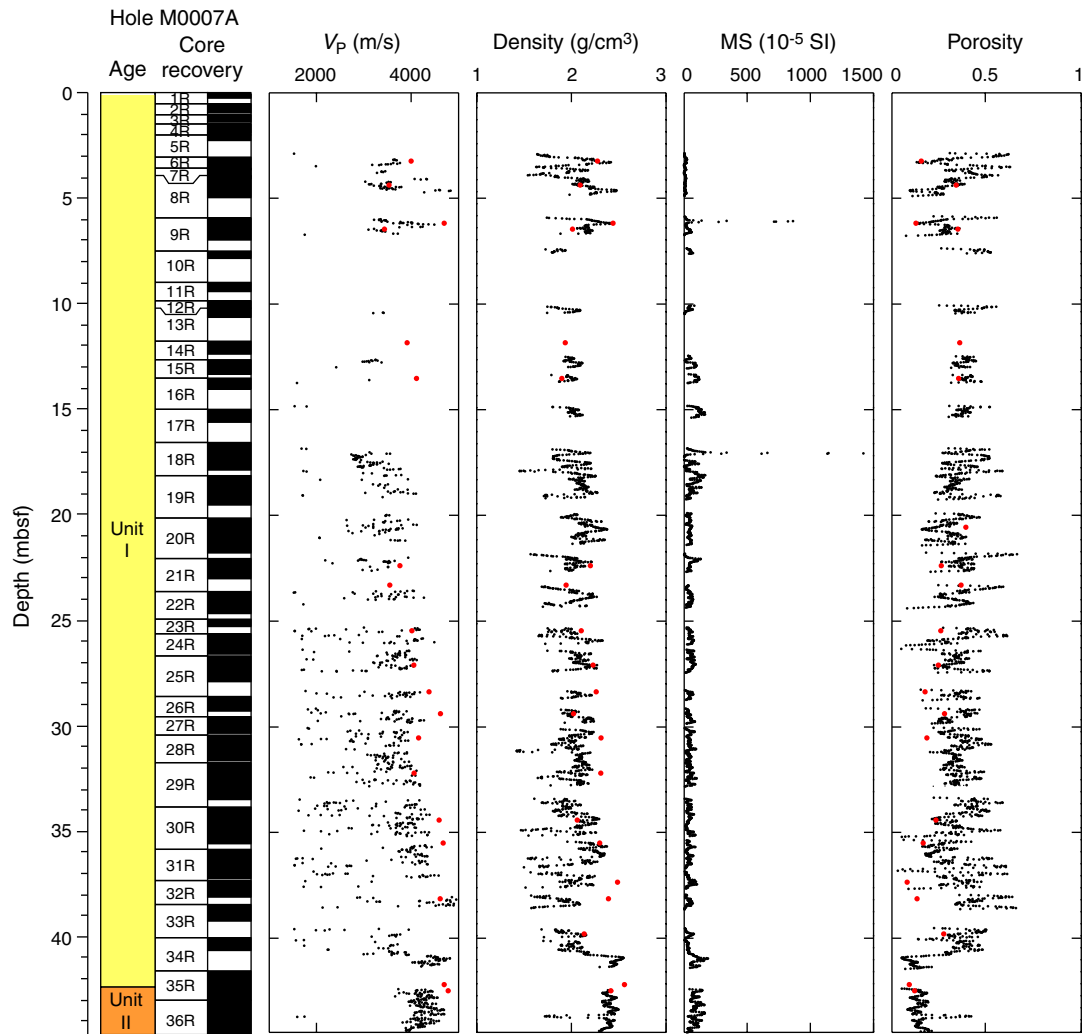


Figure F70. Cross plot of porosity with velocity for Hole M0005D. Solid lines = Wyllie time average equation (red; Wyllie et al., 1956) and Raymer modified time average equation (green; Raymer et al., 1980) for a matrix velocity of calcite (6530 m/s). Discrete measurements are superimposed (red circles).

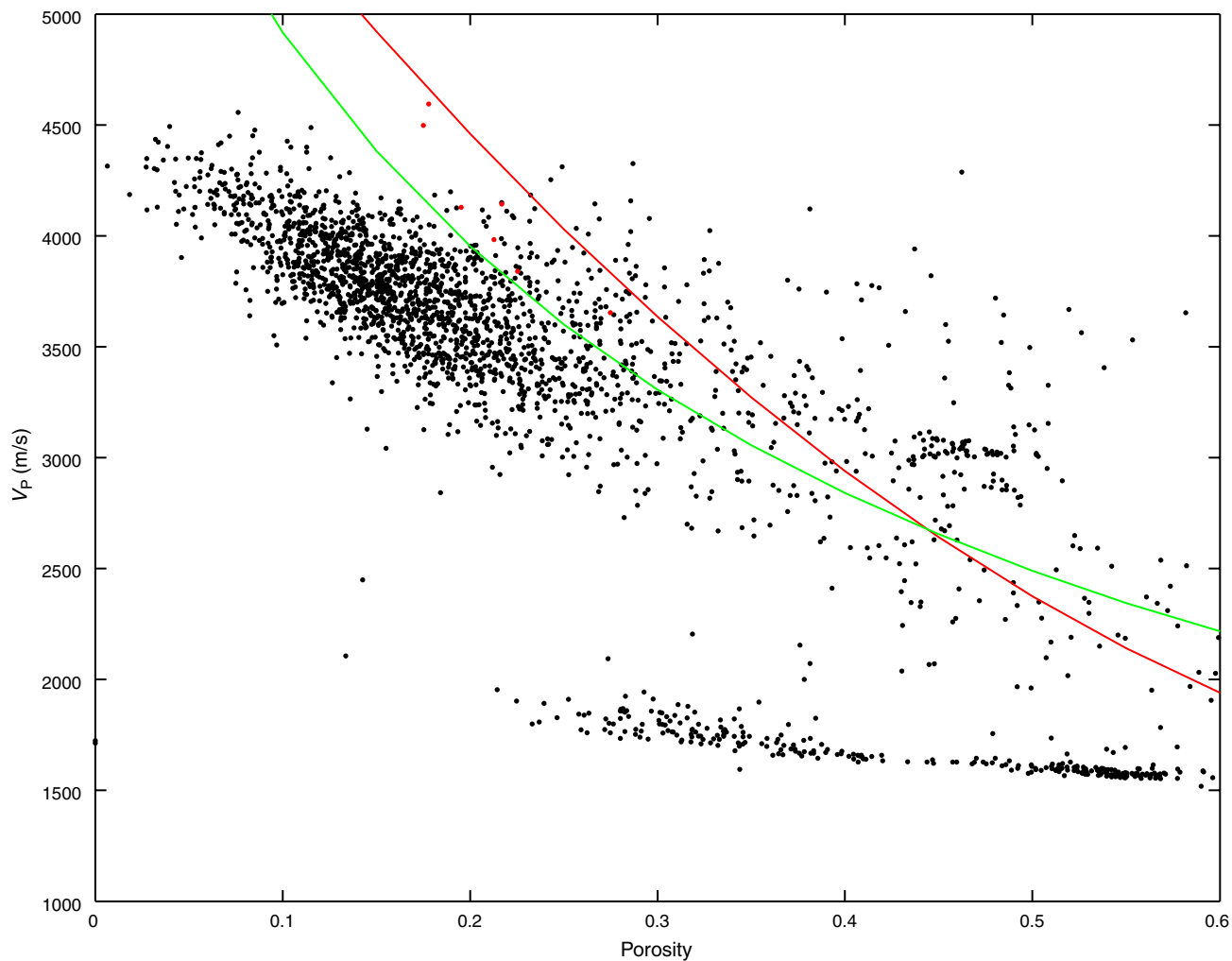


Figure F71. Comparison of MSCL velocity data (solid circles), downhole sonic log data (solid blue line), and discrete measurements (red circles) as a function of depth for Hole M0005D.

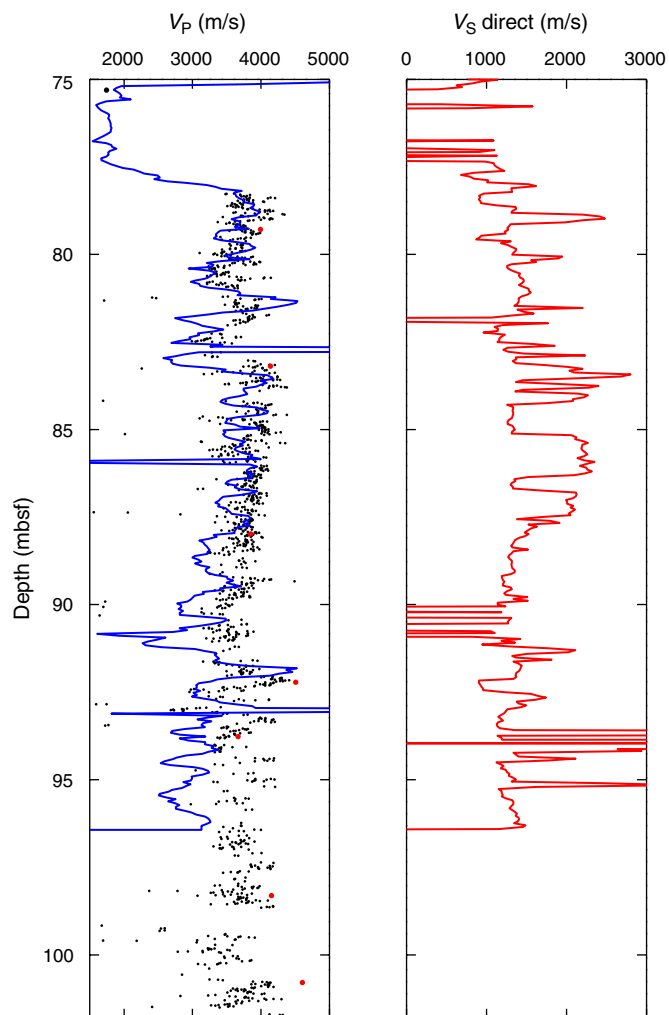


Figure F72. Comparison of multisensor core logger (MSCL) resistivity data and downhole resistivity data as a function of depth for Site M0009. DIL = dual induction tool.

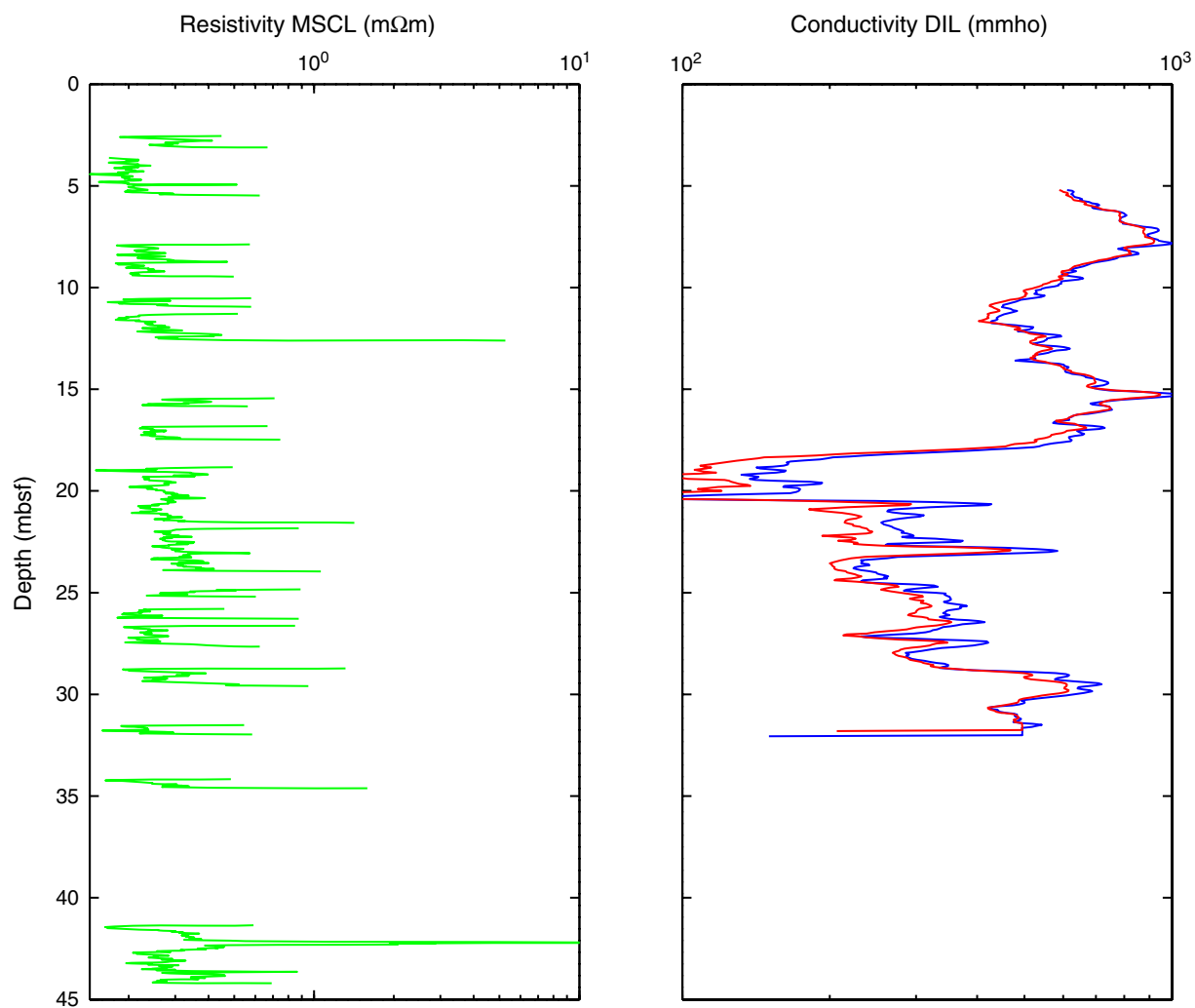


Figure F73. Color reflectance (L^*) data from Holes M0005A–M0005D and M0007A–M0007C. For plotting purposes, Holes M0005B–M0005D and M0007A–M0007C are offset from Hole M0005A by 30, 60, 90, 120, 150, and 180 L^* units, respectively.

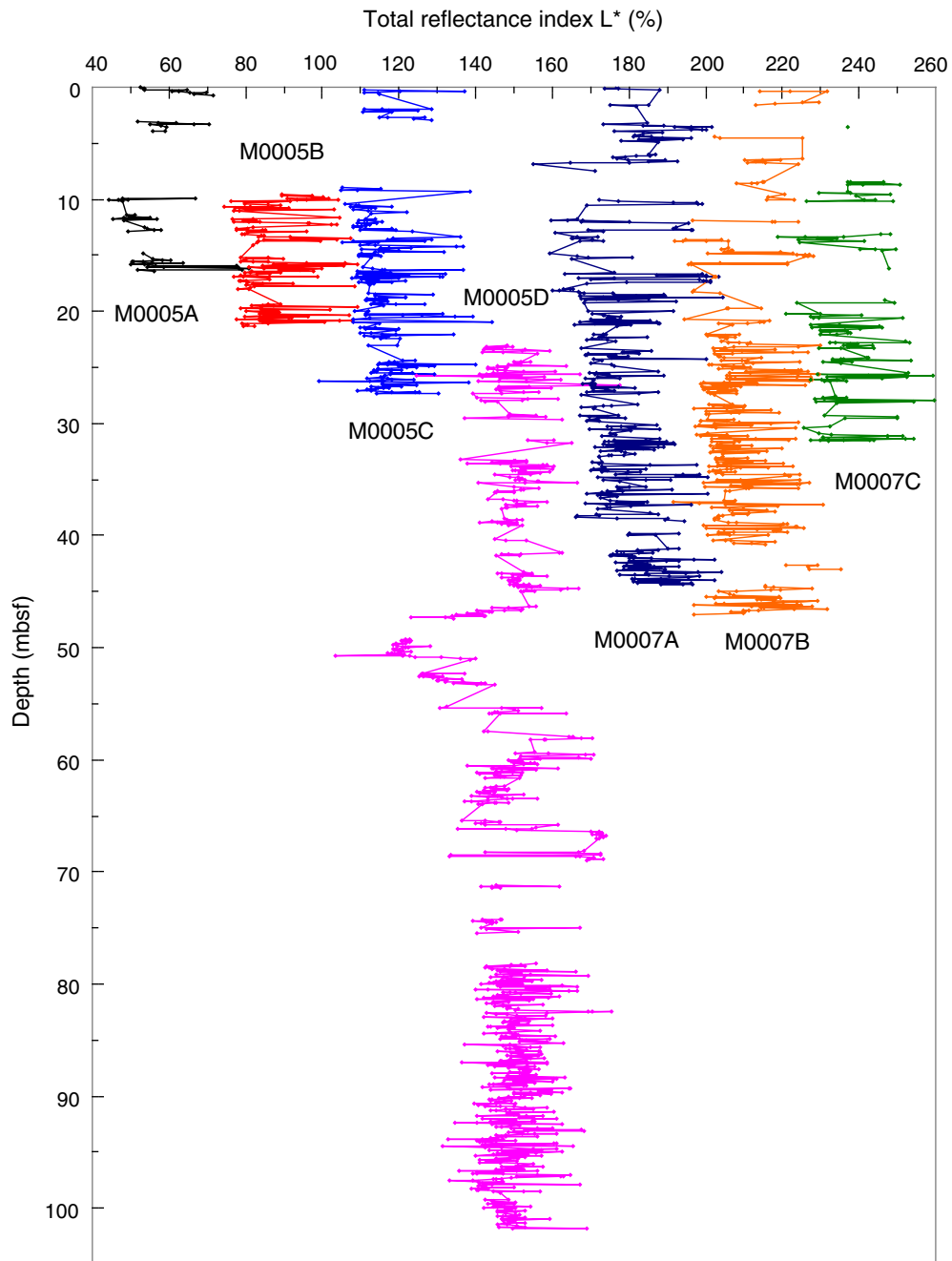


Figure F74. Wireline logging data, Hole M0005D. Mec. cal. = mechanical caliper, Ac. cal. = acoustic caliper extracted from ABI40, TGR = total gamma radiation, res. = resistivity, T = borehole fluid temperature, C = borehole fluid conductivity.

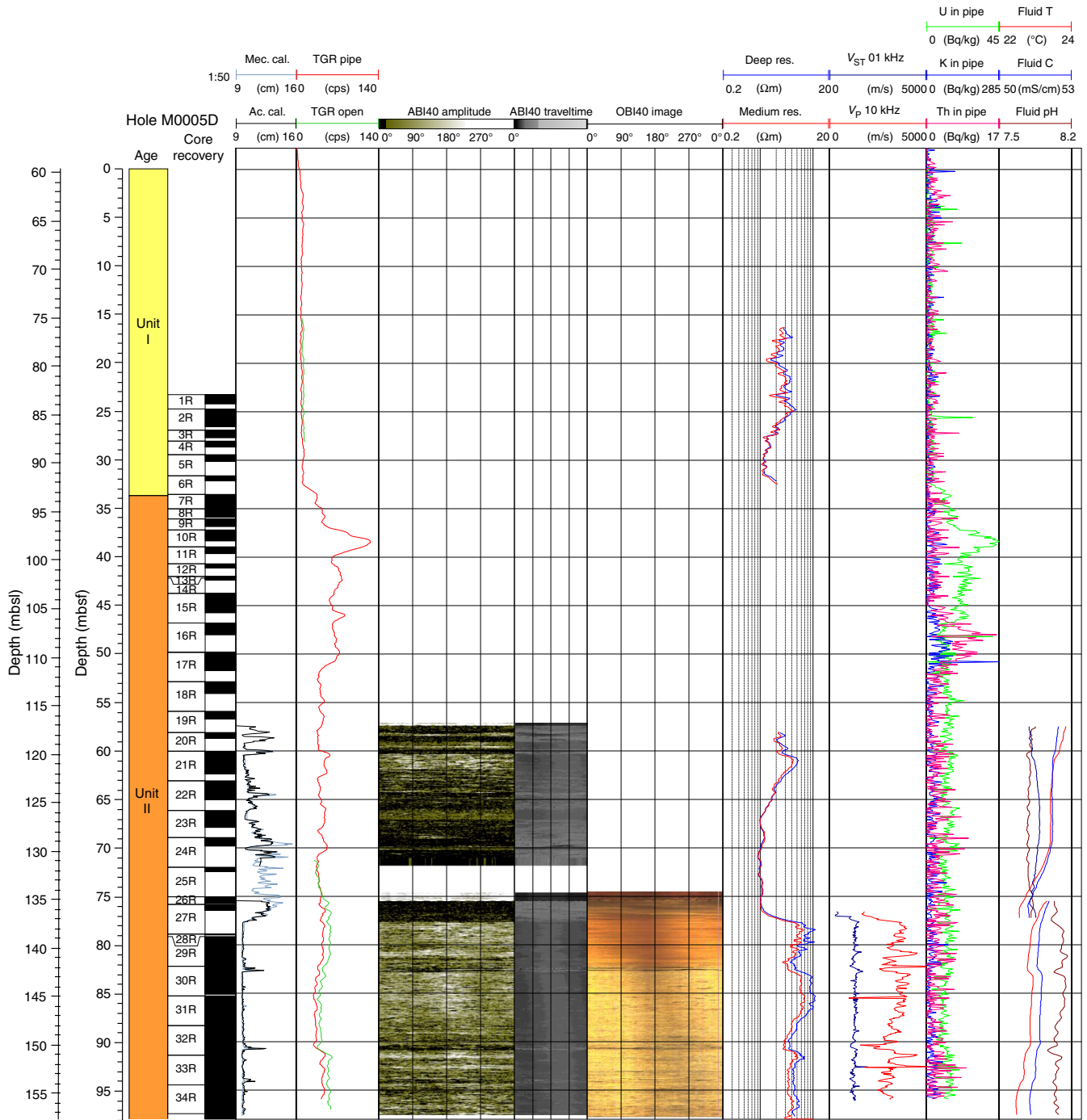


Figure F75. Wireline logging data, Hole M0005D. Cal. = caliper. (See the “DOWNHOLE” folder in “[Supplementary Material](#)” for the complete multipart figure in PDF format.)

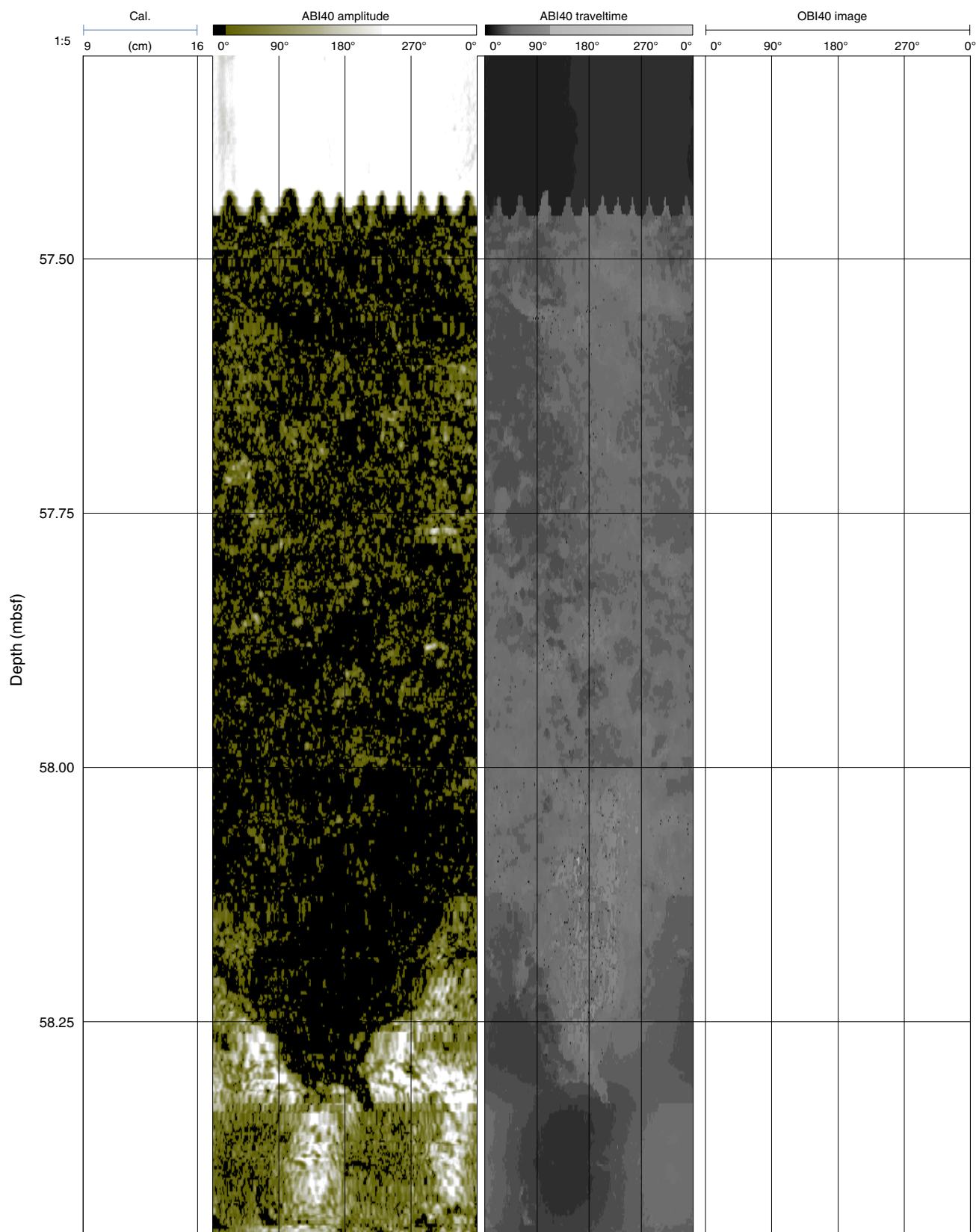


Figure F76. Wireline logging data, Hole M0007A. TGR = total gamma radiation, res. = resistivity, T = borehole fluid temperature, C = borehole fluid conductivity.

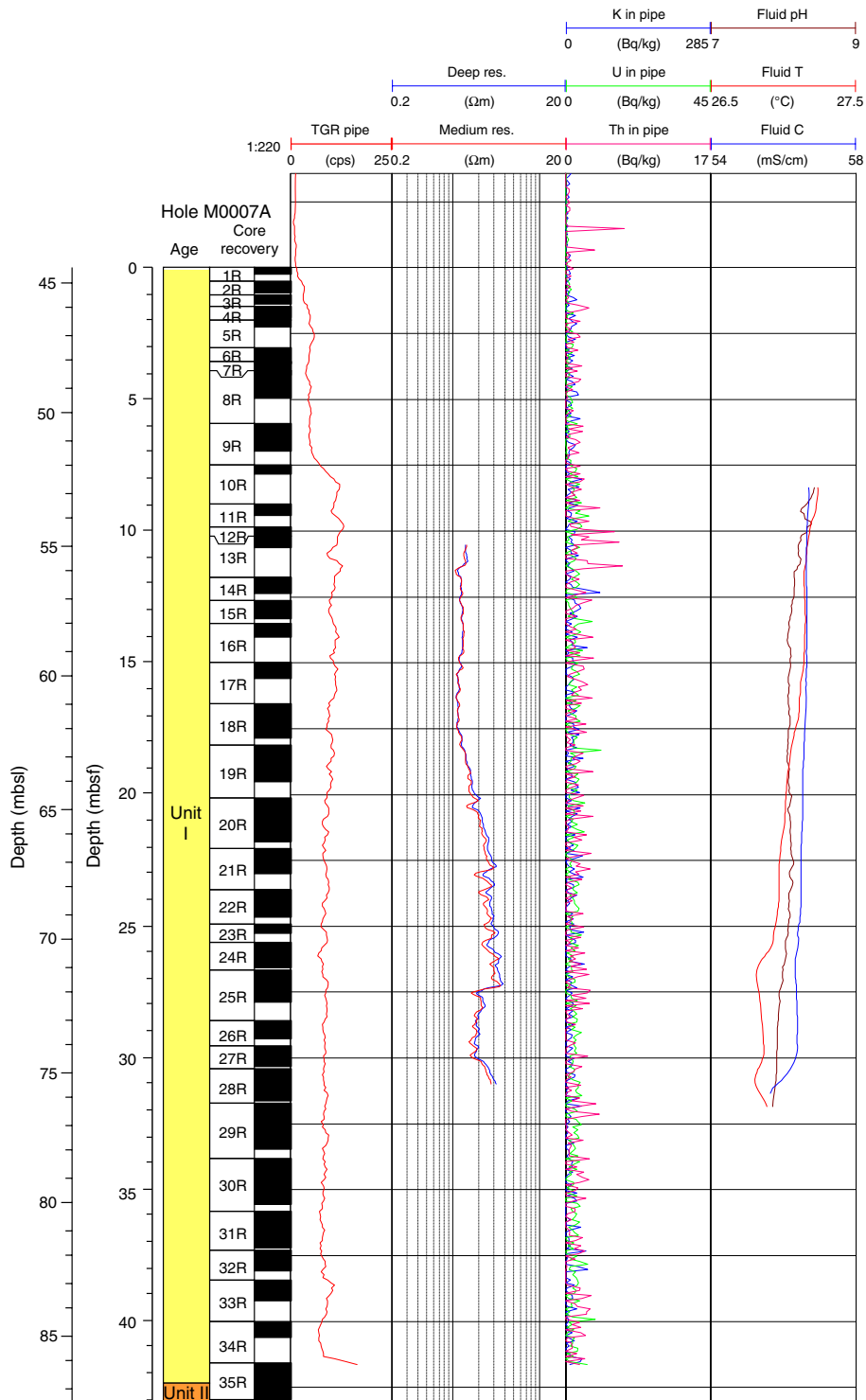


Figure F77. Wireline logging data, Hole M0007B. Ac. cal. = acoustic caliper extracted from ABI40, TGR = total gamma radiation, TT = travelttime, res. = resistivity, T = borehole fluid temperature, C = borehole fluid conductivity.

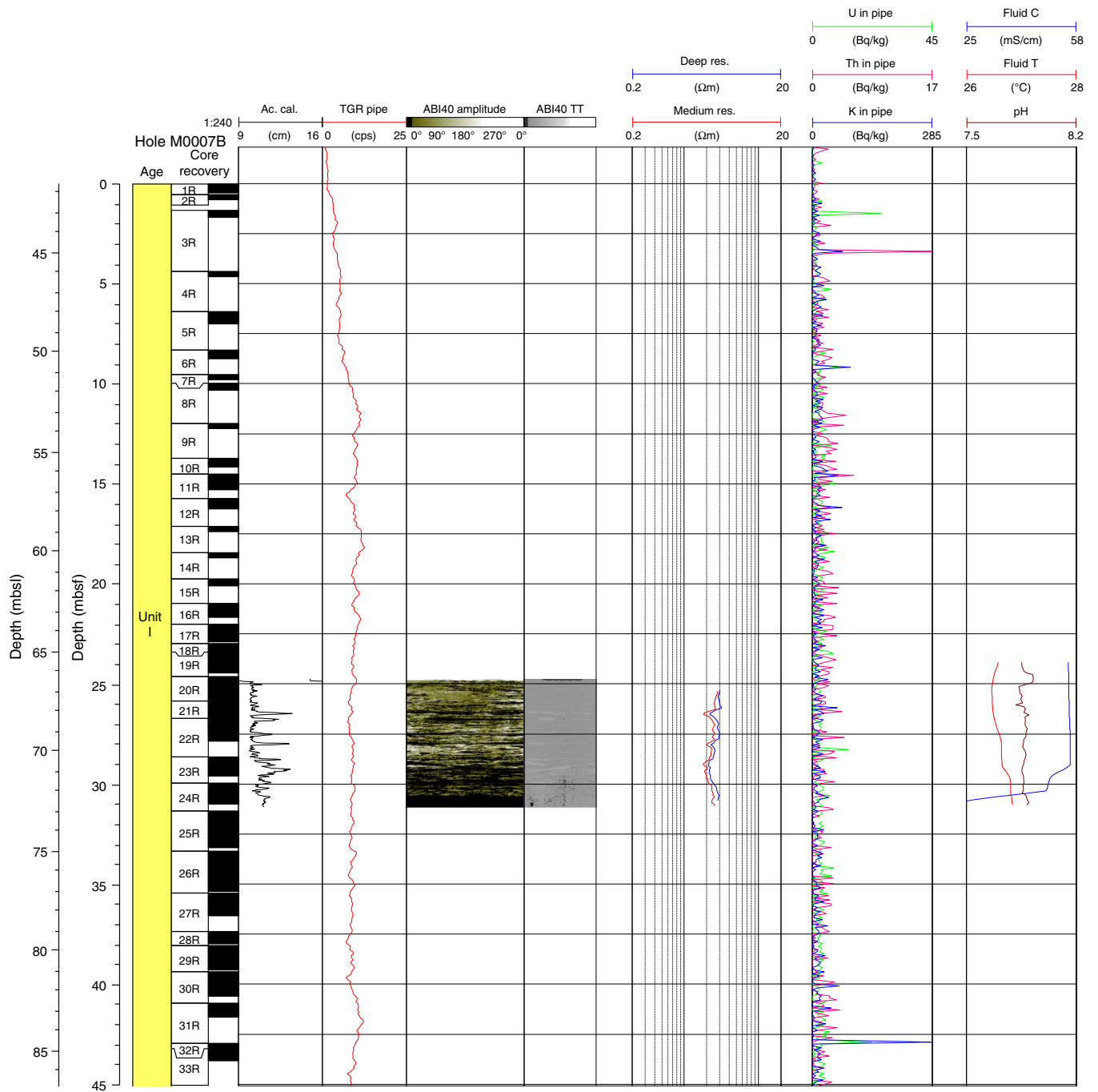


Figure F78. Wireline logging data, Hole M0007B. (See the “DOWNHOLE” folder in “Supplementary Material” for the complete multipart figure in PDF format.)

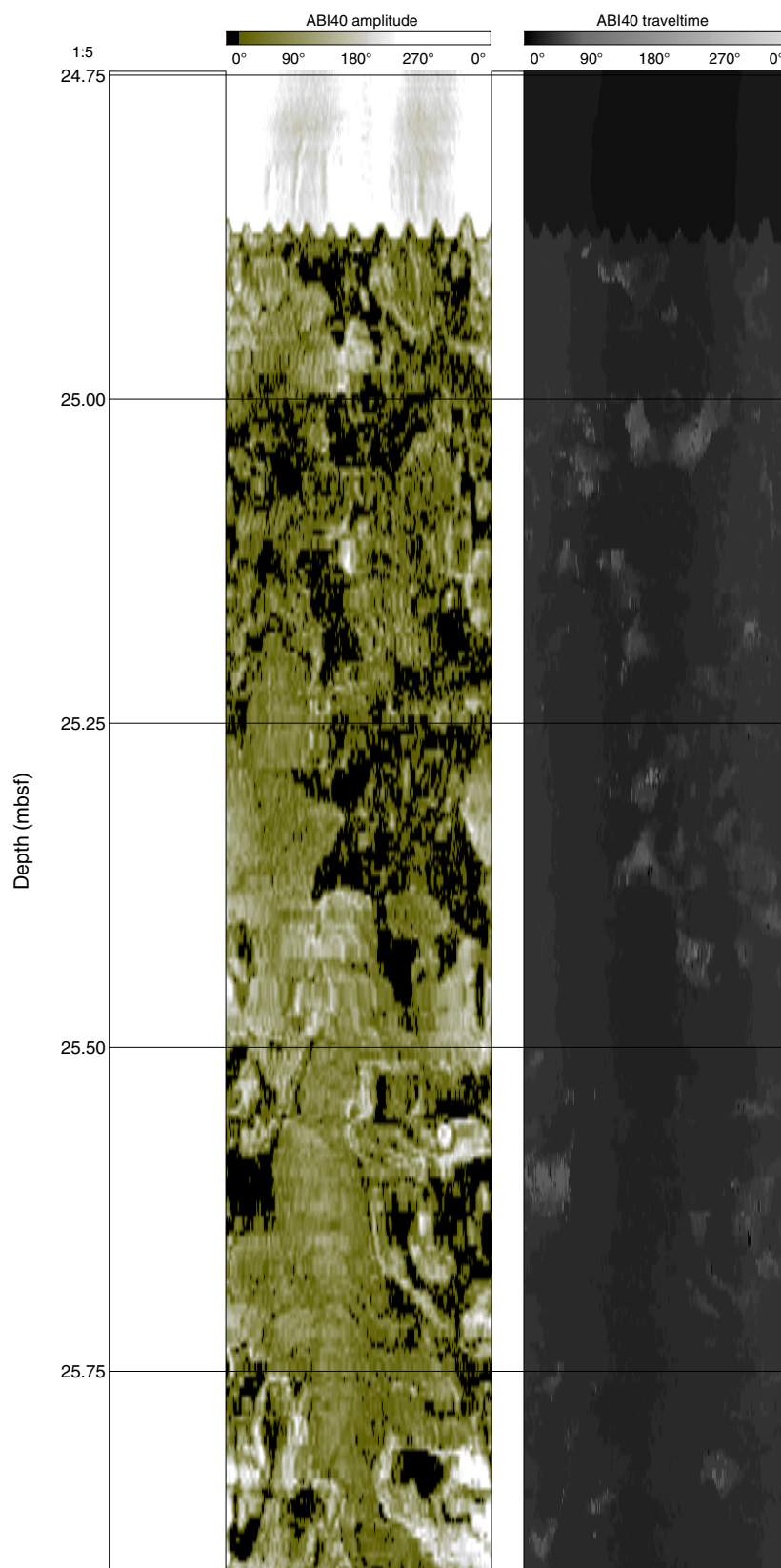


Figure F79. Maraa West pore water chemicals. A. pH. B. Alkalinity. C. Chloride. D. Ammonia. E. Magnesium. F. Potassium. (Continued on next page.)

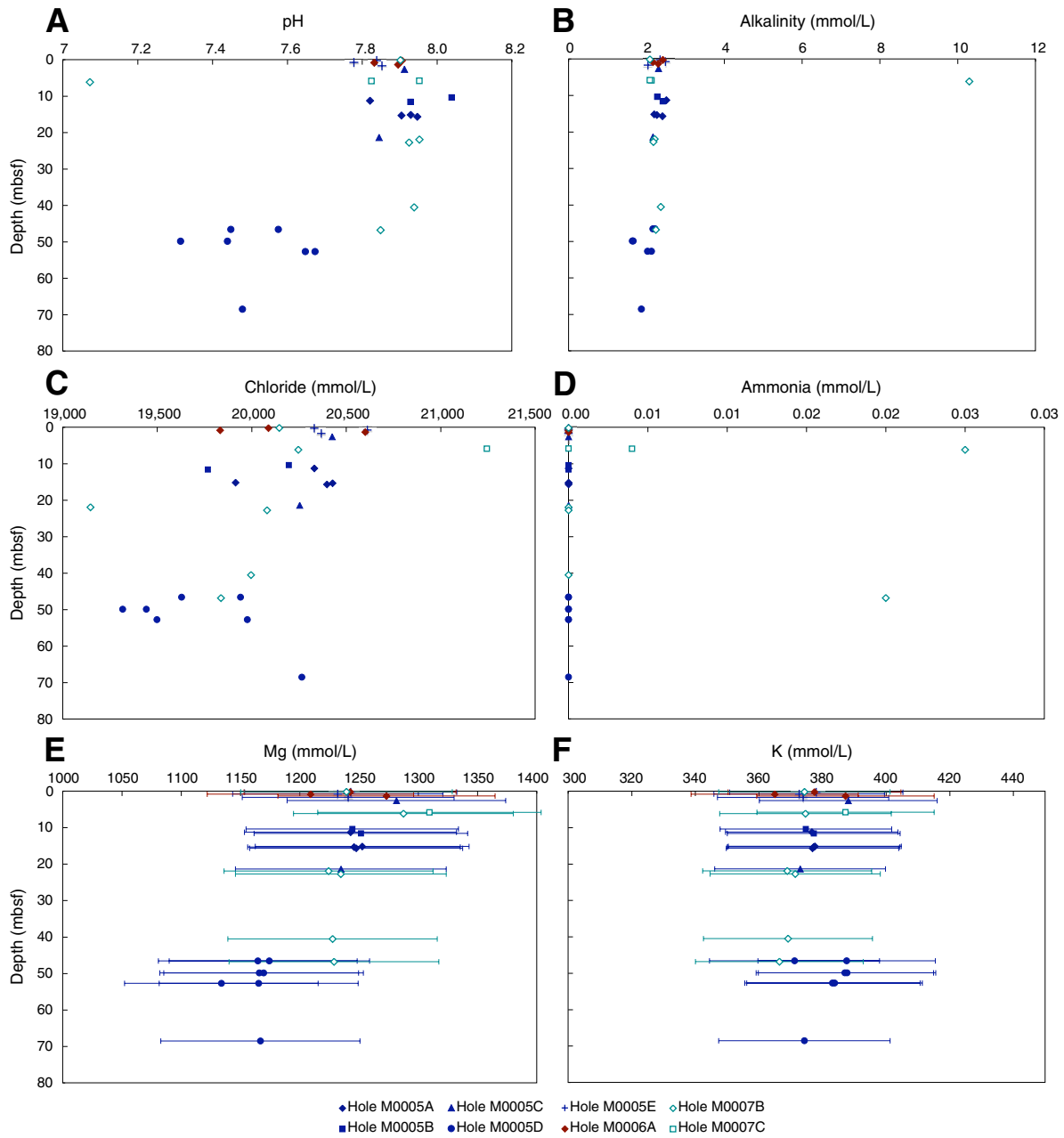


Figure F79 (continued). G. Calcium. H. Strontium. I. Lithium. J. Phosphorus. K. Manganese. L. Barium.

